Investigations of effective connectivity in small and large scale neural networks

Inaugural-Dissertation

zur

Erlangung des Doktorgrades

der Mathematisch-Naturwissenschaftlichen Fakultät

der Universität zu Köln

vorgelegt von

Nils Rosjat

aus Solingen

Köln 2016

Berichterstatter (Gutachter): PD Dr. Silvia Gruhn

Prof. Dr. Ansgar Büschges

Prof. Dr. Martin Nawrot

Tag der mündlichen Prüfung: 20.01.2016

Table of Contents

Zusammenfassung

Zur korrekten Verarbeitung von neuronalen Signalen müssen verschiedene neuronale Gruppen untereinander koordiniert werden. Um dies zu erreichen, muss zwischen den Neuronen eine Verbindung bestehen. Diese Verbindungen und insbesondere ihre Stärke sind a priori nicht bekannt und können nur in den seltensten Fällen direkt gemessen werden.

In dieser Arbeit werden drei Publikationen (Rosjat et al., 2014; Tóth et al., 2015; Popovych et al., under review) und die Ergebnisse zweier weiterer Arbeiten vorgestellt, die sich mit der Analyse von Kopplungen in experimentell gemessenen neuronalen Aktivitäten befassen. Die Arbeiten unterteilen sich in die Untersuchung von intrinsischen sowie extrinsischen intra- und intersegmentalen Verbindungen in der Stabheuschrecke *Carausius morosus* und in die Analyse und Modellierung von Kopplungen anhand von EEG-Messungen des menschlichen Gehirns bei der Ausführung von unterschiedlichen Aufgaben. In beiden Bereichen wurden unter anderem mathematische Modelle verwendet, um Hypothesen über bislang unbekannte Kopplungsmechanismen aufzustellen.

Die erste Studie befasst sich mit den durch Schizophrenie ausgelösten Veränderungen von Kopplungen im thalamo-kortikalen Kreislauf (Rosjat et al., 2014). Hierfür wurden bereits vorherig publizierte EEG-Daten aus einem Doppelklick-Paradigma verwendet, um ein mathematisches Modell, bestehend aus einer thalamischen und einer kortikalen neuronalen Population, zu erstellen. Die einzelnen Populationen bestanden aus einer Vielzahl von Phasenoszillatoren mit kontinuierlich verteilten Eigenfrequenzen. Unter Verwendung der Reduktionsmethoden von Pikovsky und Rosenblum, Ott und Antonsen sowie Watanabe und Strogatz wurden die Einflüsse der bidirektionalen Verbindungen zwischen den beiden Hirnarealen auf die Synchronisation innerhalb dieser Bereiche untersucht. Das Modell war in der Lage, die experimentellen Daten zufriedenstellend zu reproduzieren. Wir konnten beobachten, dass die Kopplungsstärke von der thalamischen zur kortikalen Region hauptsächlich die Dauer der Synchronisation beeinflusst, wohingegen die Rückkopplung zur thalamischen Region einen stärkeren Effekt auf die Synchronisationsstärke ausübt. Dies führte zu der Hypothese, dass die Rückkopplung zur thalamischen Region bei an Schizophrenie erkrankten Testpersonen vermindert sei.

In der zweiten Studie werden intersegmentale Kopplungen im Protraktor-Retraktor-

System des pro- und mesothorakal Ganglions der Stabheuschrecke *Carausius morosus* mit Hilfe von an experimentelle Daten angepassten mathematischen Modellen untersucht (Tóth et al., 2015). Wir haben dafür einerseits experimentell ermittelte und andererseits von mathematischen Modellen simulierte Phasen-Antwort-Kurven verwendet, um die Art und Stärke der Verbindungen zu untersuchen. Wir konnten zeigen, dass Verbindungen von beiden Seiten des prothorakalen zum mesothorakalen Netzwerk nötig waren, um eine gute Übereinstimmung der Phasen-Antwort-Kurven zu erzielen. Außerdem zeigte sich, dass die Stärke von exzitatorischen Verbindungen maßgeblich zu den Phasen-Antwort-Kurven beigetragen hat, wohingegen die Stärke der inhibitorischen Verbindungen keinen großen Einfluss zu haben scheint.

Die dritte Studie beschäftigt sich mit der Identifizierung eines neuronalen Markers der Bewegungsausführung (Popovych et al., under review). In dieser Arbeit haben wir die Auswirkung von intern sowie extern evozierten Bewegungen auf die Phasensynchronisation untersucht. Dafür haben wir die Signale, die von über dem motorischen Cortex platzierten Elektroden aufgezeichnet wurden, auf dem Phasenniveau der Hauptfrequenzbereiche (δ-, θ-, α-, β- und dem niedrigen γ-Bereich) hinsichtlich ihrer Phasensynchronität zwischen einzelnen Wiederholungen analysiert. Es hat sich gezeigt, dass unabhängig von der Hand, welche die Bewegung ausführt, und unabhängig von der Art, wie diese Bewegung ausgelöst wurde, eine stark lateralisierte Phasensynchronisation in den niedrigen Frequenzbereichen (δ und θ) in Elektroden über dem kontralateralen primären Motorcortex stattfindet. Diese Ergebnisse legen nahe, dass sich die Phasensynchronisation in motorischen Bereichen zusätzlich zu den etablierten Markern der ereignisbezogenen Desynchronisation und der ereignisbezogenen Synchronisation, welche sich auf Änderungen der Amplitude im α- und β-Frequenzbereich beziehen, als neuronaler Marker der Bewegungsausführung eignet.

Abstract

The correct signal processing of neuronal signals requires coordination of different groups of neurons. To achieve this there has to be a connection between those neurons. This connection and especially the strength of the connection is not known a priori and can only be measured directly in rare cases.

In this thesis I present three publications (Rosjat et al., 2014; Tóth et al., 2015; Popovych et al., under review) and the results from two additional studies focussing on the analysis of couplings in experimental measured neuronal activities. The publications can be divided into investigations of intrinsic, as well as extrinsic intra- and intersegmental connections in the stick insect *Carausius morosus* and into analysis and mathematical modeling of couplings from EEG-measurements of the human brain while subjects were performing different tasks. In both parts I made use of mathematical models to build hypotheses about so far unknown coupling mechanisms.

The first study deals with connectivity changes in the thalamo-cortical loop caused by schizophrenia (Rosjat et al., 2014). To build a mathematical model consisting of neural populations representing the thalamus and the auditory cortex we made use of published EEG-data, which were collected while subjects performed a double-click paradigm. The individual populations comprised a large number of phase oscillators with continuously distributed natural frequencies. Applying reduction methods by Pikovsky and Rosenblum, Ott and Antonsen together with the reduction method by Watanabe and Strogatz we investigated the influences of the bidirectional connections between the brain areas on the synchronization of the neuronal populations. The model was able to replicate the experimental data adequately. We observed that the coupling strength from the thalamic region to the cortical region mainly affected the duration of synchrony while the feedback to the thalamic region had a bigger effect on the strength of synchrony. This led to the hypothesis that the back coupling to the thalamic region might be reduced in schizophrenia patients.

The second study will show an analysis of intersegmental couplings in the protractor-retractor system of the pro- and mesothoracic ganglion of the stick insect *Carausius morosus* using mathematical models based on experimental data (Tóth et al., 2015). We made use of phase-response curves that were calculated experimentally on the one

hand and simulated by mathematical models on the other hand to determine the nature and the strength of their connection. We showed that connections on both sides from the prothoracic to the mesothoracic network were necessary to achieve a good agreement with the experimental phase-response curves. Additionally, it was found that the strength of the excitatory connection played a key role, while the strength of the inhibitory connection did not have a big influence on the shape of the phase-response curves.

The third study deals with the identification of a neuronal marker of movement execution (Popovych et al., under review). In this work we investigated the influence of internally and externally triggered movement on the phase synchronization in the motor system. We tested the signals, that were recorded from electrodes lying above the motor cortex, in the phase space including the major frequency bands (δ-, θ-, α-, $\beta-$ and low γ-frequencies) for inter-trial phase synchrony. The study revealed a strong lateralized phase synchronization in the lower frequency bands (δ and θ) in the electrodes above the contralateral primary motor cortex independent of the hand performing and the cue triggering the movement. The results suggest that this phase synchronization could serve as an electrophysiological marker of movement execution additionally to the well established event-related desynchronization and event-related synchronization that are based on the amplitude changes in α- and β frequency bands.

Nomenclature

CPG	Central Pattern Generator
CS	Campaniform Sensilla
CTr	Coxa-trochanter joint
DCM	Dynamic Causal Modeling
EEG	Electroencephalography
EF	Extensor-Flexor
fCO	Femoral Chordotonal Organ
FeTi	Femur-tibia joint
FFT	Fast Fourier Transform
FLB	Fold Limit Cycle Bifurcation
fMRI	functional magnetic resonance imaging
HB	Hopf Bifurcation
LD	Levator-Depressor
lM1	left Primary Motor Cortex
lPM	left Premotor Cortex
MN	Motoneurone
OA	Ott-Antonsen
ODE	Ordinary Differential Equation
PLI	Phase-locking Index
PR	Protractor-Retractor
PRC	Phase Response Curve
rM1	right Primary Motor Cortex
rPLV	rescaled phase-locking value
rPM	right Premotor Cortex
SLI	Stimulus-locking Index
SMA	Supplementary Motor Area
sPLV	single-frequency phase-locking value
ThC	Thorax-coxa joint
WS	Watanabe-Strogatz

1 Introduction

All sorts of behaviour, be it coordinated movements, processing of external inputs or planning of motions, need interactions of activities of the nervous system.

> "To move things is all that mankind can do, and for this task the sole executant is a muscle, whether it be whispering a syllable or felling a forest." (Sherrington, 1941)

The loss of such basic behavioural abilities represents a major limitation in normal day-to-day life of patients suffering from mental illnesses, such as Parkinson's disease, schizophrenia or stroke. It is the aim of this thesis to investigate the neural mechanisms underlying these basic abilities. Those fundamental actions of living organisms could either be observed on the behavioural level or recorded and analyzed on an electrophysiological level. Electrophysiology deals with electrical properties from microscopic (e.g. single-cell recordings) to a macroscopic view (e.g. whole brain recordings like electroencephalography). In this work I will approach neural activities from both the microscopic side, in extracellular nerve recordings of the stick insect using so-called hook electrodes (Schmitz et al., 1988), and the macroscopic side, in EEG recordings of the human brain.

Stick insects are often used as a model organism for neuronal studies, since their nervous system is easy to access and their walking behaviour is directly observable. Its legs consist of three leg joints that produce coordinated movements during walking and climbing. The thorax-coxa (ThC) joint is responsible for forward and backward movements, the coxa-trochanter (CTr) joint is able to move the femur of the stick insect in upward and downward direction and finally the femur-tibia (FTi) joint that is responsible for outward and inward movements of the leg. Each of the leg joints is controlled by antagonistic muscle pairs, namely the protractor-retractor (ThC), the levator-depressor (CTr) and the flexor-extensor (FTi) muscle pair (Graham and Epstein, 1985). In stick insects (Büschges, 2005) as well as in other insect species (cockroach: (Fuchs et al., 2010), cricket: (Grillner, 2003)) each muscle pair of each of the six legs is controlled by central pattern generators (CPGs). In the stick insect, these CPGs are located in the central nervous system (Büschges, 2005). Sensory feedback can effect the timing and

the magnitude of the CPG output (Büschges, 2005), what is necessary for coordinated locomotor behaviour. The main sensory organs involved in locomotion are the femoral chordotonal organ, that provides information of the movement and angular velocity of the leg (Bässler, 1967), the femoral and trochanteral campaniform sensilla, that are responsible for force and load signals (Bässler, 1977a; Akay et al., 2001, 2004), and hair plates as well as hair rows which provide information on the position of the leg relative to the body of the stick insect (Bässler, 1977a).

Previous experimental studies have shown that a single stepping front leg is able to induce rhythmic protractor-retractor motoneuron activity in the adjacent thoracic segment (Borgmann et al., 2009), whereas the last thoracic segment showed only a tonic increase in protractor-retractor motoneuron activity (Borgmann et al., 2007). In a semi-intact preparation, where all legs except for an ipsilateral pair, consisting of a front and a middle leg, were removed, a general increase in tonic motoneuron activity in the metathoracic ganglion was observed during stepping of the middle leg. However, stepping of both legs induced alternating activity in the protractor and retractor motoneurons of the metathoracic ganglion that was in phase with front leg steps (Borgmann et al., 2009). A single stepping hind leg on the other side caused a tonic increase of protractor-retractor motoneuron activity in two thirds of the experiments and rhythmic activity in the remaining third of the experiments in the mesothoracic ganglion (Borgmann et al., 2009). Additionally, it could be shown that stepping of a single hind leg also entrains a pilocarpine induced rhythm in the protractor and retractor motoneurons of the prothoracic ganglion (Grabowska, 2014).

Even though many studies focussed on the inter-segmental effects of sensory feedback, the exact contribution of those effects on the inter-leg coordination remains unclear. Mathematical models are a good tool to build hypotheses about the underlying coupling structures leading to the observed inter-segmental influences. Depending on the research question, these models could be simplified by a reduction to the phase plane as in the biomechanical cockroach model (Holmes et al., 2006; Proctor et al., 2010) or they could be based on more complex systems of Hodgkin-Huxley type neurons (Hodgkin and Huxley, 1952) that are able to describe the interactions in more detail (Daun et al., 2009; Daun-Gruhn et al., 2011; Daun-Gruhn and Tóth, 2011). The study of the precise inter-segmental influences of sensory information on motoneuron pools that control a concrete pair of muscles, thus, requests the use of the latter modeling approach. This model is not only able to reproduce different walking patterns observed in stick insects, but it also enables us to simulate various experimental paradigms by decoupling and deactivating certain leg joints from the rest of the network. Thereby an artificial deafferentation of the desired legs as used in previous experimental studies (Borgmann et al., 2009) can be produced. This model can then be used to investigate

the coupling structure and especially the nature of the connections, e.g. inhibition, excitation and coupling strengths, that are needed to achieve similar behaviour as observed in experiments.

However, the presence of the strong sensory inputs during leg movements makes it difficult to investigate the intrinsic intra- and inter-segmental interaction between the different CPG networks. In order to understand the role of this intrinsic coupling it is necessary to remove all sensory influences on the system. For this purpose a large number of studies dealt with deafferented isolated nerve cords in the state of fictive locomotion induced by the muscarinic receptor agonist pilocarpine (c.f. Büschges et al., 1995). This kind of preparation allows us to analyze the interactions of the CPG networks in the different thoracic segments.

In contrast to the stick insects nervous system, the human brain cannot be accessed easily for direct recordings of neuronal activities. Therefore, non-invasive technologies are needed to measure the brain activity. The techniques mostly used in the last decades are functional magnetic resonance imaging (fMRI), magnetoencephalography (MEG) and electroencephalography (EEG).

The human brain is an extremely complex structure that contains up to 10^{12} neurons and about 10^{13} to $5 \cdot 10^{13}$ glial cells, that do not take part directly in the synaptic interactions and electrical signaling. Every neuron can have up to 10^4 post-synaptic connections which leads to a very high complexity in the networks formed by connected neurons. To be able to capture networks in this dimension, the neurons are grouped in families, the so called brain areas. These areas are specialized on different tasks and can be distinguished by their cytoarchitecture, histological structure and organization of cells (Brodmann, 1909). The cortex can be subdivided into six cortical layers (Shipp, 2007). The cortical layers contain cells of different neuronal size, shapes and density and can be divided into three parts. The supragranular layers consist of the layers I to III. They are the main origin of corticocortical connections and consist of small pyramidal cells (layer III), small stellate cells (layer II) and nerve fibers (layer I). The second part is the internal granular layer IV that receives thalamocortical connections through stellate cells. The last part, the infragranular layers V to VI, primarily connects the cerebral cortex to subcortical layers and consists mainly of large pyramidal cells (Schusdziarra et al., 1977; Shipp, 2007; Greig et al., 2013). The composition of the six layers is different in certain cortical areas, while the motor cortex has a prominent layer V and only a small layer IV. Other cortical areas such as the primary sensory cortices, show a more pronounced granular layer (Shipp, 2007).

The various non-invasive techniques record different quantities of the brain activities

in the brain areas. In fMRI the changes of the blood-oxygen-level dependent (BOLD) signal in response to neural activity are detected. The idea behind this technique is that active brain areas consume more oxygen and thus the blood flow in these areas increases (Heeger and Ress, 2002). The advantage of this method is its excellent spatial resolution, while it has deficits in the determination of neural events at fast time-scales. MEG and EEG on the other hand measure magnetical and electrical signals. EEG measures potential differences on the scalp produced by volume currents, while MEG measures magnetic fields induced mainly by tangential primary currents based on excitatory activity (Okada et al., 1997). The simultaneous activity of about 50.000 pyramidal cells gives rise to measurable EEG and MEG signals (Murakami and Okada, 2006). Although EEG and MEG have the advantage of high temporal resolution, volume conductance leads to a poor spatial resolution. Thus, we have no detailed information on single neurons or small brain areas. This makes it necessary to use preprocessing steps like source reconstruction or spatial filtering via Laplacian references to improve the localization of the recorded signals (e.g. Van Veen et al., 1997; Dale et al., 2000; McFarland et al., 1997).

As mentioned above, the loss of basic cognitive functions is a substantial impairment to day-to-day life of patients suffering from mental diseases. Thus it is of paramount importance to understand the interplay of brain regions while performing basic cognitive tasks, such as sensory processing, movement preparation and execution, in order to increase the understanding of possible dysfunctions in the involved networks and possible improvements of their rehabilitation.

Previous studies have shown bio-markers for movement preparation and movement execution. These are, amongst others, the Bereitschaftspotential preceding self-initiated movements (Shibasaki and Hallett, 2006) and the event-related desynchronization (ERD) and event-related synchronization (ERS) in movement related tasks (Neuper et al., 2006; Pfurtscheller and da Silva, 1999). These bio-markers are based on changes of amplitudes only and do not take phase-synchronization effects into account. As seen in (Brockhaus-Dumke et al., 2008), the lack of phase-synchronization plays a key-role in auditory evoked responses in schizophrenia. Up to now it remains unclear whether similar phase-locking effects can be found in the human motor system and whether its nature is changed due to different cognitive diseases.

These phase-locking effects could be used to build mathematical models and thereby could lead to hypotheses about the modulation of the interaction between different brain areas. Based on the work by Hodgkin and Huxley (1952) many mathematical models were derived (c.f. Carlsson, 2006; an der Heiden, 2006). Most of those models only describe the coupling of a small number of neurons. Since we want to study a

bigger population of neurons, which would be expected to be involved in the human brain during execution of certain tasks, we need to find a simplified way to model the neuronal dynamics. A commonly used way to investigate the coupling structure of EEG data is dynamic causal modelling (DCM). DCM simulates the activity of infragranular, supragranular and granular layers via neural mass models using the Jansen and Rit model and estimates the coupling between the different sources of activity (Jansen and Rit, 1995; Kiebel et al., 2008). Another approach for neuronal networks of this size are ensembles of coupled phase-oscillators that can be further reduced to the mean field activity of each ensemble (Pikovsky and Rosenblum, 2011). These models can serve as an abstract phenomenological representation of the observed activities that can be adjusted to different brain regions easily. With the help of these models, insights in the general coupling structure of the investigated neural networks can be obtained.

The aim of the present thesis is to investigate coupling mechanisms and synchronization phenomena in neuronal networks on the micro- and macroscopic scale tackled by direct analysis of experimental data and by investigations of mathematical models.

The first publication (Rosjat et al., 2014) shows possible differences in the thalamocortical loop in patients suffering from schizophrenia. For this work, mathematical models based on large ensembles of phase oscillators were fitted to experimentally obtained synchronization effects in EEG data. The model was reduced to lower dimensions via the Pikovsky-Rosenblum ansatz (Pikovsky and Rosenblum, 2011). The model is - despite its abstract nature - in good agreement with the recorded EEG data. This justifies our chosen degree of approximation. The results suggest that the decrease in phase-synchronization, that is present in schizophrenia patients, is due to reduced connectivity from the auditory cortex to thalamic regions.

The second study (Tóth et al., 2015) shows an analysis of inter-segmental coupling in the protractor-retractor system of the pro- and mesothoracic ganglion of the stick insect. The mathematical model was adjusted to match the experimental condition, i.e. all legs except for a single front leg were removed. Theoretical phase-response curves (PRCs) were then fitted to the ones obtained by experiments to determine the nature and the strength of the connection between the pro- and mesothoracic segment. We showed that connections on both sides from the prothoracic to the mesothoracic network were necessary to achieve a good agreement with the experimental phase-response curves. Additionally it was found that the strength of the excitatory connection played a key role, while the strength of the inhibitory connection did not have a big influence on the shape of the phase-response curves.

The third work (Popovych et al., under review) describes synchronization phenomena on the phase and amplitude level in movement related tasks. Therefore, EEG data of young healthy participants were recorded during externally and internally triggered finger tapping movements, as well as a vision only control condition. The analysis showed low frequency intra-regional phase-synchronization in electrodes located above the pre-motor cortex, the primary motor cortex and supplementary motor areas additionally to the well-known ERD and ERS effects during movement preparation and movement execution. In contrast to phase-synchronization found in auditory double-click paradigms, there were no synchronization effects present in frequencies higher than approximately 10 Hz. The observed effect was strongest in the electrodes lying above the primary motor cortex contralateral to the moving hand.

The last part of the thesis describes the results from two additional unpublished studies. The first subsection deals with inter-regional phase-synchronization effects during

movement preparation and execution. For this purpose phase-locking metrics were used to analyze the inter-regional synchronization picked up by electrodes lying above motor related areas. The analysis showed a significant increase in phase locking that was strongest between motor regions contralateral to the moving hand and the supplementary motor area during movement preparation and execution in $\delta - \theta$ frequencies (2-7 Hz). An increase in β-phase synchronization (13-30 Hz) was observed between contralateral motor areas and the supplementary motor area, after the movement had finished.

The second subsection deals with the analysis of intrinsic connectivities in the deafferented thoracic nerve cord of the stick insect. The recorded depressor motoneuron activity was analyzed via two approaches, a first descriptive approach using phase-difference analysis and a second more sophisticated approach using dynamic causal modelling. Both approaches showed a strong agreement on the level of coupling strengths. The results suggest the existence of intra- and ipsilateral inter-segmental couplings between the segments of the pro-, meso- and metathoracic ganglia in the levator-depressor system. The study showed that the intra-segmental coupling strength in the mesothoracic ganglion is the strongest, while intra-segmental connections between meso- and metathoracic ganglia are the weakest over all experimental conditions. The connectivity in the prothoracic ganglion, that controls the behaviour of the front legs, shows a high variability between and within the different approaches. This result might reflect the independent movements from the other legs during searching movements, as well as the coupled movements during walking behaviour.

2 Published Studies

2.1 A mathematical model of dysfunction of the thalamo-cortical loop in schizophrenia

Nils Rosjat, Svitlana Popovych and Silvia Daun-Gruhn

Published in Theoretical Biology and Medical Modelling (11:45,2014)

Author Contributions

Conceived the research
Nils Rosjat, Svitlana Popovych
Silvia Daun-Gruhn

Performed the simulations
Nils Rosjat

Analyzed the data
Nils Rosjat, Svitlana Popovych
Silvia Daun-Gruhn

Figure Preparation
Nils Rosjat

First version of manuscript
Nils Rosjat

Wrote the paper
Nils Rosjat, Svitlana Popovych
Silvia Daun-Gruhn

Rosjat *et al. Theoretical Biology and Medical Modelling* 2014, **11**:45
http://www.tbiomed.com/content/11/1/45

THEORETICAL BIOLOGY AND MEDICAL MODELLING

RESEARCH Open Access

A mathematical model of dysfunction of the thalamo-cortical loop in schizophrenia

Nils Rosjat*, Svitlana Popovych and Silvia Daun-Gruhn

*Correspondence:
rosjatn@uni-koeln.de
Heisenberg Research Group of Computational Biology, Department of Animal Physiology, Institute of Zoology, University of Cologne, Zülpicher Str. 47b, 50674 Cologne, Germany

Abstract

Background: Recent experimental results suggest that impairment of auditory information processing in the thalamo-cortical loop is crucially related to schizophrenia. Large differences between schizophrenia patients and healthy controls were found in the cortical EEG signals.

Methods: We derive a phenomenological mathematical model, based on coupled phase oscillators with continuously distributed frequencies to describe the neural activity of the thalamo-cortical loop. We examine the influence of the bidirectional coupling strengths between the thalamic and the cortical area with regard to the phase-locking effects observed in the experiments. We extend this approach to a model consisting of a thalamic area coupled to two cortical areas, each comprising a set of nonidentical phase oscillators. In the investigations of our model, we applied the Ott-Antonsen theory and the Pikovsky-Rosenblum reduction methods to the original system.

Results: The results derived from our mathematical model satisfactorily reproduce the experimental data obtained by EEG measurements. Furthermore, they show that modifying the coupling strength from the thalamic region to a cortical region affects the duration of phase synchronization, while a change in the feedback to the thalamus affects the strength of synchronization in the cortex. In addition, our model provides an explanation in terms of nonlinear dynamics as to why brain waves desynchronize after a given phase reset.

Conclusion: Our model can explain functional differences seen between EEG records of healthy subjects and schizophrenia patients on a system theoretic basis. Because of this and its predictive character, the model may be considered to pave the way towards an early and reliable clinical detection of schizophrenia that is dependent on the interconnections between the thalamic and cortical regions. In particular, the model parameter that describes the strength of this connection can be used for a diagnostic classification of schizophrenia patients.

Keywords: Mathematical modeling, Phase oscillators, EEG, Synchronization

Introduction

Schizophrenia is a severe and complex mental illness causing disability [1-3]. It has been conceptualized as a disconnectivity syndrome concerning the interplay of the brain areas involved. As information on the activity of some of the deeply localized involved brain areas, such as the thalamus is not accessible to noninvasive electroencephalography (EEG) measurement, alternative methods, like mathematical models, need to be developed in order to deepen our understanding of the fundamental neural processes underlying

schizophrenia, and to detect dysfunctions in the interactions between the participating brain areas. Such methods aim at deriving reliable criteria that indicate the progress of the disease at an early stage. The early recognition is considered to be of special importance in schizophrenia.

As schizophrenia has a very high degree of complexity, due to the large number of neuronal processes involved, there is no model that treats all aspects of the disease concurrently. The model in [4], for instance, focuses on the empirical dopamine hypothesis of schizophrenia and postulates that an imbalance between glutamate and dopamine activity plays a key role in schizophrenia disorder. In particular, the authors could show that both hypoglutamatergia and hyperdopaminergia result in reduced activation of the striatal complex and thus leads to schizophrenia [4].

Heiden et al. [5] on the other hand modeled the basic neural circuit underlying schizophrenia as a dynamical system on a microstructural level of pyramidal cells (see also Mackey et al. [6]). In their model, periodic firing patterns were associated with healthy behavior, whereas aperiodic/chaotic firing patterns were associated with schizophrenic states and the switch from periodic to aperiodic firing took place due to an increase in dopamine level. In [7], the same model was analyzed in a hypo-glutamatergic setting, and it also exhibited aperiodic firing.

A top-down approach in modeling the symptoms of schizophrenia is proposed in [8,9]. These authors relate cognitive, negative and positive symptoms of schizophrenia to a reduced depth of attractor basins of the model regarded as a dynamical system. The model consisting of pools of leaky integrate-and-fire neurons for the involved pyramidal cells and inhibitory interneurons and AMPA, NMDA and $GABA_A$ synapses either developed spontaneous firing or was attracted to a high-firing state. The decrease in NMDA-receptor conductance led to a decrease in attractor stability and therefore a decrease in memory and an increase in distractability [8,9]. An additional decrease in the conductance of GABA-synapses led to jumping from spontaneous activity to attractors which could be identified with the increase of positive symptoms [8].

In [10], fMRI data of healthy and schizophrenic test persons obtained in a memory-task experiment were used to assess the connectivity between the visual, parietal and prefrontal regions using DCM as proposed by [11]. Each of these regions has a self-coupling and bidirectional all-to-all coupling. Moreover, the working memory modulates the coupling from visual to prefrontal and from prefrontal to parietal regions. The schizophrenic patients and the healthy subjects differed significantly in the self-coupling strengths, in the coupling between parietal and prefrontal regions in both directions and in the coupling from visual to prefrontral regions [10].

In contrast to the modeling studies described above, we focused our attention on the phenomena observed on the large-scale level of dysfunction of the thalamo-cortical loop in schizophrenia. We did therefore not include any explicit biophysical properties into our model. We constructed a mathematical model based on a study by [12]. In this study, the difference between healthy subjects and schizophrenia patients was investigated, using individual EEG recordings with respect to phase locking (PL) in the four frequency bands (θ, α, β and γ). The two groups of test persons showed significant difference in the strength of PL in the θ- and α-frequency band, while no significant difference in PL was observed in the other two frequency bands. The duration of PL, i.e. the time until the system desynchronize again, differed for each frequency band. However it did not differ

significantly between healthy subjects and schizophrenia patients in each of the four frequency bands.

In our earlier model [13], we described each component of the thalamo-cortical loop as a single phase oscillator, where each of them operated at its natural frequency. We used phase oscillators for the description of the dynamics in each brain area, since previous studies suggested that the timing of the brain rhythms, i.e. the phases, were more important than their amplitudes [12]. The coupling between these oscillators was expressed in form of weighted phase differences with suitable coefficients, which were determined from the natural frequencies of the oscillators. Using this model, we were able to explain the difference in phase locking in the respective frequency bands of the two groups of test persons depending on the feedback from the cortex to the thalamus. In this model, however, the synchronization effect observed directly after the given auditory stimulus did not abate and vanish after a given period of time, contrary to what was seen in the experiments [12]. We had therefore to change our mathematical model in order to be able to account for the desynchronization effects, too.

In the present study we extended this mathematical model such that now each area of the thalamo-cortical loop is represented by a large population of phase oscillators. The coupling between populations is driven by a complex meanfield (definition see below). To reduce this high-dimensional model to a low dimensional system which still reflects the behavior observed in the EEG data and to allow its analysis, we use the reduction methods of Watanabe- Strogatz [14], Ott-Antonsen [15] and Pikovsky-Rosenblum [16]. The mathematical analysis of the model offers a conducive explanation for the underlying mechanisms leading to the differences observed between healthy subjects and schizophrenia patients, as seen in the experiments by [12]. Our results suggest that the differences are due to a decrease in strength of the coupling from the auditory cortex to the thalamus in schizophrenia patients. Even so, our model is a rather abstract description of the neural dynamics that take place in the thalamo-cortical loop. A decrease in coupling strength can occur due to changes in the dopamine, glutamate or serotonin concentrations. This means in any case a reduction in signal transduction from the auditory cortex to the thalamus. Furthermore, our analysis of the reduced system reveals that the mechanism underlying the abolition of synchrony observed in all four brain wave bands is based on a fold limit cycle bifurcation that takes place when the coupling between the auditory cortex and the thalamus is changed (in either direction). Our model additionally predicts that a change in coupling strength from the thalamus to the auditory cortex, however, affects the duration of phase synchrony.

The paper is organized as follows. In section “The experimental setup and results”, we review the experimental setup and the results of the study by [12]. In section “Mathematical model”, we present the general structure of the thalamo-cortical loop and set up a mathematical model which we use to analyze first the behavior of two coupled brain regions, the thalamus and one cortical region, and then that of three coupled ones, the thalamus and two cortical regions.

The experimental setup and results

The mathematical model presented below is based on experimental results (for details of the experiment and methods used see [12]). In the following, we outline the experiment performed in [12]. Two groups of participants were investigated during the experiment:

the first group consisted of 32 schizophrenia patients and the second of 32 healthy subjects. The experiment was based on the well-established paired click paradigm [17]. It consisted of 96 paired clicks (S_1 and S_2). Each click had a duration of 1 ms. The interstimulus interval between the two clicks within a pair lasted 500 ms, and the inter-trial interval between pairs of clicks 10 s. The EEG was continuously recorded using 32 electrodes during the whole experiment. Data from the vertex electrode Cz were taken for the analysis, because the cortex around the location of this electrode performs sensory and motor functions, see [18]. The recorded data have been divided into epochs of 1500 ms (500 ms prior to S_1 and 500 ms following stimulus S_2). The occurence of stimulus S_1 in each segment was set to $t = 0$, hence the stimulus of each segment appeared at $t = 0$. To obtain detailed information on the temporal and spectral properties of the EEG, a single-trial analysis was applied to the epochs. Thus a complex Morlet wavelet transformation in the frequency range from 3 Hz to 60 Hz in 1 Hz steps was performed to compute the phases of the single-trial data. A typical result is displayed in Figure 1 (adapted from [13]) where the cosine of the single trial phase after the wavelet transformation for a fixed frequency 54 Hz is shown. It includes 82 superimposed segments. Uniform distribution of the phases prior stimulus onset, i.e. for $t \in [-50, 0]$ is clearly visible, while the so called phase locking effect after the stimulus, i.e. for $t \in [0, 75]$, and the effect of desynchronisation after $t = 75$ ms can also be clearly discerned.

The stimulus locking index

$$SLI(t) = \left| \frac{1}{n} \sum_{k=1}^{n} e^{2\pi i \phi_k(t)} \right| \tag{1}$$

defined in [19], can be used to measure the degree of phase locking for a certain frequency at time t. We denote the number of repetitions of the auditory double clicks by n and the phase of the k-th oscillation at time t by $\phi_k(t)$. Values near 0 indicate a uniform distribution of phases and values near 1 nearly synchronized phases. It was found that schizophrenia patients produced significantly less phase locking in lower frequency bands after the first stimulus than healthy subjects [12].

Table 1 shows the *SLI* and the duration of synchronization for the two groups of subjects for the θ- and α-frequency band for which significant differences were found in the *SLI* (see [12]). Based on these experimental results, we constructed a mathematical model

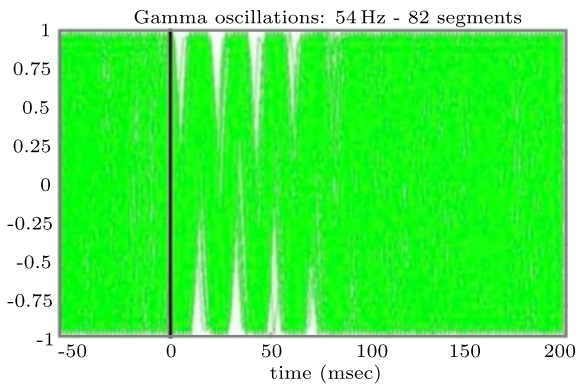

Figure 1 Experimental data. The cosine of the phases, derived from EEG data of a single participant, expressing a frequency of 54 Hz is shown (from [13]).

Table 1 Example behavior of cortical regions

	Max. SLI		Duration
	Patients	Control	[ms]
θ	.30	.37	400
α	.19	.26	250

Columns 1-2: Maximum SLI values (from [12]); Column 3: Approximate duration of stimulus responses ([12], Figure two).

of the thalamo-cortical loop and used it to explain the observed differences between the neural activities of schizophrenia patients and healthy subjects.

Mathematical model

Our model of the thalamo-cortical loop is based on the results of [4,12,13,20]. According to the experimental findings in these sources, we assume that essentially three main brain areas are actively involved in auditory signal processing, i.e. the thalamic auditory relay nucleus (here for the sake of simplicity, they are referred to as thalamus), the thalamic reticular nucleus (here named TRN) and areas of the auditory cortex. An auditory input signal reaches the thalamus and then propagates to the auditory cortex. From the auditory cortex, the signal propagates to higher cerebral regions such as the prefrontal cortex and back to the TRN, which inhibits the thalamus. Furthermore, backpropagation from higher regions such as the prefrontal cortex modulates the activity of the thalamus. These inhibitory and modulating influences lead to a reduced response of the thalamus to the second of the two clicks [21-23]. Since we are only interested in the dynamics after the first and before the second stimulus, we neglected the impact of the TRN. This means that only the thalamus and different regions of the auditory cortex are present in our model. It can be assumed that the different cortical regions act in different oscillatory frequency ranges, which correspond to the θ, α, β and γ ranges. The structure of the thalamo-cortical loop used in our model is shown in Figure 2.

In our earlier work [13], we described each part of the thalamo-cortical loop by a single phase oscillator. Each oscillator had a natural frequency, which was chosen according to biological/experimental observations. We assumed, that coupling between all phases is a form of weighted phase difference with suitable coefficients to be determined from the natural frequencies. With this model, it was possible to reproduce the effects that correspond to phase locking as observed in the EEG data of the two groups of subjects. However, in contrast to what the data showed (see Figure 1, t $>$ 75 ms), the oscillators

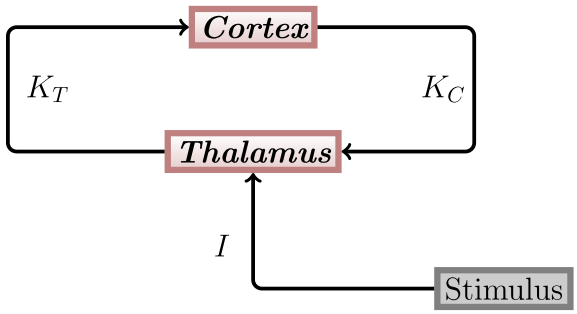

Figure 2 Thalamo-cortical loop. The general structure of the thalamo-cortical loop used in our modeling study. K_T and K_C denote coupling strengths between the thalamus and the auditory cortex. Both the thalamus and the cortex are represented by one population of oscillators each. I denotes the stimulation strength.

remained in the synchronized state perpetually, and their phases did not desynchronize again. To overcome this major drawback of our old model, we now describe each element of the thalamo-cortical loop as a large ensemble of nonidentical phase oscillators. Each oscillator in the population has a natural frequency ω, which is chosen from a Lorentz distribution $n(x)$. The coupling between populations is driven by a complex meanfield. In the experiments, repeated stimulations were used in order to obtain stimulation moments at different phases. In our mathematical model we use 1000 oscillators with distributed phases in each population and stimulate each oscillator at $t = 0$. Since we choose the initial conditions for each oscillator to be different, the results obtained by stimulating them at only one point in time are comparable to the experimental conditions.

First, we will consider a minimal mathematical model, which consists of only two populations of oscillators, one for the thalamus and one for the θ-frequency band of the auditory cortex. We will use this simplified model to understand the mechanism behind the transition from the synchronized to the desynchronized state after stimulation (as seen in Figure 1).

Minimal mathematical model (two populations)

In the minimal model, two populations of oscillators are coupled via their complex mean fields as shown in Figure 3. One of them describes brain wave activity in the thalamus and the other one in the cortex, in this case in the θ-band. In the course of this work, we will refer to these populations as thalamus population and cortex population, respectively.

The system describing the neural activities of the two populations reads as follows

$$\frac{d\phi_T(\omega_T)}{dt} = \omega_T + K_C R_C \sin(\theta_C - \phi_T(\omega_T)) + I(t)\cos(\phi_T(\omega_T)), \tag{2}$$

$$\frac{d\phi_C(\omega_C)}{dt} = \omega_C + K_T R_T \sin(\theta_T - \phi_C(\omega_C)), \tag{3}$$

where ω_T and ω_C are continuous parameters distributed in each ensemble of oscillators as

$$n_a(\omega_a) = \frac{2}{\pi(1 + 4(\omega_a - \tilde{\omega}_a)^2)}, \quad a = \{T, C\} \tag{4}$$

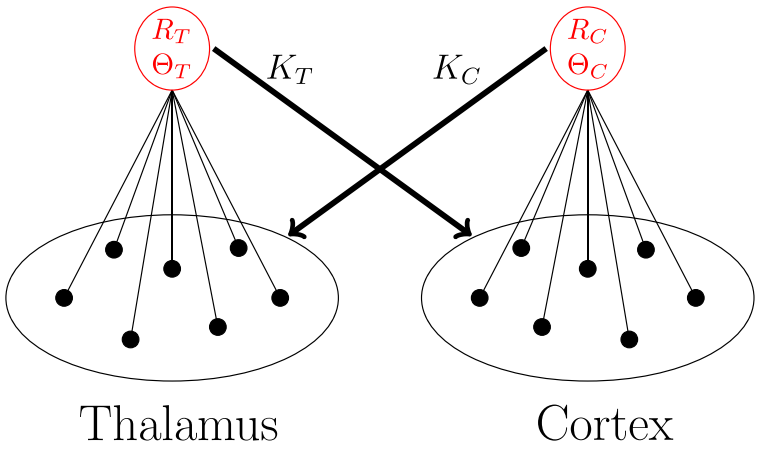

Figure 3 Mean field coupling. Visualization of the complex mean field coupling between the thalamic region (*T*) and a single cortical region (*C*). Black represents the individual oscillators and red their complex mean fields. The oscillators of one population are coupled through the mean phases Θ and the degree of synchronization *R* of the oscillators in the other population. See text for details.

and represent the natural frequencies of the oscillators. ϕ_T and ϕ_C denote the phases of the oscillators of the thalamus and cortex populations, respectively. The state of each population can be described by the distribution density $W(x,\phi,t) = n(x)w(x,\phi,t)$, with the conditional distribution density of oscillators denoted by $w(x,\phi,t)$ [16].

Each oscillator in the cortical population is coupled to the complex mean field

$$Y_T = R_T e^{i\theta_T} = \int n(x) \int_{-\pi}^{\pi} e^{i\phi_T} w(x,\phi_T,t) d\phi dx \tag{5}$$

of the thalamic population and each oscillator in the thalamic population is coupled to the complex mean field

$$Y_C = R_C e^{i\theta_C} = \int n(x) \int_{-\pi}^{\pi} e^{i\phi_C} w(x,\phi_C,t) d\phi dx \tag{6}$$

of the cortical populations (see Figure 3). Coupling strengths are denoted by K_T and K_C, respectively.

The thalamus population is stimulated by an external stimulus that acts directly on it (see Figure 2). This stimulus is represented by the term $I(t)\cos(\phi_T)$ where

$$I(t) = \begin{cases} I & \text{during stimulus,} \\ 0 & \text{otherwise.} \end{cases} \tag{7}$$

A complete analysis of the model can be performed by means of the Watanabe-Strogatz (WS) theory [14]. With this theory an N-dimensional system of identical oscillators can be reduced to a three-dimensional system with the global variables ρ, ϕ and ψ. Here ρ is the global amplitute, ϕ and ψ are global phases. The original phase variables can be reconstructed from the obtained WS variables by means of the time-dependent transformation. The theory is described in more detail in the Appendix.

Following [14-16,24], we transform system (2)-(3) using Equation 36 (see Appendix) and obtain a reduced system of WS equations with the new variable ρ_T, ϕ_T, ψ_T and ρ_C, ϕ_C, ψ_C. By additionally introducing $z_a(\omega_a) = \rho_a e^{i\phi_a}$ and the phase shift $\alpha_a(\omega_a) = \phi_a - \psi_a$, $(a = T, C)$, we obtain

$$\frac{dz_T(\omega_T)}{dt} = i\omega_T z_T(\omega_T) + \frac{K_C}{2}\left(Y_C - Y_C^* z_T(\omega_T)^2\right) + \frac{I(t)i}{2}\left(1 + z_T(\omega_T)^2\right), \tag{8}$$

$$\frac{d\alpha_T(\omega_T)}{dt} = \omega_T + \mathrm{Im}\left(z_T(\omega_T)^*\left(K_C Y_C + I(t)i\right)\right), \tag{9}$$

$$\frac{dz_C(\omega_C)}{dt} = i\omega_C z_C(\omega_C) + \frac{K_T}{2}\left(Y_T - Y_T^* z_C(\omega_C)^2\right), \tag{10}$$

$$\frac{d\alpha_C(\omega_C)}{dt} = \omega_C + \mathrm{Im}\left(z_C(\omega_C)^* K_T Y_T\right). \tag{11}$$

Here, $i = \sqrt{-1}$ and A^* denotes the conjugate complex of A.

Now we consider this reduced set of equations with respect to the Ott-Antonsen manifold [25]. In this case, $z(\omega)$ no longer depends on $\alpha(\omega)$, and the mean fields Y_C and Y_T can therefore be written as

$$Y_a = R_a e^{i\theta_a} = \int n_a(x) z_a(x) dx, \qquad (a = T, C). \tag{12}$$

Following the work by Ott and Antonsen for a similar distribution [25], the integrals in Equation (12) can be calculated by applying the residue theorem, under an additional assumption that $z_a(\omega)$ $(a = T, C)$ is analytic in the upper half-plane. This calculation yields

$$Y_T = z_T(\tilde{\omega}_T + i/2), \tag{13}$$

$$Y_C = z_C(\tilde{\omega}_C + i/2). \tag{14}$$

Thus Equation (8) for $\omega_T = \tilde{\omega}_T + i/2$ and Equation (10) for $\omega_C = \tilde{\omega}_C + i/2$ provide a 2-dimensional system of complex ODEs that describe the behavior of the order parameter of the thalamic and the cortex population, respectively:

$$\frac{dY_T}{dt} = \left(\tilde{\omega}_T i - \frac{1}{2}\right) Y_T + \frac{1}{2}\left(K_C Y_C + I(t)i - Y_T^2\left(K_C Y_C^* - I(t)i\right)\right) \tag{15}$$

$$\frac{dY_C}{dt} = \left(\tilde{\omega}_C i - \frac{1}{2}\right) Y_C + \frac{K_T}{2}\left(Y_T - Y_C^2 Y_T^*\right) \tag{16}$$

In the following, we will investigate this system of two complex differential equations, i.e. its dynamics during the post-stimulus interval.

Analysis of the model behavior in the post-stimulation interval

For the analysis of eqs. (15)-(16) in the post-stimulus interval, i.e. when $I(t) = 0$, we transform them to a 4-dimensional system of real ODEs via $Y_T = x_T + iy_T$ and $Y_C = x_C + iy_C$. This leads to

$$\frac{dx_T}{dt} = -\frac{x_T}{2} - \omega_T y_T + \frac{K_C}{2}\left(x_C - \left(x_T^2 - y_T^2\right) x_C - 2x_T y_T y_C\right) \tag{17}$$

$$\frac{dy_T}{dt} = \omega_T x_T - \frac{1}{2} y_T + \frac{1}{2} K_C \left(y_C - 2x_T y_T x_C + \left(x_T^2 - y_T^2\right) y_C\right) \tag{18}$$

$$\frac{dx_C}{dt} = -\frac{1}{2} x_C - \omega_C y_C + \frac{1}{2} K_T \left(x_T - \left(x_C^2 - y_C^2\right) x_T - 2x_C y_C y_T\right) \tag{19}$$

$$\frac{dy_C}{dt} = \omega_C x_C - \frac{1}{2} y_C + \frac{1}{2} K_T \left(y_T - 2x_C y_C x_T + \left(x_C^2 - y_C^2\right) y_T\right). \tag{20}$$

In a next step, we linearize this new system about its fixed point $x_F = (0, 0, 0, 0)$ and investigate the stability of this fixed point with the coupling strengths K_C and K_T as parameters. The linearized system reads:

$$\begin{pmatrix} \frac{dx_T}{dt} \\ \frac{dy_T}{dt} \\ \frac{dx_C}{dt} \\ \frac{dy_C}{dt} \end{pmatrix} = A \begin{pmatrix} x_T \\ y_T \\ x_C \\ y_C \end{pmatrix} \quad \text{with} \tag{21}$$

$$A = \begin{pmatrix} -\frac{1}{2} & -\omega_T & \frac{K_C}{2} & 0 \\ \omega_T & -\frac{1}{2} & 0 & \frac{K_C}{2} \\ \frac{K_T}{2} & 0 & -\frac{1}{2} & -\omega_C \\ 0 & \frac{K_T}{2} & \omega_C & -\frac{1}{2} \end{pmatrix}. \tag{22}$$

A one-dimensional bifurcation diagram is displayed in Figure 4. For the calculation of this diagram, we fix one of the coupling parameters, $K_C = 1.2$, and show the dependence of one of the system variables (x_C) on the second coupling parameter K_T. The system has a fixed point $x_F = (0, 0, 0, 0)$, which is stable for $K_T < K_T^{HB}$. At $K_T = K_T^{HB} = \frac{(\omega_T - \omega_C)^2 + 1}{K_C}$ a Hopf bifurcation (HB) occurs in the system, i.e. a complex conjugate pair of eigenvalues of A passes through the imaginary axis (see Figure 4). At this point, the branch of stable fixed points (x_F, red line in Figure 4) loses its stability because it collapses into a branch of unstable periodic orbits (x_{PU}, blue circles). Additionally, the system exibits a fold limit cycle bifurcation (FLB) at $K_T^{FLB} < K_T^{HB}$. At this bifurcation point, two periodic orbits, a stable (x_{PS}, green discs) and an unstable one (blue circles) are born. The bifurcation diagram reveals three parameter regions in which the system displays different behavior. In region I $\left(0 < K_T < K_T^{FLB}\right)$ we have a stable fixed point $x_F = (0, 0, 0, 0)$, which corresponds to the state of full desynchronization in the non-reduced system (2)-(3). In region III $\left(K_T > K_T^{HB}\right)$ the fixed point x_F has lost its stability and all trajectories are attracted to the

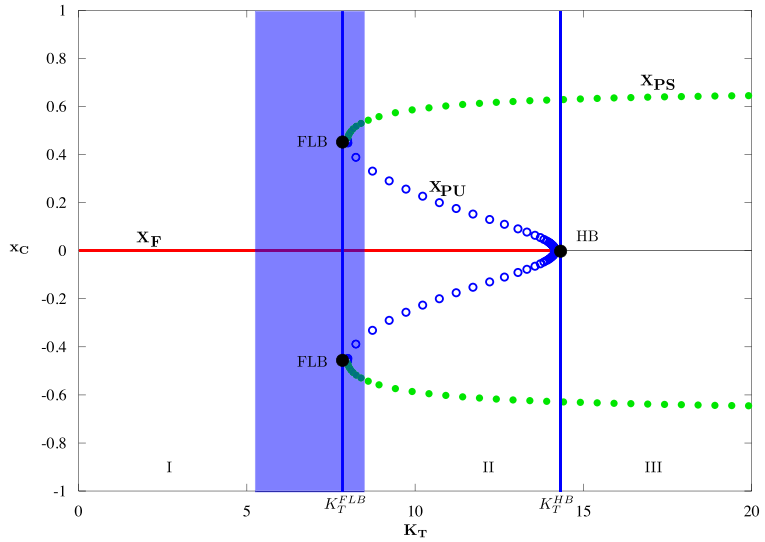

Figure 4 Bifurcation diagram. Bifurcation diagram in the ($K_T - x_C$)-plane. The coupling strength from the cortex to the thalamus has been set to $K_C = 1.2$ and the coupling strength K_T from the thalamus to the cortex is varied; $\tilde{\omega}_C = 3$ Hz and $\tilde{\omega}_T = 7$ Hz. Red line: stable fixed points (x_F), black line: unstable fixed points; green filled circles represent the maximum and minimum of stable periodic orbits (x_{PS}) while the blue circles represent the maximum and minimum of unstable periodic orbits (x_{PU}). Bifurcation points, i.e. the fold limit cycle bifurcation (FLB) at K_T^{FLB} and the Hopf-bifurcation (HB) at K_T^{HB} are marked with vertical blue lines. The light blue box represents the parameter region where the initially synchronized system desynchronizes in finite time (like in Figure 1).

stable periodic orbit x_{PS} (filled green circles in Figure 4). This corresponds to a state near perfect synchronization of the non-reduced system. In region II $\left(K_T^{FLB} < K_T < K_T^{HB}\right)$, the system is bistable. It can exhibit fixed point solutions as well as periodic ones. Both behaviors are separated by an unstable periodic orbit x_{PU}. Depending on the initial conditions of the system, the trajectory will stay in the region of attraction of the fixed point x_F or is attracted by the stable periodic orbit x_{PS}.

Let us now focus on the blue region surrounding the bifurcation points FLB. It is possible to choose a value of the parameter K_T inside this region such that the trajectory is resetted to a state near the periodic orbit and drops back to the stable fixed point after a certain amount of time.

Figure 5 shows the behavior of the reduced system (left) and the corresponding behavior of the non-reduced system (right) for the three parameter regions described above. Red lines in the figures of the left column indicate the maximum amplitude of the solutions. Black thick lines in the figures of the right column indicate the SLIs. In region I (see Figure 4), i.e. for low value of K_T, e.g. $K_T = 1$, the reduced system exhibits a stable fix point solution (Figure 5(a), left), and the corresponding non-reduced system is in the desynchronization regime (Figure 5(a), right), hence SLI = 0. For K_T in region III (see Figure 4), e.g. $K_T = 16$, the stable periodic orbit of the reduced system is shown in

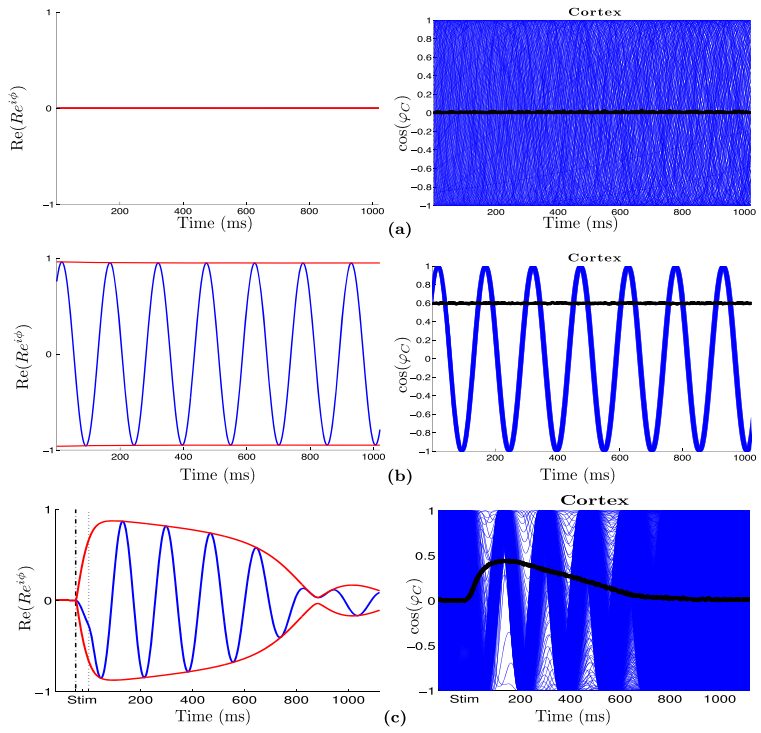

Figure 5 Bifurcation behaviors. The real part of the solution of the reduced system (left) and the corresponding cosine of the solution of the non-reduced system (right) for **(a)** $K_T = 1$ in region I, **(b)** $K_T = 16$ in region III and **(c)** $K_T = 5.5$ in region II of Figure 4 are shown. In (c) the behavior of both systems is shown during and after stimulation. For the reduced system, red lines indicate the maximum amplitude of the solutions (panels in the left column). For the non-reduced system, the oscillators' (only 200 out of $N = 1000$ displayed) activities are shown as blue curves, and the corresponding max SLI is plotted in black (panels in the right column). $K_C = 1.2$, $\tilde{\omega}_C = 3$ Hz, $\tilde{\omega}_T = 7$ Hz. The stimulus intensity was set to $I = 100$ and had a duration of 50 ms for all simuli.

Figure 5(b) on the left and the corresponding synchronization regime of the non-reduced system on the right with SLI = 0.6. In Figure 5(c) K_T is fixed near K_T^{FLB} ($K_T = 5.5$, left edge of blue region in Figure 4). With this parameter choice, we observe the same dynamics as seen in the experiments: before stimulation we have desynchronization in the non-reduced system and a fix point in the reduced one. After the stimulation interval (marked with vertical dash lines), we see a phase reset, and the phases of the oscillators of the non-reduced system are now synchronized (thin wave). After some time (t $>$ 700 ms) they desynchronize again. The length of the synchronization state can be modulated by changing the distance of K_T to K_T^{FLB}. The closer K_T is set to K_T^{FLB} the longer the trajectory will stay in the state of synchronization before it desynchronizes again.

In Figure 6, top left, the maximum SLI of the cortex population for different pairs of coupling strengths (K_C, K_T) is shown. For this we stimulated the system of two populations ($N = 1000$ oscillators each) with a stimulation strength of $I = 100$ for 50 ms and calculated $\max_t \frac{1}{1000} \sum_{j=1}^{1000} e^{2\pi i \varphi_{C_j}(t)}$ for each fixed pair (K_C, K_T). The dependence of the peak of the frequency distribution on these parameters was calculated using the fast Fourier transformation (MATLAB function FFT). It is shown in the bottom left panel of Figure 6. The coupling strengths K_T and K_C were varied independently from 0 to 10 with a step

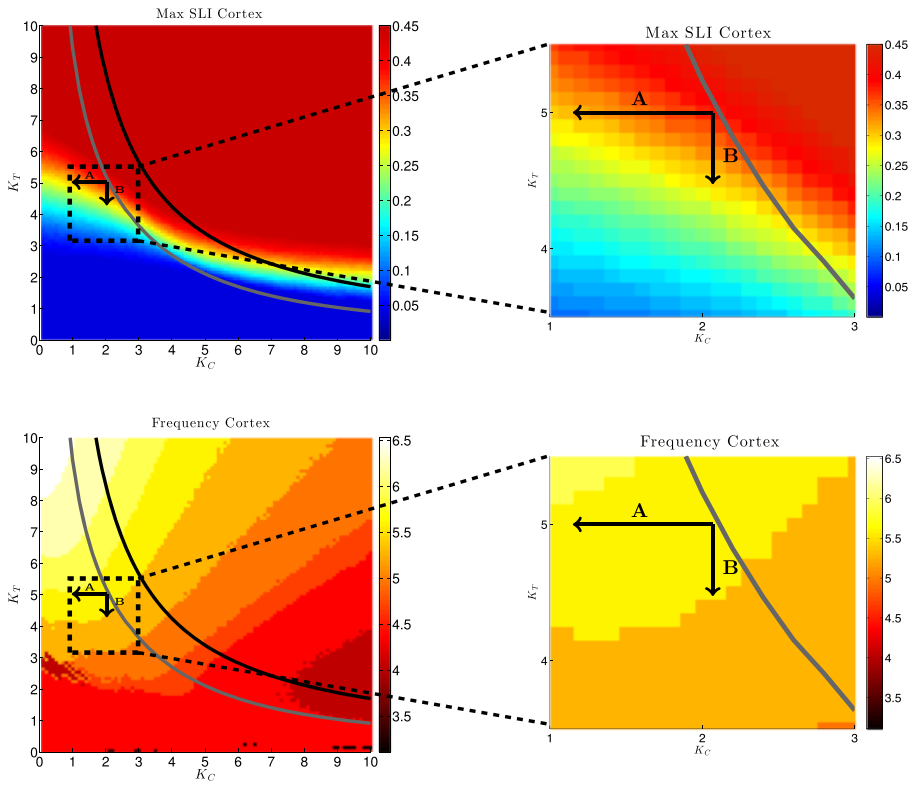

Figure 6 Coupling parameter dependence. Left: Maximal SLI (top) and mean frequency (bottom) of the oscillators in the cortical region (for $\tilde{\omega}_C = 3$ Hz, $\tilde{\omega}_T = 7$ Hz and $N = 1000$) as functions of the coupling strengths K_C and K_T. Right: enlargments of the marked areas in the corresponding panels. Solid curves mark Hopf-Bifurcations (black) and fold-limit cycle bifurcations (gray) of the reduced system. The arrows A and B show possible transitions from a level of high synchronization ($K_C = 2, K_T = 5$) to a level of lower synchronization (tip of arrow A: $K_C = 1.1, K_T = 5$; tip of arrow B: $K_C = 2, K_T = 4.5$).

size of 0.05. The grey and black curves in the K_C-K_T plane represent the branches of fold limit cycle bifurcations (FLBs) of the periodic orbits and of Hopf-bifurcations (HBs) of the fixed points, respectively. As seen in Figure 4, only parameter values to the left and close to the grey curve and parameter values which yield $SLI \geq 0.3$ guarantee a strong synchronized population which desynchronizes in finite time. The closer the coupling parameters are set to the branch of FLBs the longer the population will stay in the synchronized state. When the value of the coupling parameter K_T is decreased the system moves away from the curve of FLBs, thus the synchronization of the system becomes weaker and shorter. This happens even for small changes in K_T (direction denoted by B in Figure 6, top left). Changing the value of the coupling parameter K_C, however, has a much weaker effect on the strength of synchronization (direction denoted by A in Figure 6, top left). An enlargement of this region of interest is shown in Figure 6, top right.

We know from the experimental data of [12] that schizophrenia patients show a lower synchronization in the θ-band than healthy subjects (max SLI = 0.3 and 0.37, respectively). If we now change the parameters K_C and K_T such that the SLI changes from 0.37 to 0.3 (in the A or B direction or in a direction representing a linear combination of the two), the mean frequency of the θ-oscillators does only minimally change, i.e. it remains approximately 6 Hz. A major change in the mean frequency should of course not happen when the conditions of the system are changed from the healthy to the schizophrenic state. Figure 6, bottom left shows the mean frequency of the cortical oscillators for different pairs of coupling parameters (K_C, K_T). An enlargement of the region of interest is shown in Figure 6, bottom right.

Summing up, our model simulations nicely show that the neural dynamics observed in EEG data of schizophrenia patients and healthy subjects strongly depend on the strength of the coupling between the thalamus and the cortex: decreasing one or both of the coupling parameters K_T or K_C in an appropriate manner decreases the max SLI of the system and changes the time the system stays synchronized but leaves its mean frequency nearly unchanged.

Model with three populations

In this section, we consider the extension of our minimal model to three populations of coupled phase oscillators, where one of them describes brain activity in the thalamus and the other two θ- and α-brain waves in the auditory cortex. We only consider the θ- and α-frequency band here since the experimental data of [12] showed significant differences between schizophrenia patients and healthy subjects in these frequency bands, only.

Our extended system has the form

$$\frac{d\phi_T(\omega_T)}{dt} = \omega_T + \sum_{j=1}^{2} K_{C_j} R_{C_j} \sin\left(\theta_{C_j} - \phi_T(\omega_T)\right) + I(t)\cos\left(\phi_T(\omega_T)\right), \tag{23}$$

$$\frac{d\phi_{C_1}(\omega_{C_1})}{dt} = \omega_{C_1} + K_{T_1} R_T \sin\left(\theta_T - \phi_{C_1}(\omega_{C_1})\right), \tag{24}$$

$$\frac{d\phi_{C_2}(\omega_{C_2})}{dt} = \omega_{C_2} + K_{T_2} R_T \sin\left(\theta_T - \phi_{C_2}(\omega_{C_2})\right). \tag{25}$$

All notations are the same as in the minimal model. ϕ_T and ϕ_{C_1}, ϕ_{C_2} are the phases corresponding to the oscillators of the thalamus population and the oscillators of the θ cortex

and α cortex populations, respectively. ω_T, ω_{C_1} and ω_{C_2} represent the natural frequencies of the corresponding oscillators chosen from the distribution described in Equation 4.

Each oscillator of both cortical populations is coupled to the complex mean field

$$Y_T = R_T e^{i\theta_T} = \int n(x) \int_{-\pi}^{\pi} e^{i\phi_T} w(x, \phi_T, t) d\phi dx$$

of the thalamic population with the corresponding coupling parameters $K_{T_j}, j = 1, 2$. Each oscillator in the thalamic population is coupled to both complex mean fields

$$Y_{C_j} = R_{C_j} e^{i\theta_{C_j}} = \int n(x) \int_{-\pi}^{\pi} e^{i\phi_{C_j}} w(x, \phi_{C_j}, t) d\phi dx, \qquad j = 1, 2$$

of the θ and α cortical populations with the corresponding coupling parameter K_{C_j}, $j = 1, 2$.

For the sake of simplicity and as a first approximation, we assume, that there is no direct connection between the two cortical populations. Note, that these populations are considered as functionally distinct groups in the cortex, not as anatomically distinct ones. They, however, influence each other indirectly through the feedback they receive from the thalamic population. Figure 7 shows a schematic illustration of the thalamo-cortical loop with two cortex populations. The thalamus population is stimulated with the same external stimulus as in the case of the minimal model (see Equation 7).

Again, we apply the Watanabe-Strogatz ansatz [14] and its extension by Pikovsky and Rosenblum [16] to the system (23)-(25) and obtain

$$\frac{dz_T(\omega_T)}{dt} = i\omega_T z_T(\omega_T) + \sum_{j=1}^{2} \frac{K_{C_j}}{2} \left(Y_{C_j} - Y_{C_j}^* z_T(\omega_T)^2 \right) + \frac{I(t)i}{2} \left(1 + z_T(\omega_T)^2 \right), \quad (26)$$

$$\frac{d\alpha_T(\omega_T)}{dt} = \omega_T + \mathrm{Im}\left(z_T(\omega_T)^* \left(K_{C_1} Y_{C_1} + K_{C_2} Y_{C_2} + I(t)i \right) \right), \quad (27)$$

$$\frac{dz_{C_1}(\omega_{C_1})}{dt} = i\omega_{C_1} z_{C_1}(\omega_{C_1}) + \frac{K_{T_1}}{2} \left(Y_T - Y_T^* z_{C_1}(\omega_{C_1})^2 \right), \quad (28)$$

$$\frac{d\alpha_{C_1}(\omega_{C_1})}{dt} = \omega_{C_1} + \mathrm{Im}\left(z_{C_1}(\omega_{C_1})^* K_{T_1} Y_T \right), \quad (29)$$

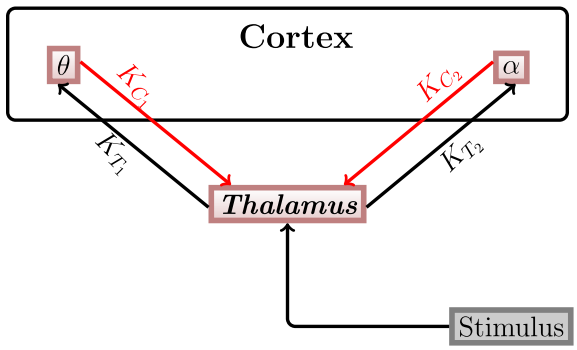

Figure 7 Three population structure. Scheme of the three-population model. Fixed couplings are shown in black and variable ones in red.

$$\frac{dz_{C_2}(\omega_{C_2})}{dt} = i\omega_{C_2} z_{C_2}(\omega_{C_2}) + \frac{K_{T_2}}{2}\left(Y_T - Y_T^* z_{C_2}(\omega_{C_2})^2\right), \tag{30}$$

$$\frac{d\alpha_{C_2}(\omega_{C_2})}{dt} = \omega_{C_2} + \mathrm{Im}\left(z_{C_2}(\omega_{C_2})^* K_{T_2} Y_T\right). \tag{31}$$

This system can again be reduced to a 3-dimensional system of complex ODEs representing the dynamics of the order parameters. The reduced system has the form:

$$\begin{aligned}\frac{dY_T}{dt} &= \left(\tilde{\omega}_T i - \frac{1}{2}\right) Y_T + \frac{1}{2}\left(I(t)i + Y_T^2 I(t)i\right) + \\ &\quad + \frac{1}{2}\sum_{j=1}^{2}\left(K_{C_j} Y_{C_j} - Y_T^2 K_{C_j} Y_{C_j}^*\right),\end{aligned} \tag{32}$$

$$\frac{dY_{C_1}}{dt} = \left(\tilde{\omega}_{C_1} i - \frac{1}{2}\right) Y_{C_1} + \frac{K_{T_1}}{2}\left(Y_T - Y_{C_1}^2 Y_T^*\right), \tag{33}$$

$$\frac{dY_{C_2}}{dt} = \left(\tilde{\omega}_{C_2} i - \frac{1}{2}\right) Y_{C_2} + \frac{K_{T_2}}{2}\left(Y_T - Y_{C_2}^2 Y_T^*\right). \tag{34}$$

The main results of the analysis of this model are illustrated in Figure 8. The panels of the figure on the left show the maximum SLI and the frequency for both cortex populations over the plane of the coupling parameters K_{C_1} and K_{C_2}. The right column shows enlargements of a region of interest of each of the figures shown in the left column. In these simulations we fixed the coupling from the thalamus population to the θ- and α-populations, i.e. $K_{T_1} = 5.5$ and $K_{T_2} = 7$, respectively. For each parameter pair (K_{C_2}, K_{C_1}), we stimulated the system ($N = 1000$ oscillators in each of the three populations) with a stimulus intensity of $I = 100$ for 50 ms and calculated the maximum SLI as $\max_t \frac{1}{1000}\sum_{j=1}^{1000} e^{2\pi i \varphi_{C_j}(t)}$. The results are shown in the first and third row of Figure 8. The figures in the second and fourth row of Figure 8 show the mean frequency of the θ- and α-populations, respectively, as functions of the coupling strengths K_{C_1} and K_{C_2}. The coupling strengths K_{C_1} and K_{C_2} were varied independently from 0 to 10 with a step size of 0.05. The grey and black curves again denote the branches of fold limit cycle bifurcations (FLBs) of the periodic orbits and of Hopf bifurcations (HBs) of the fixed points, respectively.

Using these simulations, we can now navigate through the (K_{C_2}, K_{C_1}) parameter plane and find pairs of coupling parameter values at which our model exhibits brain dynamics as observed in healthy subjects or in schizophrenia patients. To change the dynamics of the model from the healthy to the schizophrenic state, the parameter pairs need to be chosen such that: i) the max SLI of the θ-brain waves changes from 0.37 to 0.3; ii) the one of the α-waves from 0.26 to 0.19; iii) the frequencies of the θ- and α-populations change only minimally, i.e. they remain approximately $5 - 7$ Hz for the θ- and $9 - 12$ Hz for the α-population.

With the letters P and C, we label the positions in the (K_{C_2}, K_{C_1}) parameter plane which correspond to the max SLIs and frequencies observed in schizophrenia patients and healthy subjects, respectively. For healthy subjects the coupling constants are $K_{C_2} = 3.9, K_{C_1} = 2.2$, for schizophrenia patients $K_{C_2} = 3.2, K_{C_1} = 1.2$. We can see that schizophrenia patients, compared to healthy subjects, have a reduced feedback from both cortex populations to the thalamus.

We therefore hypothesize based on our model that schizophrenia patients have deficits in signal transduction from the auditory cortex back to the thalamus.

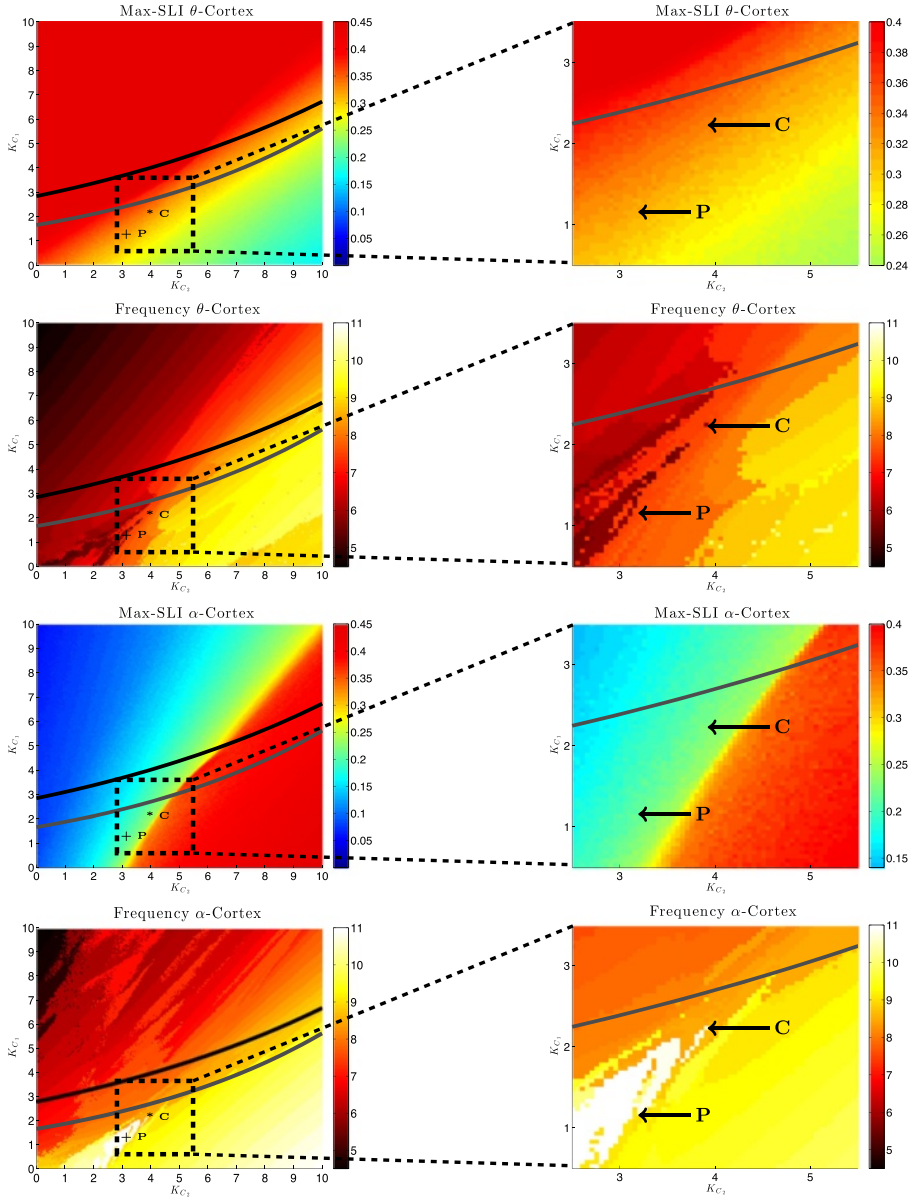

Figure 8 Coupling parameter dependence for three populations. Left: maximum SLI and frequency of the θ-population ($\tilde{\omega}_{C_1} = 3$ Hz; top two) and the α-population ($\tilde{\omega}_{C_1} = 14$ Hz; bottom two) as functions of the coupling parameters K_{C_2} and K_{C_1}. Right: enlargement of the marked areas. The points in the corresponding left panels C ($K_{C_2} = 3.9, K_{C_1} = 1.2$) and P ($K_{C_2} = 3.2, K_{C_1} = 1.2$) mark parameter choices that yield the max SLIs and frequencies observed in healthy subjects (controls) and schizophrenia patients, repectively. The coupling parameters from the thalamus ($\tilde{\omega}_T = 7$ Hz) to the cortex are fixed at $K_{T_1} = 5.5$ and $K_{T_2} = 7.0$. Solid curves mark branches of Hopf bifurcations (black) and of fold limit cycle bifurcations (gray) of the reduced system.

Figure 9 shows the behaviour of the θ- and α-populations in the case of schizophrenia patients, i.e. the coupling parameters are $K_{T_1} = 5.5$, $K_{T_2} = 7$, $K_{C_2} = 3.2, K_{C_1} = 1.2$. The cosine of the phases of 200 oscillators is shown (in total we calculated N=1000 oscillators in each population). The system was stimulated at $t = 0$. The black lines indicate the max SLI. Before the stimulation, i.e. $t \in [-100, 0]$, we have a uniform distribution of the phases, which means that the oscillators in each population are desynchronized, i.e.

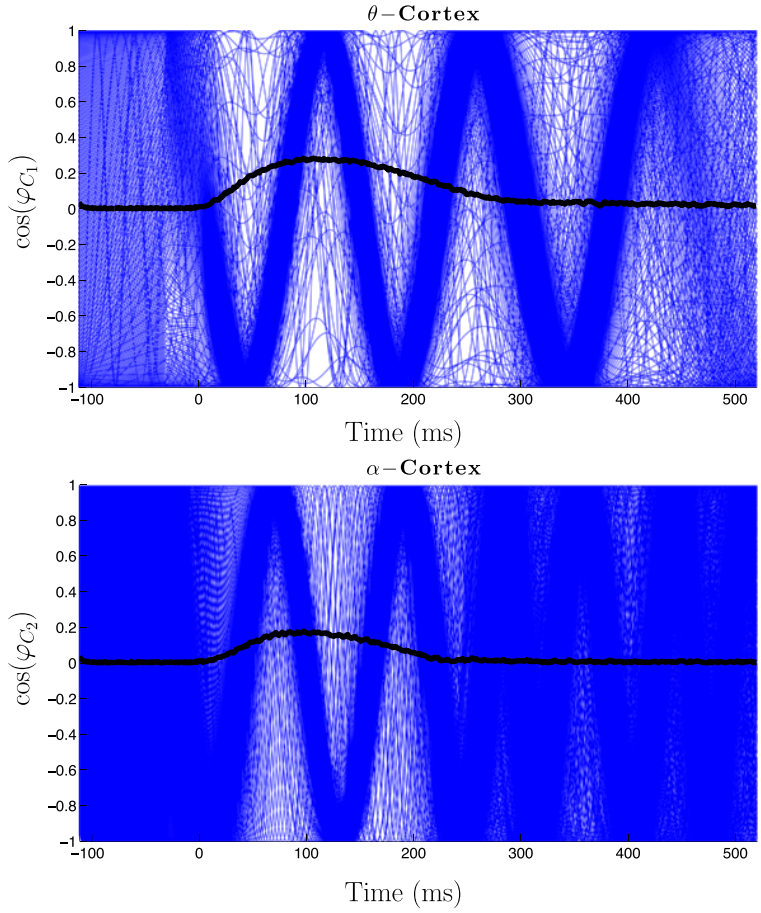

Figure 9 Dynamic behavior of cortical regions. An example of the desynchronization in the two cortical areas of the non-reduced system (only 200 of $N = 1000$ oscillators are shown); $\tilde{\omega}_{C_1} = 3$ Hz $\tilde{\omega}_{C_2} = 14$ Hz, $\tilde{\omega}_T = 7$ Hz, $K_{T_1} = 5.5$, $K_{T_2} = 7.0$, $K_{C_2} = 3.2$, $K_{C_1} = 1.2$. The max SLI is shown in black. Frequency of coupled oscillators in the phase-locking interval: 6 Hz for θ-population and 9.4 Hz for α-population.

max SLI $= 0$. Directly after the stimulation at $t = 0$ a phase reset occurs and the phases of the oscillators synchronize (thin blue waves), hence now max SLI > 0. After a certain time, they desynchronize again: the desynchronization in the α-population happens earlier (at ≈ 250 ms) followed by that in the θ-population (at ≈ 400 ms). These simulation results fully agree with the experimental data [12].

Discussion

We have constructed a mathematical model which describes some aspects of the dysfunction in neural activity of the thalamo-cortical loop during schizophrenia. This model is, in contrast to the models introduced at the beginning [5,7,8,10], an abstract description of the neural activity of the brain regions involved. The description is based on synchronization phenomena as found in the EEG records of healthy subjects and schizophrenia patients. The model allows us to study the interaction of the brain areas involved in a systematic way and to detect the effects of changes of the couplings between them.

A major advantage of our model is that it provides insight into activities of brain areas not directly accessible by EEG measurements. A second advantage is its flexibility:

since we did not include any explicit biophysical properties into our model and stayed on a phenomenological macrostructural level, it can be adjusted to fit similar effects in other diseases, e.g. Morbus Parkinson [5] or bipolar disorder [26]. Patients suffering from Morbus Parkinson show a decrease in post-movement synchronization in the β-band [27] in the motor cortex. To simulate the system dynamics underlying this disease, it is possible to extend our model by including oscillators with β-frequencies in the cortex population (as done by the extension of our model from initially 2 to 3 populations). In a graph-theoretical analysis, Kim et al. [26] could show that only synchronization in α frequencies is significantly lower in patients with bipolar disorder than in healthy controls. Thus it would be possible to adjust the coupling strengths in our model in a way that it could appropriately reproduce the symptoms of this disease.

We have seen that the description of each area by a population of phase oscillators with distributed frequencies instead of only a single one per region allows the model to exhibit phase desynchronization in addition to phase-resetting after a given auditory stimulus. With this model it is now possible to get insights into the brain dynamics of the thalamic region which are not accessible to EEG measurements and to investigate the impact of different connection topologies between the thalamic and cortical brain regions on the duration and strength of synchronization in the respective brain frequency bands.

By analyzing our model, we have seen that it supports the current view [9] that the coupling between the thalamic and the cortical regions is responsible for dysfunction of the thalamo-cortical loop in schizophrenia. In particular, our model shows that a reduction in the strength of coupling from the thalamic to a cortical region, i.e. decreasing the coupling parameters K_{T_i}, shortens the time interval of phase synchronization after stimulus. The closer K_{T_i} is to the fold limit cycle bifurcation the longer the state of high synchrony lasts. A reduction in the strength of the coupling from the cortical regions back to the thalamus, i.e. decreasing the coupling parameters K_{C_i}, however reduces the strength of synchronization. Comparing this with the findings in [12] yields that patients differ mostly in the θ- and α-frequency bands in that they have a significantly lower coupling K_{C_i} from the cortex to the thalamus and only a little weaker coupling K_{T_i} from the thalamus to the cortex, than healthy subjects.

The bifurcation analysis of our model was only possible, because we were able to reduce this large-scale model to systems of only two or three dimensions by using the Ott-Antonsen theory and the reduction methods by Pikovsky and Rosenblum. Thanks to these reduction methods, we could do so without loosing the desynchronization phenomena observed in experiments and exhibited by the large-scale model. The bifurcation analysis helped us to understand the mechanisms underlying the desynchronization which follows the initial phase reset after the auditory stimulus. As far as we are aware of, our model can show for the first time which bifurcations underlie the changes in the simulated brain dynamics.

We have, furthermore, seen that the mechanism of desynchronization is preserved if the model is extended from initially 2 to 3 regions to describe the neural activity in the thalamo-cortical loop. In this model, however, both parameter regions which correspond to data of schizophrenia patients and of healthy subjects are rather small (see little island in Figure 8). For the sake of simplicity and as a first approximation, we did not

include any direct couplings between the cortical regions. Preliminary results (simulation results not shown) suggest that the size of this parameter region will increase, if additional intra-cortical connections are included in the model, and the mechanisms of desynchronization will still be preserved. However, further investigations will be needed to gather firm evidence that supports the preliminary results.

Simulation results obtained with our model support the notion that schizophrenia is not caused by focal brain abnormalities, but results from pathological interactions between brain regions [28]. In contrast to other studies that found abnormal functional connectivity between temporal and frontal regions, as measured by PET and fMRI [29-31], our model hypothesizes that it is the feedback from the thalamus to the auditory cortex that causes the disabilities, even in the absense of direct coupling between cortical frequencies.

Of course, the validity of our model needs to be further tested by comparing the simulation results with experimental ones obtained in new measurements. The "disconnection hypothesis" suggests that the core pathology of schizophrenia is an impaired neuromodulation of synaptic plasticity that leads to abnormal functional integration of neural systems, i.e., "dysconnectivity" [32,33]. A possible next step would therefore be to investigate the influence of medications like eicosapentaenoic acid [34], pregnenolone [35,36] or antipsychotics [37] on the functional signal transduction by calculating individual SLIs from the EEG data or in a DCM study [38]. This would provide information on the coupling between the thalamus and the auditory cortex in schizophrenia patients. One could then compare whether a regeneration of functions can be linked to a restored connection strength between thalamus and cortex.

Moreover, EEG measurements on individual patients and the calculation of their individual coupling strength between the thalamus and the cortex could then be used as a tool to diagnostically classify the different types of schizophrenia. The advantage of this approach would be that the grouping of patients would not simply be driven by data but would be constrained by a well-founded and carefully specified theory.

In order to explain the experimental observations we consider in this paper a simple and plausible model which inherits properties of the coupling of the Kuramoto model. Despite the simplicity of the model, we observed good agreement between experimental data and numerical simulations. This justifies our chosen degree of approximation. Of course more sophisticated phase models including the nonresonance case [39,40] as well as detailed networks of the brain regions of interest could improve the quality of that results. Particularly, if we extended our model to include other brain regions with distinct natural frequencies, such as β- or γ-bands, we should definitely consider models that incorporate the nonresonance property.

Conclusion

Our model can explain functional differences seen between EEG records of healthy subjects and schizophrenia patients on a system theoretic basis. Because of this and its predictive character, the model may be considered to pave the way towards an early and reliable clinical detection of schizophrenia that is dependent on the interconnections between the thalamic and cortical regions. In particular, the model parameter that describes the strength of this connection can be used for a diagnostic classification of schizophrenia patients.

Appendix

Mathematical theory

In this section, we will present the main reduction methods that are used to analyze our systems in section "Mathematical model". The Pikovsky-Rosenblum ansatz [16] is an extension of the reduction method by Watanabe and Strogatz [14] which covers infinitely large systems of nonidentical phase oscillators. The general model treated in this theory reads:

$$\frac{d\phi(x,t)}{dt} = \omega(x,t) + \mathrm{Im}\left[H(x,t)e^{-i\phi}\right]. \tag{35}$$

The natural frequencies of the oscillators are denoted by $\omega(x,t)$. They depend on a continuous parameter x. The oscillators are coupled via a complex field $H(x,t)$. The state of the system can be described by the distribution density $W(x,\phi,t)$ which is determined by the distribution density of the parameter $n(x)$ and the conditional distribution density of oscillators $w(x,\phi,t)$, written as

$$W(x,\phi,t) = n(x)w(x,\phi,t).$$

According to the idea presented in [14], three new variables $\rho(x,t)$, $\Phi(x,t)$, $\Psi(x,t)$ and constants of motion $\psi(x)$ are introduced to the original system of equations via the transformation

$$e^{i\phi} = e^{i\Phi}\frac{\rho + e^{i(\psi-\Psi)}}{\rho e^{i(\psi-\Psi)} + 1}, \tag{36}$$

which transforms the time-dependent density $w(x,\phi,t)$ to a stationary density $\sigma(x,\psi)$ with the new variables $\Phi(x,t)$, $\Psi(x,t)$ and $\rho(x,t)$ which satisfy the following

$$\frac{\partial\rho(x,t)}{\partial t} = \frac{1-\rho^2}{2}\mathrm{Re}\left(H(x,t)e^{-i\Phi}\right), \tag{37}$$

$$\frac{\partial\Phi(x,t)}{\partial t} = \omega(x,t) + \frac{1+\rho^2}{2\rho}\mathrm{Im}\left(H(x,t)e^{-i\Phi}\right), \tag{38}$$

$$\frac{\partial\Psi(x,t)}{\partial t} = \frac{1-\rho^2}{2\rho}\mathrm{Im}\left(H(x,t)e^{-i\Phi}\right). \tag{39}$$

As three new variables are added to the system, additional constraints have to be defined to guarantee that the transformation (36) determines ρ, Φ, Ψ uniquely. These constraints are defined in [14,16] as follows:

$$\int_{-\pi}^{\pi}\sigma(\psi,x)e^{i\psi}d\psi = 0$$

and

$$Re\int_{-\pi}^{\pi}\sigma(\psi,x)e^{i2\psi}d\psi = 0.$$

In section "Mathematical model", we apply this ansatz to populations of oscillators with complex mean field coupling. It is therefore important to determine the order parameters of each subpopulation. In [16] it was shown that

$$Y = Re^{i\Theta} = \int n(x)Z(x)dx = \int n(x)\gamma(x)z(x)dx$$

holds. This simplifies further if the constants of motion are distributed uniformly in which case $\gamma(x) = 1$ (see [16]).

In [15,25] the same general model (35) is treated with a different ansatz. Their idea was to extend the density function $W(x, \phi, t)$ to a Fourier series:

$$W(x,\phi,t) = \frac{n(x)}{2\pi}\left\{1 + \left[\sum_{m=1}^{\infty} f_m(x,t)e^{-im\phi} + \text{c.c.}\right]\right\},$$

where *c.c.* denotes complex conjugate. Ott and Antonsen have shown that the continuity equation that expresses the conservation of the number of oscillators is fullfilled if the Fourier coefficients f_m can be written in terms of a single function F^m. This set of solutions is the so-called OA-manifold. Pikovsky and Rosenblum argued in [16] that the OA-manifold corresponds to the case of uniformly distributed constants of motion in the Watanabe-Strogatz Theory. Ott and Antonsen discussed in [25] that the OA-manifold is the only attractive region in terms of long-time evolution under the assumption that the parameter distribution $n(x)$ is continuous. This makes it possible to reduce the systems to the OA-manifold for purposes of a long-time analysis.

Competing interests
The authors declare that they have no competing interests.

Authors' contributions
Conceiving the research: NR, SP, SDG. Performance of numerical simulations: NR. Data analysis: NR, SP, SDG. Manuscript writing: NR, SP, SDG. All authors have read and approved the final mansucript.

Acknowledgements
We would like to thank Drs. T. Küpper, R. Müller and T.I. Toth for useful discussions in the course of the work.

Received: 3 September 2014 Accepted: 15 October 2014
Published: 18 October 2014

References

1. Liddle PF: **The symptoms of chronic schizophrenia. A re-examination of the positive-negative dichotomy.** *Br J Psychiatry* 1987, **151:**145–151.
2. Green MF: **What are the functional consequences of neurocognitive deficits in schizophrenia?** *Am J Psychiatry* 1996, **153:**321–330.
3. Mueser KT, McGurk SR: **Schizophrenia.** *Lancet* 2004, **363**(9426):2063–2072.
4. Carlsson A: **The neurochemical circuitry of schizophrenia.** *Pharmacopsychiatry* 2006, **39:**10–14.
5. an der Heiden U: **Schizophrenia as a dynamical disease.** *Pharmacopsychiatry* 2006, **39**(S1):36–42.
6. Mackey MC, an der Heiden U: **Dynamical diseases and bifurcations: understanding functional disorder in physiological systems.** *Funkt Biol Med* 1982, **1:**156–164.
7. Zendehrouh S, Bakouie F, Gharibzadeh S, Rostami A: **Mathematical modeling of schizophrenia.** *J Paramedical Sci* 2010, **1:**26–32.
8. Loh M, Rolls ET, Deco G: **A dynamical systems hypothesis of schizophrenia.** *PLoS Comput Biol* 2007, **3**(11):e228.
9. Rolls E, Loh M, Deco G, Winterer G: **Computational models of schizophrenia and dopamine modulation in the prefrontal cortex.** *Nat Rev Neurosci* 2008, **9:**696–709.
10. Brodersen K, Deserno L, Schlagenhauf F, Penny W, Buhmann J, Stephan K: **Dissecting psychiatric spectrum disorders by generative embedding.** *NeuroImage: Clinical* 2014, **4:**98–111.
11. Deserno L, Sterzer P, Wüstenberg T, Heinz A, Schlagenhauf F: **Reduced prefrontal-parietal effective connectivity and working memory deficits in schizophrenia.** *J Neurosci* 2012, **32:**12–20.
12. Brockhaus-Dumke A, Müller R, Faigle U, Klosterkötter J: **Sensory gating revisited: relation between brain oscillations and auditory evoked potentials in schizophrenia.** *Schizophr Res* 2008, **99:**238–249.
13. Popovych S, Küpper T, Müller R, Brockhaus-Dumke A: **Modelling disturbance in early sensory processing in schizophrenia.** *GAMM-Mitteilungen* 2009, **32:**93–104.
14. Watanabe S, Strogatz S: **Constants of motion for superconducting Josephson arrays.** *Physica D* 1994, **74:**197–253.
15. Ott E, Antonsen T: **Long time evolution of phase oscillator systems.** *Chaos* 2009, **19:**023117.
16. Pikovsky A, Rosenblum M: **Dynamics of heterogeneous oscillator ensembles in terms of collective variables.** *Physica D* 2011, **240:**872–881.
17. Potter D, Summerfelt A, Gold J, Buchanan RW: **Review of clinical correlates of P50 sensory gating abnormalities in patients with schizophrenia.** *Schizophr Bull* 2006, **32**(4):692–700.
18. Teplan M: **Fundamentals of EEG measurement.** *Meas Sci Rev* 2002, **2:**1–11.
19. Tass PA: **Stimulus-locked transient phase dynamics, synchronization and desynchronization of two oscillators.** *Europhys Lett* 2002, **59**(2):199.

20. Llinás R, Ribary U, Jeanmonod D, Kronberg E, Mitra P: **Thalamocortical dyrhythmia: a neurological and neuropsychiatric syndrome characterized by magnetoencephalography.** *PNAS* 1999, **96**(26):15222–15227.
21. Ferrarelli F, Tononi G: **The thalamic reticular nucleus and schizophrenia.** *Schizophr Bull* 2011, **37**(2):306–315.
22. McAlonan K, Brown VJ, Bowman EM: **Thalamic reticular nucleus activation reflects attentional gating during classical conditioning.** *J Neurosci* 2000, **20**(23):8897–8901.
23. Krause M, Hoffmann WE, Hajós M: **Auditory sensory gating in hippocampus and reticular thalamic neurons in anesthetized rats.** *Biol Psychiatry* 2003, **53**(3):244–253.
24. Pikovsky A, Rosenblum M: **Partially integrable dynamics of hierarchical populations of coupled oscillators.** *Phys Rev Lett* 2008, **101**(4):264103.
25. Ott E, Antonsen T: **Low dimensional behavior of large systems of globally coupled oscillators.** *Chaos* 2008, **18:**037113.
26. Kim DJ, Bolbecker AR, Howell J, Rass O, Sporns O, Hetrick WP, Breier A, O'Donnell BF: **Disturbed resting state EEG synchronization in bipolar disorder: a graph-theoretic analysis.** *NeuroImage: Clinical* 2013, **2:**414–423.
27. Pfurtscheller G, Pichler-Zalaudek K, Ortmayr B, Diez J, Reisecker F: **Postmovement beta synchronization in patients with Parkinson's Disease.** *J Clin Neurophysiol* 1998, **15**(3):243–250.
28. Stephan KE, Friston KJ, Frith CD: **Dysconnection in schizophrenia: from abnormal synaptic plasticity to failures of self-monitoring.** *Schizophr Bull* 2009, **35**(3):509–527.
29. Friston KJ, Frith CD, Fletcher P, Liddle PF, Frackowiak RS: **Functional topography: multidimensional scaling and functional connectivity in the brain.** *Cereb Cortex* 1996, **6:**156–164.
30. Lawrie SM, Buechel C, Whalley HC, Frith CD, Friston KJ, Johnstone EC: **Reduced frontotemporal functional connectivity in schizophrenia associated with auditory hallucinations.** *Biol Psychiatry* 2002, **51:**1008–1011.
31. Meyer-Lindenberg AS, Olsen RK, Kohn PD: **Regionally specific disturbance of dorsolateral prefrontal hippocampal functional connectivity in schizophrenia.** *Arch Gen Psychiatry* 2005, **62:**379–386.
32. Friston KJ: **Theoretical neurobiology and schizophrenia.** *Br Med Bull* 1996, **52:**644–655.
33. Friston KJ: **The disconnection hypothesis.** *Schizophr Res* 1998, **30:**115–125.
34. Peet M, Brind J, Ramchand CN, Shah S, Vankar GK: **Two double-blind placebo-controlled pilot studies of eicosapentaenoic acid in the treatment of schizophrenia.** *Schizophr Res* 2001, **49**(3):243–251.
35. Marx CE, Keefe RSE, Buchanan RW, Hamer RM, Kilts JD, Bradford DW, Strauss JL, Naylor JC, Payne VM, Lieberman JA, Savitz AJ, Leimone LA, Dunn L, Porcu P, Morrow AL, Shampine LJ: **Proof-of-concept trial with the neurosteroid pregnenolone targeting cognitive and negative symptoms in schizophrenia.** *Neuropsychopharmacology* 2009, **34**(8):1885–1903.
36. Ritsner MS, Gibel A, Shleifer T, Boguslavsky I, Zayed A, Maayan R, Weizman A, Lerner V: **Pregnenolone and dehydroepiandrosterone as an adjunctive treatment in schizophrenia and schizoaffective disorder: an 8-week, double-blind, randomized, controlled, 2-center, parallel-group trial.** *J Clin Psychiatry* 2010, **71**(10):1351–1362.
37. Carlsson A: **Antipsychotic drugs, neurotransmitters, and schizophrenia.** *Am J Psychiatry* 1978, **135**(2):164–173.
38. Friston K, Harrison L, Penny W: **Dynamic causal modelling.** *NeuroImage* 2003, **19:**1273–1302.
39. Komarov M, Pikovsky A: **Effects of nonresonant interaction in ensembles of phase oscillators.** *Phys Rev E* 2011, **84:**016210.
40. Komarov M, Pikovsky A: **Dynamics of multifrequency oscillator communities.** *Phys Rev Lett* 2003, **110:**134101.

doi:10.1186/1742-4682-11-45
Cite this article as: Rosjat *et al.*: A mathematical model of dysfunction of the thalamo-cortical loop in schizophrenia. *Theoretical Biology and Medical Modelling* 2014 **11**:45.

2.2 Investigating inter-segmental connections between thoracic ganglia in the stick insect by means of experimental and simulated phase response curves

Tibor Istvan Tóth, Martyna Grabowska, Nils Rosjat, Katja Hellekes, Anke Borgmann, Silvia Daun-Gruhn

Published in Biological Cybernetics (109:349–362,2015)

Author Contributions

Conceived the research
Tibor Istvan Tóth, Nils Rosjat
Martyna Grabowska, Katja Hellekes
Anke Borgmann, Silvia Daun-Gruhn

Performed the experiments
Martyna Grabowska, Anke Borgmann
Katja Hellekes

Performed the simulations
Tibor Istvan Tóth, Nils Rosjat

Analyzed the data
Tibor Istvan Tóth, Nils Rosjat
Anke Borgmann, Silvia Daun-Gruhn

Figure Preparation
Tibor Istvan Tóth, Nils Rosjat

First version of manuscript
Tibor Istvan Tóth

Wrote the paper
Tibor Istvan Tóth, Nils Rosjat
Silvia Daun-Gruhn

Biol Cybern (2015) 109:349–362
DOI 10.1007/s00422-015-0647-5

ORIGINAL PAPER

Biological Cybernetics

Investigating inter-segmental connections between thoracic ganglia in the stick insect by means of experimental and simulated phase response curves

Tibor I. Tóth · Martyna Grabowska · Nils Rosjat · Katja Hellekes · Anke Borgmann · Silvia Daun-Gruhn

Received: 9 July 2014 / Accepted: 6 February 2015 / Published online: 25 February 2015

Abstract The neuronal networks that control the motion of the individual legs in insects, in particular in the stick insect, are located in the pro-, meso- and meta-thoracic ganglia. They ensure high flexibility of movement control. Thus, the legs can move in an apparently independent way, e.g., during search movements, but also in tight coordination during locomotion. The latter is evidently a very important behavioural mode. It has, therefore, inspired a large number of studies, all aiming at uncovering the nature of the inter-leg coordination. One of the basic questions has been as to how the individual control networks in the three thoracic ganglia are connected to each other. One way to study this problem is to use phase response curves. They can reveal properties of the coupling between oscillatory systems, such as the central pattern generators in the control networks in the thoracic ganglia. In this paper, we report results that we have achieved by means of a combined experimental and modelling approach. We have calculated phase response curves from data obtained in as yet unpublished experiments as well as from those in previously published ones. By using models of the connected pro- and meso-thoracic control networks of the protractor and retractor neuromuscular systems, we have also produced simulated phase response curves and compared them with the experimental ones. In this way, we could gain important information of the nature of the connections between the aforementioned control networks. Specifically, we have found that connections from both the protractor and the retractor "sides" of the pro-thoracic network to the meso-thoracic one are necessary for producing phase response curves that show close similarity to the experimental ones. Furthermore, the strength of the excitatory connections has been proven to be crucial, while the inhibitory connections have essentially been irrelevant. We, thus, suggest that this type of connection might also be present in the stick insect, and possibly in other insect species.

Keywords Phase response curves · Network model · Peripheral stimulation · Inter-segmental coordination · Stick insect

T. I. Tóth · M. Grabowska · N. Rosjat · S. Daun-Gruhn ( )
Heisenberg Research Group of Computational Biology, Department of Animal Physiology, Institute of Zoology, University of Cologne, Zülpicher Str. 47b, 50674, Cologne, Germany
e-mail: sgruhn@uni-koeln.de

K. Hellekes · A. Borgmann
Department of Animal Physiology, Institute of Zoology, University of Cologne, Cologne, Germany

K. Hellekes
Present address:
Research Institute of Molecular Pathology, Vienna, Austria

1 Introduction

The three thoracic ganglia: the pro-, meso- and meta-thoracic in insects, and in the stick insect in particular, contain the neuronal apparatuses that control the motion of the individual legs of the animal. The thoracic control mechanisms enjoy, on the one hand, considerable functional autonomy, that is, they are capable of moving the individual legs in an apparently independent way during search movements, on the other hand, their activity is precisely coordinated during normal locomotion, i.e., walking. This hints at a complex and flexible control mechanism of the leg movements in these animals that is capable of bringing about tight inter-leg coordination by suitable synaptic connections between the segmental neuronal control networks. It comes, therefore, as no surprise that the nature, the structure, and mechanisms of the inter-leg coordination have been the subject of a number

of studies on a variety of insects (Hughes 1952; Wilson 1966; Delcomyn 1971, 1981; Pearson and Franklin 1984; Graham 1985; Laurent and Burrows 1989a,b; Cruse et al. 1990, 2009; Ritzmann and Büschges 2007), and on the stick insect, in particular (e.g., Graham 1972; Ludwar et al. 2005; Borgmann et al. 2007, 2009, 2011; Grabowska 2012). These studies dealt with various aspects of the inter-segmental coordination during locomotion: some of them were behavioural studies (e.g., Hughes 1952; Wilson 1966; Graham 1972, 1985; Cruse et al. 1990; Grabowska 2012), while others (e.g., Laurent and Burrows 1989a,b; Ludwar et al. 2005; Borgmann et al. 2007, 2009, 2011) used electrophysiological techniques. The latter techniques are suitable to uncover the elementary mechanisms that underlie inter-segmental coordination, and ultimately locomotion (normal walking) itself. A further advantage of these techniques is that they can reveal structure and function of small local neuronal networks that take part in the coordination processes, and by that, they lend themselves to mathematical modelling of their functions.

This is exactly the kind of approach that we employ in this study in order to help advance our understanding in this field. Specifically, we want to find out more about the nature of the inter-segmental neuronal connections descending from the pro-thoracic ganglion to the meso- and meta-thoracic ganglions. To this end, we make use of phase response curves (PRCs). PRCs are an effective means for uncovering properties of coupled oscillatory systems (e.g., Winfree 2000; Schultheiss et al. 2012). In this paper, we thus report on the analysis and simulation of PRCs and their role in uncovering properties of the underlying inter-segmental coordination. The simulated PRCs obtained from two different models were compared to experimental PRCs from as yet unpublished and from earlier experiments (Borgmann et al. 2009), while varying the type and strength of synaptic connections from the pro-thoracic protractor–retractor central pattern generator (CPG) to the meso-thoracic one. We found close similarity between these experimental PRCs and the simulated ones obtained from the CPG activities at a strong excitatory synaptic connection on the "protractor side" and a moderate one on "the retractor side." We thus suggest that connections of similar nature might also be present in the stick insect's local neuronal networks that control muscle activity.

2 Materials and methods

We first provide a summary of the experimental procedures, and then we will treat the inter-segmental model.

2.1 Short description of the experiments

The experiments to be described here consist of three groups. One of them comprises experiments that were performed and published earlier (Borgmann et al. 2007, 2009). The other two groups contain as yet unpublished experiments. The basic experimental procedures are the same for both groups. Their description can be found elsewhere (Akay et al. 2007; Borgmann et al. 2007, 2009, 2011). Here, we present the procedures that were applied in the hitherto unpublished experiments. In both groups of them, all legs of a stick insect but the front right one were amputated at mid-coxa. In the first group of experiments, the front leg was cut at the middle of the femur. The femur was then shaved with a scalpel blade in order to remove the sensory hairs. By the removal of the tibia, the femoral chordotonal organ (fCO) was, of course, also rendered ineffective. Then 5×10^{-4} M pilocarpine was administered to the meso-thoracic ganglion alone (split-bath preparation, Borgmann et al. (2009)) in order to elicit (nearly) periodic oscillation in the CPGs of the meso-thoracic ganglion. The campaniform sensilla (CS) of the front leg were then directly stimulated while the meso-thoracic CPG was oscillating. The stimulation technique applied was the same as in Akay et al. (2007). An increase of load on the leg was mimicked by bending the femur against the fixed coxa joint from anterior to posterior using a piezo-electric device. The time course of the stimulus was a ramp function of constant duration and amplitude having a very fast rising phase (as indicated in Fig. 1a). It was applied at different phases of the pilocarpine-induced periodic oscillation of the meso-thoracic protractor–retractor CPG. The oscillatory activity was extracellularly recorded from the meso-thoracic protractor motoneurones (MNs). In particular, the length T until the next MN activity after the stimulus was measured and related to the average period length T_{p0} as follows:

$$\phi = \frac{d}{T_{p0}} \tag{1}$$

$$\Delta\phi = \frac{T - T_{p0}}{T_{p0}} \tag{2}$$

Thus, the PRC was created as a function $\Delta\phi$ of the phase ϕ of the stimulus timing (see also Fig. 1a). The average period T_{p0} was calculated as the average of at least three periods (denoted T_p in Fig. 1a) immediately preceding the stimulus. d is the time interval from the start of an oscillatory period (start of a protractor burst) to the application of the stimulus (cf. Fig. 1a). These experiments were performed on five animals. Since not all phases (ϕ) could be obtained in a single experiment, the $\phi - \Delta\phi$ data from all (successful) experiments on five animals were pooled to a single data set in order to construct a PRC with as many phase points (ϕ) as possible. The resulting PRC is shown in Fig. 1b.

In the second group of hitherto unpublished experiments, the left front leg was intact and was placed on a tread wheel. The wheel was moved backwards in order to force forward stepping of the leg. The movement of the leg was started

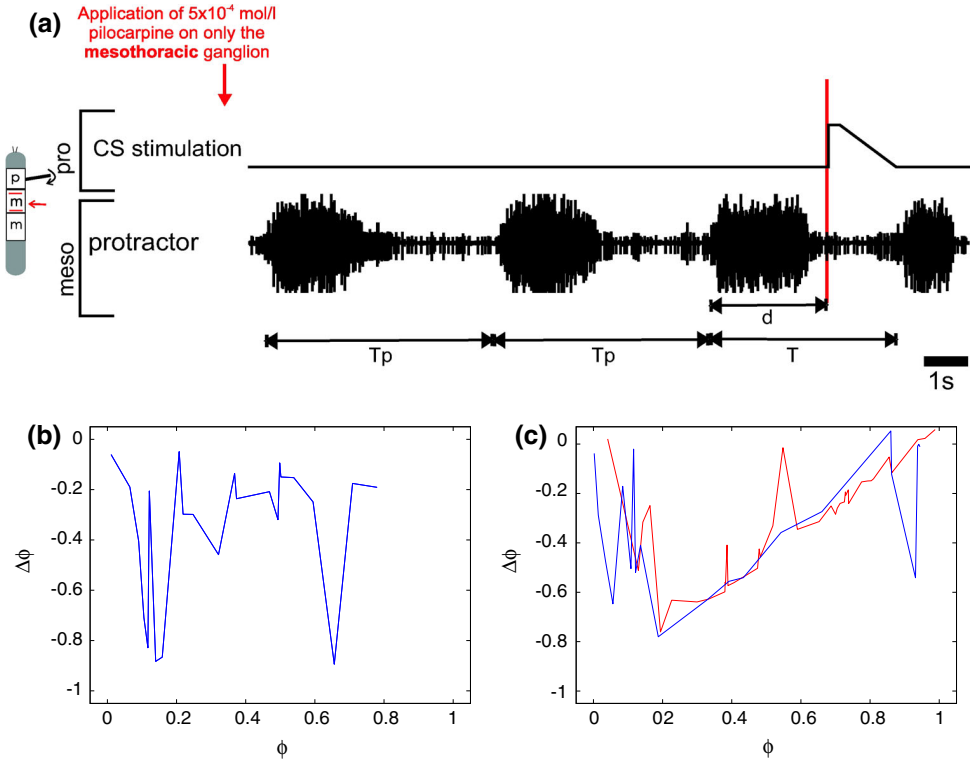

Fig. 1 Experimental records from the meso-thoracic protractor MNs. **a** Administration of pilocarpine to the meso-thoracic ganglion as indicated at the top of the panel. Note the time quantities T and T_p and their relations to $\Delta\phi$ the phase-shift induced by the stimulus. d is the time elapsed between the start of an oscillatory period and the application of the stimulus. **b** Phase response curve obtained with stimulation of the femoral campaniform sensilla; **c** phase response curves obtained during forced (*red curve*) and free (*blue curve*) front leg stepping. (The latter is adapted from Borgmann et al. (2009), their Fig. 2C, with permission). Note also that the period (T_p) in panel (**a**) is normalized to one in panels (**b**) and (**c**). In these experiments, $T_p \approx 7.5$ s and $T_p \approx 6.2$ s for the forced and free stepping, respectively (colour figure online)

at different phases (ϕ) of the pilocarpine-induced oscillation of the protractor–retractor CPG in the meso-thoracic ganglion. This process ensured a nearly natural and simultaneous stimulation of CS, the hair fields, and the fCO (Bässler 1977, 1983; Büschges and Gruhn 2008; Schmitz 1986a,b). The $\Delta\phi$ values of the PRC were produced from the experimental data the same way as in the preceding case. The PRC was then constructed by pooling the phase points obtained from five animals. The resulting PRC is the red curve in Fig. 1c.

In the experiments that were published earlier in Borgmann et al. (2009) front-leg stepping of the animals was monitored on a passive treadmill. Only spontaneous front leg stepping sequences were taken into account in order to be free of effects that abdominal stimulation with a paint brush may cause. Here, too, CS, the hair fields, and the fCO were, thus, stimulated in a natural way (Bässler 1977, 1983; Büschges and Gruhn 2008; Schmitz 1986a,b). The stepping coincidentally occurred at different phases of the oscillatory period, and again the PRC was constructed by pooling the phase data from five animals the same way as in the hitherto unpublished experiments. The resulting PRC is the blue curve in Fig. 1c. Both PRCs in Fig. 1c are rather erratic in the range $0 \leq \phi < 0.2$. The reason for this we shall explain in detail in the Results.

Thus, the experimental PRCs should be deemed to be unreliable in this range of ϕ (cf. Fig. 1c).

2.2 Network models used in the simulations

We used two types of models in the simulations: one "skeleton" model comprising only the protractor–retractor CPGs of the pro- and meso-thoracic ganglia and the excitatory and inhibitory synaptic pathways between the two CPGs (Fig. 2); and a model obtained by extending a detailed 1-leg model of the stick insect (Knops et al. 2013). In the "skeleton" model, both excitatory and inhibitory synaptic pathways run ipsilaterally from the pro-thoracic CPG to the meso-thoracic one. Moreover, these pathways are present both on the "protractor side" and the "retractor side", as indicated in Fig. 2. There is, however, no specific sensory input to the CPGs. With this simple model, we aimed at finding out whether a direct excitatory stimulus alone can give rise to PRCs similar to those constructed from the experimental data. In this model, the stimulus currents I_{sr} and I_{sp} were, thus, directly applied to

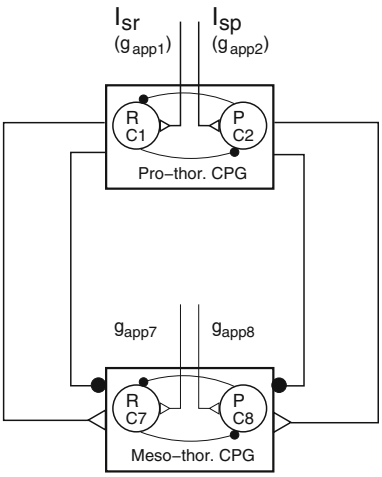

Fig. 2 The "skeleton" model consisting only of the pro-thoracic and meso-thoracic protractor–retractor CPGs (as indicated), and the excitatory and inhibitory synaptic pathways from the former CPG to the latter. Here, *R* stands for retractor and *P* for protractor; furthermore, *Pro-thor.* for pro-thoracic, and *Meso-thor.* for meso-thoracic. The numbering C1, C2, C7, and C8 of the CPG neurons was done for reasons of consistency with the extended 1-leg model, which will be introduced below. I_{sr} and I_{sp} are the stimulus currents to the retractor and the protractor neuron of the pro-thoracic CPG, respectively. The conductances of the (central) drives to the CPG neurons (g_{app1} etc.) are also given for the sake of consistency with the 1-leg model. The parentheses around g_{app1} and g_{app2} indicate that the stimulus current to the CPG neurons C1 and C2 was applied directly and not by changing the value of g_{app1} or g_{app2}. The empty triangles on the meso-thoracic CPG denote excitatory synapses, the filled circles are inhibitory synapses whose pathways originate at the pro-thoracic CPG

the retractor or the protractor neuron of the pro-thoracic ganglion on top of the "normal" excitation, which ensured the oscillatory behaviour of the CPGs. The simulated PRC was calculated from the activity of the protractor neuron of the meso-thoracic CPG.

The 1-leg model represents the intact front leg of the stick insect in the aforementioned experiments and is basically the model in Knops et al. (2013). This model is then complemented by adding a local control network to play the role of the meso-thoracic protractor–retractor local control network. It receives both excitatory and inhibitory synaptic connections from its pro-thoracic counterpart (Fig. 3). This arrangement corresponds in essence to the experimental conditions, where all legs, except one front leg, are amputated. Also, the local control networks in the meta-thoracic ganglion played no role in the experimental investigations. They were, therefore, completely omitted from the models used in present study.

In more detail, the extended network model in Fig. 3 contains the three main neuro-muscular systems and their interconnections in the intact front leg (pro-thoracic level): the protractor–rectractor (PR), the levator–depressor (LD), and the extensor–flexor (EF) system.

There is, however, a difference to the model in Knops et al. (2013). In contrast to it, in the present version of the leg-model, the (lumped) position signal γ (in a hexagon in Fig. 3) contributes to the excitation of the LD system. This excitatory connection, together with the excitatory effect of the β signal on the CPG of the EF system (cf. Fig. 3) can bring about the autonomous stepping movements in the intact leg. At the same time, the β signal represents the peripheral sensory signals to the PR system. It thus replaces the abstract sensory signals and their gating in the abstract sensory neurons in the model by Daun-Gruhn and Toth (2011). The intra-EF effect of γ is omitted here, because it was found much weaker in the simulations than the inter-joint effect of γ just described.

Since all other legs were amputated, none of the LD and EF systems of the other legs appear in the models used in this study. Hence, no sensory inputs are effective at the meso- and meta-thoracic levels, in contrast to the inter-segmental model in Daun-Gruhn and Toth (2011). Even the EF system of the front leg is unnecessary for the simulations. The oblique lines in Fig. 3 indicate that the latter sub-system is severed from the LD system. Hence, it could have been omitted, as in Fig. 6. We, nevertheless, kept it in Fig. 3 in order to illustrate the model of an intact leg. The PR system of the middle leg (meso-thoracic level) was, however, added since the aim of the present study was to uncover possible connections from the pro- to the meso-thoracic PR system. As far as the meta-thoracic level is concerned, the PR system of the hind leg remained in the experiments formally intact but played no part, directly or indirectly, in the experiments. It was, therefore, not incorporated into the model used here.

The model in Fig. 3 is built from several topologically similar units (e.g., PR control network). These units or sub-systems consist of a local neuronal network controlling the activity of an antagonistic muscle pair. The properties of one such sub-system arise mainly from direct or indirect experimental evidence and to some extent from physiologically reasonable assumptions. A detailed description of the experimental evidence and the assumptions can be found in Borgmann et al. (2011), Daun-Gruhn and Toth (2011), Daun-Gruhn et al. (2011), Toth and Daun-Gruhn (2011), Toth et al. (2012), and Knops et al. (2013). One of the main properties based on experimental findings is that the MNs do not receive a direct excitatory drive from the CPG but inhibition (Büschges 1995) presumably via inhibitory (non-spiking) interneurons (Büschges 1998). However, central excitatory signals do act on them uniformly (Westmark et al. 2009). The topology of the local networks faithfully mirrors this finding. In addition, the presence of a layer of pre-motor inhibitory interneurons (IN1 etc.) increases the flexibility of the local networks in controlling the activity of the attached antagonistic muscle pair. The activity of the CPGs is governed by, presumably central, inputs denoted as g_{app1} etc., where g_{app1} etc. are the conductances of the excitatory input currents to

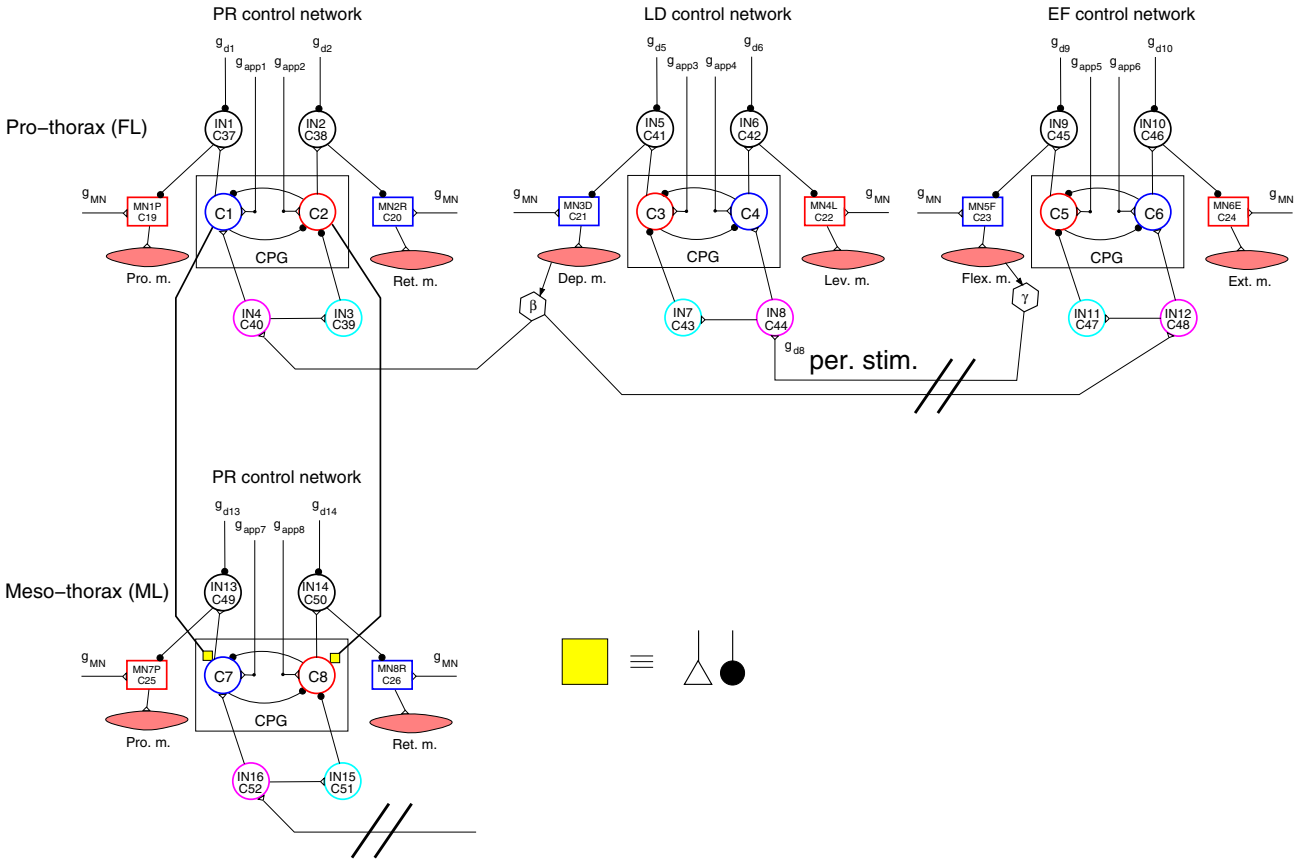

Fig. 3 The extended neuromuscular model used in the simulations. The pro-thoracic segment (front leg) is intact, i.e., it contains, beside the protractor–retractor local neuronal network and muscles, both the complete levator–depressor and extensor–flexor neuromuscular sub-systems. At the meso-thoracic segment, only the protractor–retractor sub-system is present in analogy to the amputation of the middle leg. The three sub-systems at the meta-thoracic level are omitted altogether, since they are considered to be irrelevant for purposes of mimicking the experimental arrangements. In the (extended) neuromuscular model, each local neuronal network (PR control network etc.) controls the activity of an antagonistic muscle pair (Pro. m–Ret. m etc.). Parts of a local neuronal network: CPG consisting of two, mutually inhibitory neurones (C1–C2 etc.), as indicated; two pre-motor inhibitory interneurones (IN1, IN2 etc.), two modulatory interneurons (IN3, IN4 etc.), and two motoneurons [MN(P), MN(R) etc.]. *Empty triangles* on neurons: excitatory synapses; *filled circles* on neurons: inhibitory synapses; *filled yellow squares* on neurons C7 and C8: separate excitatory and inhibitory synapses lumped together for the sake of simplicity. The insert on the *right hand side* indicates this fact. Their paths originate in the CPG neurons C1 and C2, respectively. Hexagons with β and γ written in them: sources of afferent signals encoded in the levation angle β and the femur-tibia angle γ, respectively. $g_{\mathrm{app}1}$, $g_{\mathrm{app}2}$ etc.: conductances of the (central) excitatory inputs to the CPG neurones; g_{d1}, g_{d2} etc.: conductances of the (central) inhibitory inputs to the inhibitory pre-motor neurons; g_{MN}: conductance of the central excitatory input to all motoneurons. *Thick oblique double lines* synaptic connection is cut. Further *abbreviations*: *FL* front leg, *ML* middle leg, *PR* protractor–retractor, *LD* levator–depressor, *EF* extensor–flexor, *per. stim.* site of the peripheral stimulation. Note that for technical reasons, the neurons have also been numbered consecutively. For a more detailed explanation, see text

the CPG neurones, and by the excitatory and inhibitory outputs of the "modulatory" interneurons. For example, IN3 and IN4 are such modulatory neurons in the pro-thoracic PR control network (Fig. 3). The modulatory interneurons are, in turn, driven by sensory signals that encode load and position (touch-down of the tarsus). In the model, these signals are represented by the levation angle β and the angle at the femur-tibia joint γ (and their critical values for signalizing, for example, touch-down) (Fig. 3).

In modelling the neuro-muscular coupling, each action potential of a MN contributes to the contraction of the attached muscle. In this way, co-contractions of an antagonistic muscle pair could easily be mimicked. A detailed explanation of the model of the neuromuscular coupling is in Toth et al. (2012). The muscle model is, in essence, a simplified and linearized Hill model (Hill 1953). It takes the specific geometry at each leg joint into account. The form of the equations of mechanical motion is, therefore, different at each leg joint. However, at each joint, the (velocity-dependent) torque generated by the viscosity during muscle contraction is one component of the total torque developed (cf. Toth et al. 2012; Knops et al. 2013).

We used simple Hodgkin–Huxley-type neuron models (Hodgkin and Huxley 1952) in constructing the models of the local networks. All model neurons, except for the MNs, were non-spiking ones containing only one voltage-gated current,which was a slowly inactivating sodium current I_{NaP} with instantaneous activation kinetics (Daun et al. 2009; Daun-Gruhn and Toth 2011). The model of the MNs admitted the usual Na–K action potentials and, in addition, adaptation of the firing frequency (Daun-Gruhn and Toth 2011). For emulating the synaptic activity, a simple model was used in which the synaptic activation was described by a sigmoid (Boltzmann-) function of the presynaptic potential (Daun-Gruhn and Toth 2011).

The inter-segmental coupling from the pro-thoracic to the meso-thoracic CPG consisted of both excitatory and inhibitory synaptic pathways from the pro-thoracic to the meso-thoracic CPG. (These synapses are represented, lumped together, by yellow squares on the CPG neurons C7 and C8 in Fig. 3). Moreover, the pathways were bilateral, i.e., connecting the protractor neuron of the pro-thoracic CPG to that of the meso-thoracic CPG, and similarly, the retractor neuron of the pro-thoracic CPG to that of the meso-thoracic CPG (pathways: bold lines from C1 to C7 and from C2 to C8, respectively, as shown in Fig. 3). The direction of the connection reflects experimental findings (Borgmann et al. 2007, 2009). Note that both the CPGs of the PR systems and the type of connection between them were the same in the "skeleton" model (Fig. 2) and in the extended 1-leg model (Fig. 3).

The site of peripheral stimulation in the model was assigned to the input of the modulatory interneuron IN8 of the LD neuromuscular sub-system, as indicated in Fig. 3. Cutting the sensory pathways of the γ signal from the EF sub-system to IN8 (indicated by oblique double lines in Fig. 3), the latter became an input site of the model. Then, varying the value of the conductance g_{d8} of the input current, we could mimic the experimental stimuli in the model. It is important to bear in mind that, in the model, peripheral stimulation at the IN8, as indicated in Fig. 3 always induces mechanical movement in the LD neuromuscular system. Selective CS stimulation is, therefore, not possible in the model. It is more appropriate to assume that the simulated PRCs better correspond to the experimental ones that were obtained during front leg stepping, especially forced front leg stepping of the stick insect. This point will become important when the synaptic connections from the pro-thoracic CPG to the meso-thoracic one depend on signals from sense organs responding to (angular) velocity.

The model was implemented in the form of a computer program written in the programming language C and was run under the Linux operating system. The program contains the numerical values of all system parameters. It is freely available from the authors on request.

3 Results

3.1 Experimental phase response curves

Figure 1 shows the PRCs obtained in the experiments: one, by directly stimulating CS of the front leg alone (Fig. 1b), and two, when the stimulus was produced by free or forced front leg stepping (blue and red curve in Fig. 1c, respectively). (Note that the blue PRC in Fig. 1c was previously published in Borgmann et al. (2009): their Fig. 2C). The PRC in Fig. 1b exhibits apparently little regularity. Perhaps, a weak linear trend may be discerned in the interval $0.2 \leq \phi \leq 0.6$.

The experimental PRCs obtained during free or forced stepping of the intact front leg look quite similar (Fig. 1c). In contrast to the PRC in Fig. 1b, there is a large interval of ϕ ($[0.2, 0.8]$) in which they behave linearly. Moreover, the slopes of these linear segments are approximately equal (1.05 and 0.95 for the blue and the red PRC, respectively). The similarity between them might not be very surprising, since both of them were produced from data during front leg stepping. That is, in both cases not only the CS but also the hair fields and the fCO were simultaneously stimulated. The difference between them is that during forced stepping the start of a step can more accurately be controlled.

As for the differences between the PRC in Fig. 1b and the PRCs in Fig. 1c, we think that direct CS stimulation alone fails to produce sufficient sensory input in the first group of hitherto unpublished experiments, in order to produce PRCs with a high enough signal to noise ratio. By contrast, in the experiments in which the stimulation evoked multimodal sensory input by making the front leg step, sufficient sensory input was provided to produce PRCs with clear deterministic trends. All three PRCs display erratic behaviour in the interval [0.0, 0.2]. This hints at a common origin in all measurements. In measurements at small phase (ϕ) values, the stimulus can start during a discharge of the protractor MNs. Thus, the stimulus directly interferes with the MN activity. This interference is strongly nonlinear; hence, it can lead to large uncertainties as to the starting point of the next MN burst. The phase shift $\Delta\phi$ can, therefore, be subject to large deviations. Indeed, all three PRCs show such large deviations for small phases ($\phi \leq 0.2$) (cf. Fig. 1b, c). We think that the suspected weak linearity in the PRC in Fig. 1b is a sign of the CS-induced excitation in the protractor MNs. However, this effect is rather weak, since CS stimulation alone is insufficient to produce the clear phase relationship in that PRC. For this reason, we did not pursue a comparison of this experimental PRC obtained with direct CS stimulation with the simulation results. Nevertheless, these data proved useful in showing the differences between experimental PRCs that were obtained in different experimental conditions.

3.2 Simulated phase response curves obtained with the "skeleton" model

The so-called "skeleton" model comprised only the pro- and meso-thoracic protractor–retractor CPGs with excitatory and inhibitory synaptic pathways from the pro-thoracic to the meso-thoracic CPG on both the "retractor" and the "protractor side" (Fig. 2). Both the pro- and meso-thoracic CPG were autonomously oscillating due to setting the values of the conductances g_{app1}, g_{app2}, g_{app7} and g_{app8} of the central drive to the CPG neurons C1, C2, C7, and C8 to suitable values ($g_{\mathrm{app1}} = g_{\mathrm{app7}} = 0.1925\,\mathrm{nS}$, $g_{\mathrm{app2}} = g_{\mathrm{app8}} = 0.1875\,\mathrm{nS}$). Although the period of the oscillations was much shorter than that in the experiments ($T_{\mathrm{per}} \approx 124$ ms), the relation of roughly 1:3 between protractor and retractor phase was preserved.

The system received direct stimuli to the neurons of the pro-thoracic CPG. When a stimulus of $I_{\mathrm{sr}} = 3$ nA was applied, in addition to the driving currents I_{app1} and I_{app2}, on the "retractor side" and no stimulus was applied to the "protractor side", we obtained PRCs quite similar to the experimental one. Other combinations of stimuli (e.g., I_{sp} alone or I_{sp} and I_{sr}) did not yield acceptable results.

Similarity of PRCs was judged by the presence and coincidence of linear parts of both PRCs. More precisely, we regarded a simulated PRC to be in satisfactory agreement with, or similar to, the experimental one, if the linear parts of both PRCs started nearly at the same phase ϕ, they were approximately of the same length, and their slope was also nearly of the same value (≈ 1.0).

For the resulting PRC in Fig. 4, the following synaptic strengths (conductances) were used: $g_{\mathrm{s,e}}(7, 1) = 0.17\,\mathrm{nS}$, $g_{\mathrm{s,i}}(7, 1) = 0.1\,\mathrm{nS}$, $g_{\mathrm{s,e}}(8, 2) = 0.17\,\mathrm{nS}$, $g_{\mathrm{s,i}}(8, 2) = 0.1$ nS. Here, $g_{\mathrm{s,x}}(k, j)$ denotes the synaptic conductance from neuron j to neuron k, and $x = e$ means excitatory, $x = i$ inhibitory synapse. We used the same numbering of the CPG neurons as in the extended 1-leg model for the sake of comparability (cf. Fig. 3). However, other symmetric combinations of the conductance values were also possible in order to obtain satisfactory simulated PRCs. The range for $g_{\mathrm{s,e}}(7, 1)$ and $g_{\mathrm{s,e}}(8, 2)$ was found to be $[0.1, 0.18]\,\mathrm{nS}$, and a somewhat larger range $[0.02, 0.2]\,\mathrm{nS}$ for $g_{\mathrm{s,i}}(7, 1)$ and $g_{\mathrm{s,i}}(8, 2)$. Thus, excitatory connections were necessary to produce PRCs that were similar to the experimental one, whereas even weak inhibitory connections sufficed to get such results. When the synaptic conductances fell into the above ranges, the simulated PRC showed fairly good agreement with the experimental one, especially in its linear part (Fig. 4).

Asymmetric value combinations of the synaptic conductances, that is, when the conductance values on the "protractor side" differed from those on the "retractor side", were also tested. Choosing the conductance values 0.17, 0.1, 0.05 and 0 nS that are to represent strong, moderate, weak and no synaptic connection, respectively, we found four cases with satisfactory agreement between experimental and simulated PRC. In all such cases, the excitatory connection on the "protractor side" ($g_{\mathrm{s,e}}(8, 2)$) was strong. The excitatory connection on the "retractor side" ($g_{\mathrm{s,e}}(7, 1)$) was in three cases of moderate strength, and weak in one case. The inhibitory connection on the "protractor side" ($g_{\mathrm{s,i}}(8, 2)$) was moderate in three cases and strong in one, while the inhibitory connection on the "retractor side" ($g_{\mathrm{s,i}}(7, 1)$) was zero (no connection) in two cases, and of moderate strength in the other two. From this, it can be seen that a strong excitatory connection on the "protractor side" and, essentially, a moderate excitatory connection on the "retractor side" are necessary for a satisfactory simulation result. The same is true for the inhibitory connection on the "protractor side", while the presence of the inhibitory connection on the "retractor side" is, at certain value combinations of the conductances of the other connections, not required.

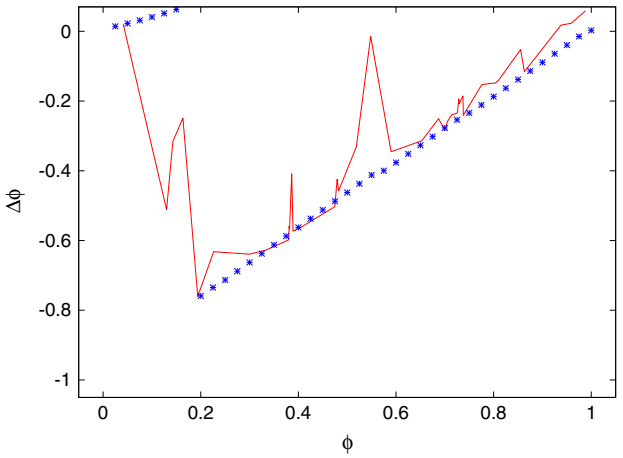

Fig. 4 Simulated phase response curve (*blue points*) obtained with the "skeleton" model, and its comparison with the experimental one: forced front leg stepping (*red continuous line*). Note the similarity in the linear parts of the two curves (colour figure online)

3.3 Simulated phase response curves obtained with the extended 1-leg model

We carried out simulations with a variety of synaptic strengths, expressed by the synaptic conductances of the excitatory and inhibitory synapses on the CPG neurons C7 and C8 (cf. Fig. 3). We found in preliminary simulations that $g_{\mathrm{syn}} = 0.01\,\mathrm{nS}$ proved to be a weak connection, $g_{\mathrm{syn}} = 0.04\,\mathrm{nS}$ an intermediate, and $g_{\mathrm{syn}} = 0.1\,\mathrm{nS}$ a strong one for both excitatory and inhibitory synapses on C7 and C8. The latter synaptic strength proved to be so strong for the excitatory synapse on C7 ("retractor" CPG neurone) that, when applied, the oscillatory behaviour of the meso-thoracic CPG (C7–C8) was abolished regardless of the value of the

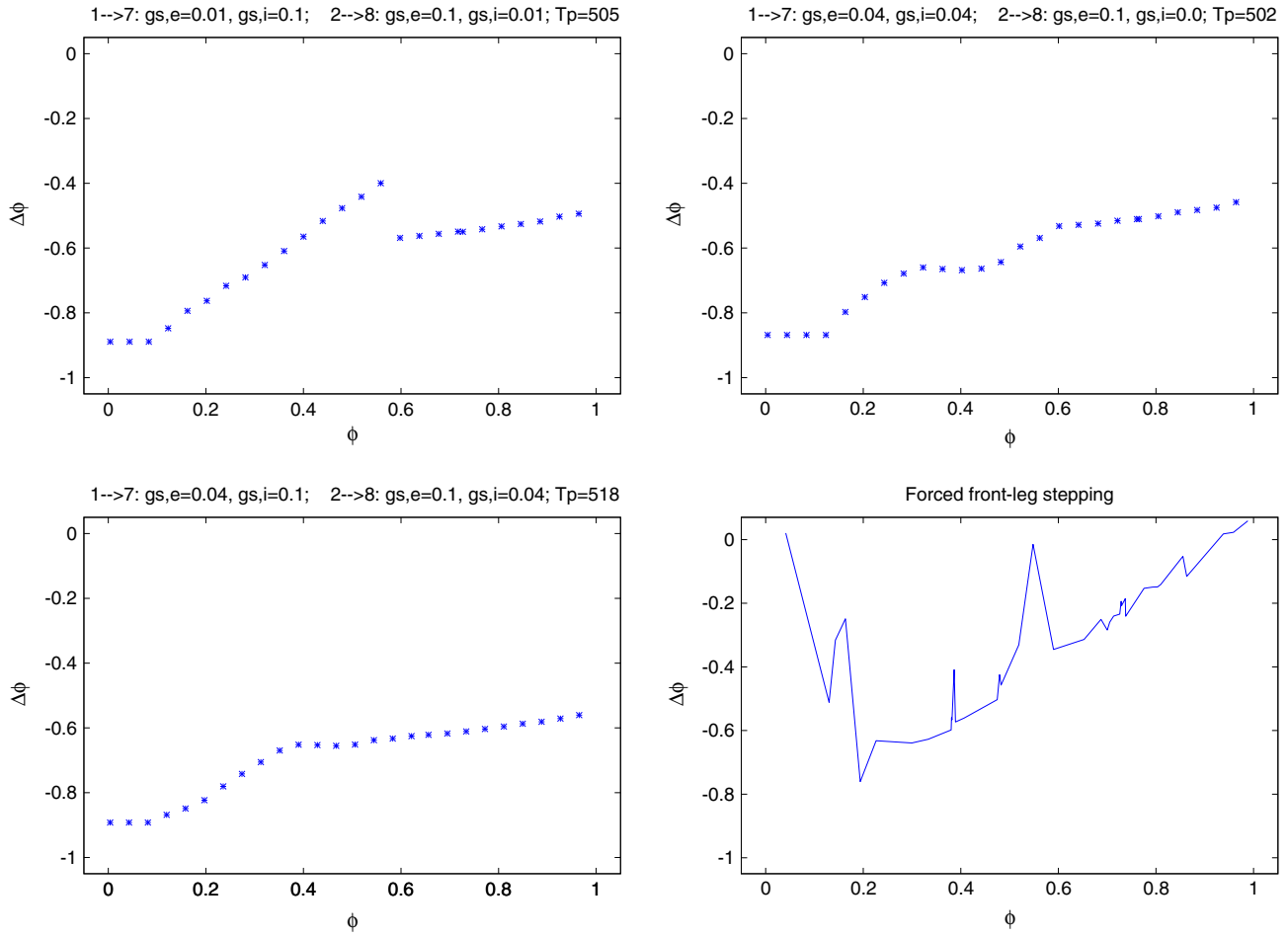

Fig. 5 Simulated phase response *curves* for three sets of synaptic connection strengths from the pro-thoracic to the meso-thoracic CPG, as indicated above the individual panels. The panel at the *bottom right* is the experimental phase response curve obtained with forced front leg stepping. 1 → 7 above the panels showing simulation results means synaptic connection from neuron C1–C7; 2 → 8 has an analogous meaning; $g_{s,e}$ stands for the conductance of excitatory synapse, $g_{s,i}$ for that of inhibitory one. T_p means the actual period in the meso-thoracic CPG. In the experiments, the period was about 7.5 s. The simulated phase response curves are only vaguely similar to the experimental one. For further explanations, see text

other synaptic conductances (not illustrated). This value for the excitatory synapse on C7 was, therefore, excluded from the subsequent simulation trials.

Furthermore, we found that the value combination of the synaptic strengths on the "protractor side", i.e., from C2 to C8, strongly affected the length of the oscillatory period in the meso-thoracic CPG (C7–C8) even in the absence of ramp stimulation at interneuron IN8 peripheral stimulation). Note that in the absence of stimuli at interneuron IN8, the "protractor" CPG neurone C2 remained in the depolarized state; hence, its counterpart C1 was permanently kept at rest, thus, no excitatory or inhibitory synaptic signal could be transmitted on the "retractor side", i.e., from C1 to C7 (cf. Fig. 3). With no synaptic connection, the period in the meso-thoracic CPG was 1173 ms, which was reduced to 502 ms, when the excitatory connection $g_{\mathrm{syn,e}}(8, 2)$ was increased to 0.1 nS. Other values of this synaptic conductance yielded periods between these values, but it is worth mentioning that even a weak excitatory connection of 0.01 nS reduced the period substantially (to $T_{\mathrm{per}} < 900$ ms). Some combinations of these excitatory and inhibitory connections even abolished the oscillatory behaviour in the meso-thoracic CPG, i.e., when $g_{\mathrm{syn,e}}(8, 2) \leq 0.01$ nS and $g_{\mathrm{syn,i}}(8, 2) \geq g_{\mathrm{syn,e}}(8, 2)$).

We ran simulations with 11 representative combinations of synaptic connections on both the "retractor" and the "protractor side" (i.e., connections from C1 to C7 and from C2 to C8, respectively). These were the combinations that yielded oscillatory behaviour in the meso-thoracic CPG (C7–C8), although with shortened periods, as mentioned above. For each of them, we constructed the PRC. Three resulting PRCs that showed the best agreement with the experimental PRC relative to the other simulation results are displayed in Fig. 5. Even so, the similarity between the simulated PRCs and the experimental one remained, for sev-

eral reasons, rather limited. Firstly, the range of $\Delta\phi$ values in the simulations is much smaller ($\leq$0.5) than in the experiment ($\approx$0.8). Also, the (nearly) linear part with slope about 1, present in the experimental PRC, is missing in all but one simulated PRCs. Even in the only simulated PRC where it is present, the PRC undergoes a sudden change at $\phi \approx 0.56$, which is absent in the experimental one. There is one more essential shortcoming of the simulated PRCs obtained so far with the extended 1-leg model: the oscillatory period in the simulations strongly reduced to values less than 1 s as soon as at least some of the synaptic strengths from the pro-thoracic CPG (C1–C2) to the meso-thoracic one (C7–C8) became intermediate (0.04 nS) or strong (0.1 nS). In Fig. 5, in fact, all periods are about 0.5 s. Such shortening of oscillatory periods were never observed in the experiments. There, the oscillatory periods were between 2 and 7.5 s (hitherto unpublished experiments and Borgmann et al. 2007, 2009). In summary, we can, thus, state that the connection scheme in the model that makes use of "static" synapses from the pro-thoracic CPG (C1–C2) to the meso-thoracic one (C7–C8) is unsatisfactory; hence, there is a call for change in the model's properties, in particular, in the connection properties.

Thus, we modified the aforementioned synaptic connections in a later version of the model. The main change was that, in steady state, that is, when no movement of the front leg took place or no peripheral stimulus was applied to IN8, no synaptic signal was present on the CPG neurones C7 and C8 from the pro-thoracic CPG (C1–C2). In physiological terms, this means that the above synaptic connections now also depended on the (angular) velocity signals produced by the velocity-dependent sense organs (hair fields and fCO, (Büschges and Gruhn 2008)) in the front leg. The modified model is displayed in Fig. 6. The main difference between the preceding version of the model and the one displayed in Fig. 6 is that in the latter version, the synaptic connection from the pro-thoracic to the meso-thoracic CPG are effective only if the LD control network is active, i.e., produced changes in the angle β, hence, $|d\beta/dt| > 0$. This turned out to be a substantial change as the results of simulations with this version of the model will show below.

We carried out simulations for all 192 combinations of the four synaptic strengths (conductance values) of the synapses on the meso-thoracic CPG from the pro-thoracic CPG for which oscillatory behaviour occurred in the meso-thoracic CPG. The four values of synaptic conductances used were 0.0 nS (no connection), 0.01 nS (weak connection), 0.04 nS (moderate connection), and 0.1 nS (strong connection). As it turned out, at some combinations of the synaptic strengths, the oscillation in the meso-thoracic CPG was abolished by the peripheral stimulation (at IN8) (cf. Fig. 6). In the first group of cases in which that happened, only a moderate excitatory connection was present from the CPG neurone C1 to the CPG neurone C7 (cf. Fig. 6), i.e., $g_{s,e}(7, 1) = 0.04$ nS and $g_{s,i}(7, 1) = 0.0$ nS, and on the "protractor side", we had $g_{s,e}(8, 2) \leq g_{s,i}(8, 2)$ and $g_{s,i}(8, 2) \geq 0.04$ nS. In the second group of cases, there was also a weak inhibitory synaptic connection from C1 to C7 ($g_{s,1}(7, 1) = 0.01$ nS), and the inhibitory synaptic connection from C2 to C8 was strong ($g_{s,i}(8, 2) = 0.1$ nS). The number of such cases in the two groups amounted to ten. Thus, the total number of cases in which the meso-thoracic CPG showed oscillatory behaviour was 182. From these 182 cases, which can be subdivided according to the combinations of the values of the synaptic conductances from C2 to C8 into 16 groups, we chose 1–3 representatives from each of these groups for which we computed the full PRC. From these results, altogether 25 cases were selected for display in Fig. 7. In each panel of Fig. 7, two or three simulated PRCs showing nearly identical behaviour are displayed. We clustered the results such that the left column in Fig. 7 contain results that partially agree with the experimental one, the middle column results that show a good agreement with the experimental one, and in the right column, the simulation results are in no agreement with the experimental one.

The criteria for the goodness of agreement are as defined before for simulated PRCs obtained with the "skeleton" model. Accordingly, at good agreement (middle column of panels in Fig. 7), the lengths of the linear parts of the PRCs almost exactly coincided, although the slope of the experimental PRC was somewhat smaller than that of the simulated ones ($\approx$0.95 vs. $\approx$1.00). In the group of results with partial agreement (left column of panels in Fig. 7), at least half of the linear parts coincided.

The clustering enabled us to find common properties in the connection strengths, i.e., common values of the synaptic conductances from the pro-thoracic to the meso-thoracic CPG. Thus, we found $g_{s,e}(7, 1) = 0.04$ nS and $g_{s,e}(8, 2) = 0.1$ nS for all simulated PRCs in the middle column, while the strength of the inhibitory connections varied the whole range of admissible values (0.0–0.1 nS). Thus, the value of the inhibitory connections was irrelevant for the good agreement of these simulated PRCs with the experimental one. For the simulated PRCs in the left column, we have $g_{s,e}(7, 1) = g_{s,e}(8, 2) = 0.04$ nS, while the inhibitory connection on the "protractor side" varies between weak and moderate strength and on the "retractor side" it takes all admissible values. Thus, partial agreement seems to occur essentially due to the weaker excitatory connection (smaller value of $g_{s,e}(8, 2)$) on the "protractor side".

In the cases in which the agreement between simulation and experimental results was poor, the excitatory synaptic connection from the pro-thoracic CPG to the meso-thoracic one on the "protractor side" was absent or weak ($g_{s,e}(8, 2) \leq 0.01$ nS), and the excitatory connection on the "retractor side" was in most cases moderate and in a few

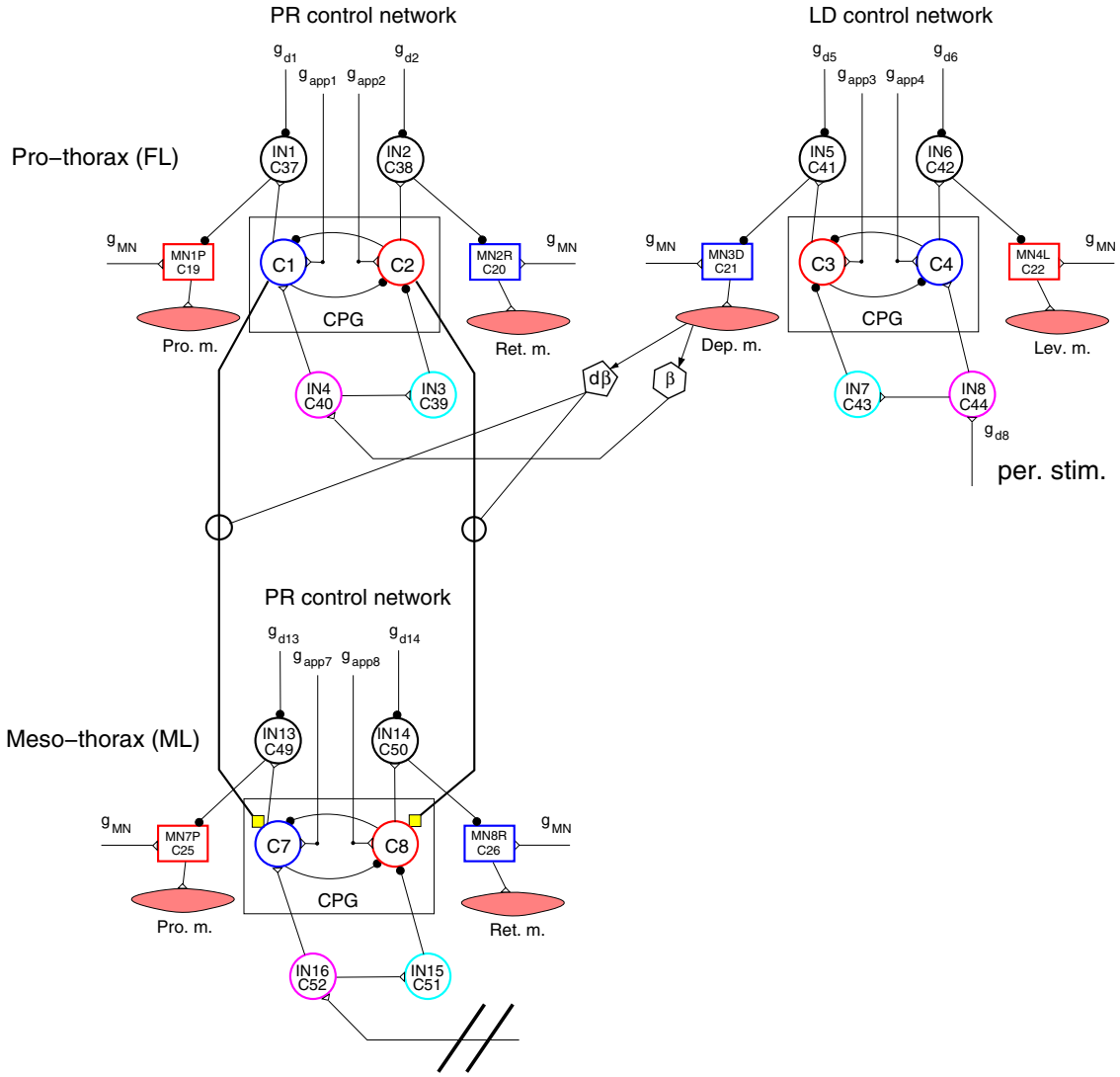

Fig. 6 Modified network model that includes velocity-sensitive gating. $\mathrm{d}\beta$ in a pentagon: velocity-dependent sensory signal, proportional to the angular velocity $\mathrm{d}\beta/\mathrm{d}t$. *Circles* on the synaptic paths from the pro-thoracic CPG to the meso-thoracic one symbolize the gating function that depends on the angular velocity $\mathrm{d}\beta/\mathrm{d}t$. Other parts of the model are identical to those in Fig. 3, except for the pro-thoracic EF control network, which is omitted here for the sake of simplicity

cases weak ($g_{\mathrm{s,e}}(7,1) = 0.04\,\mathrm{nS}$ and $g_{\mathrm{s,e}}(7,1) = 0.01\,\mathrm{nS}$, respectively).

In summary, we found that a strong excitatory connection from the pro-thoracic CPG to the meso-thoracic one was necessary on the "protractor side" and a moderate excitatory connection on the "retractor side". These conditions together were also sufficient to achieve good agreement between simulated and experimental PRCs.

4 Discussion

The main goal of this study has been to make progress in understanding the structure and function of, in particular, the inter-segmental coordination between the thoracic neural networks of the stick insect. We studied the connections between the pro- and meso-thoracic ganglia by means of models that produced simulated PRCs, and made use of corresponding results of hitherto unpublished, and of earlier, published experiments (Borgmann et al. 2009). In one group of the as yet unpublished experiments, the data for the PRC were obtained by directly stimulating the CS. In the other group, forced stepping of the intact front leg was induced at different phase values (ϕ) of the oscillatory period of the protractor–retractor CPG of the meso-thoracic ganglion. The PRC was then constructed as described in Materials and methods.

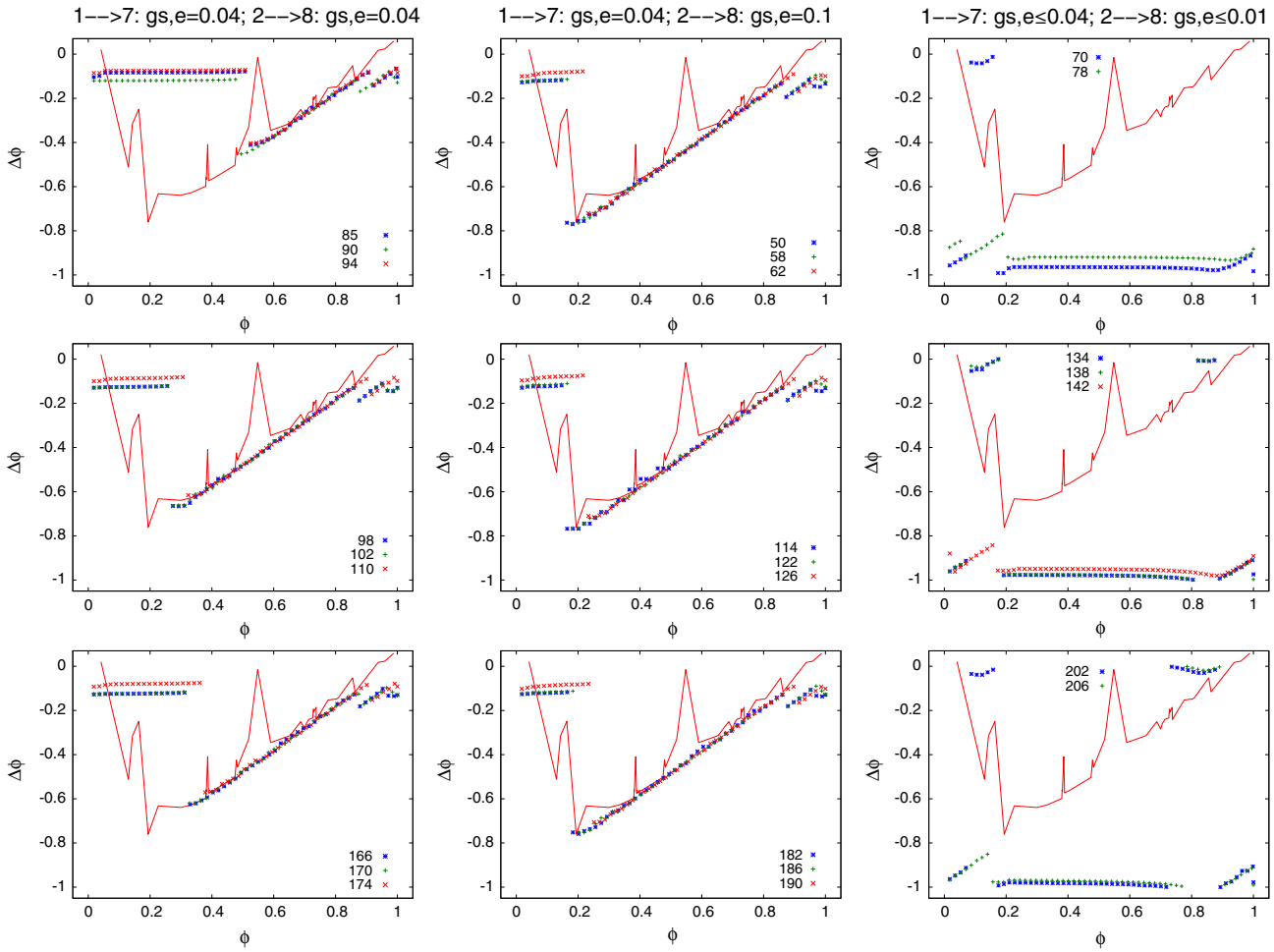

Fig. 7 Simulated phase response curves obtained with the gated synaptic connections from the pro-thoracic CPG to the meso-thoracic one. For the sake of direct comparability, the phase response curve obtained in experiments with forced front leg stepping is drawn in every panel as a *continuous line*. The simulated curves are drawn as a sequence of discrete points using a different point type and colour for each curve within the same panel. The simulation results are clustered such that the *first column* shows simulated phase response curves that partially agree with the experimental one, the *second column* shows the simulated results with a good agreement with the experimental one, and in the *third column*, simulation results with no agreement with the experimental one are displayed. On the *top of each column*, the values of the conductances of the excitatory synapses characteristic for that group of simulated phase response curves are shown. The numbers in the legend of each panel are the (technical) codes for the actual combinations of the four synaptic strengths at the four synapses from the pro-thoracic to the meso-thoracic CPG. The notation is the same as in Fig. 5

In the simulations, we used a "skeleton" model of the inter-segmental coupling (Fig. 2) and an extended version of our existing 1-leg model (Toth et al. 2012; Knops et al. 2013) (cf. Figs. 3 and 6), to produce simulated PRCs. Our approach was to compare the experimental and simulated PRCs under the basic assumption that if the PRCs are similar so are the systems that generate them. In this study, it was not our goal to invent or introduce a substantially new model but rather to apply our existing one to the above task. As it turned out, this could only be done with some modification of the original model.

We carried out the task in two stages: first using a simple "skeleton" model in order to check whether any meaningful results would arise when coupling two CPGs directly using both excitatory and inhibitory bilateral synaptic connections. Then we tried to reproduce the experimental results (PRCs) by means of a more detailed, biologically more relevant model, which we called the (extended) 1-leg model. In the "skeleton" model, the stimuli were directly applied to the neurons of the pro-thoracic CPG, while they acted indirectly, via the β signal and interneuron IN4, on the neurons of the pro-thoracic CPG in the extended 1-leg model. As mentioned earlier, peripheral stimuli in the extended 1-leg model always induced mechanical movement in the LD neuromuscular system. This movement of the femur corresponds well to (forced) front leg stepping in the experiments. A com-

parison with the experimental PRC obtained with direct and selective CS stimulation would, thus, be problematic. Furthermore, this PRC is also very noisy. The noise almost fully masked a possibly present linear part of that PRC. We do not have an explanation as to the source of the noise, we would only suggest that perhaps the efficacy of the CS stimuli alone was not high enough to produce reliable response signals in the protractor MNs. In addition, the pro-thoracic protractor–retractor CPG might also have been far away, in the system theoretic sense, from its oscillatory state it is in during normal locomotion. Interestingly, there seems to be some preliminary experimental evidence that stimulation of the fCO alone has no discernible effect on the activity of the meso-thoracic CPG, at least for the conditions in which those experiments were performed (K. Hellekes unpublished results). One may assume that, during front leg stepping, additional excitatory signals representing leg movement (e.g., position, angular velocity), apart from the CS-induced signal, arrive at the protractor MNs, and, thus, a robust phase relationship will be established resulting in a less noisy PRC. The simulations support the hypothesis that apart from the position-dependent sensory signals, signals that encode the angular velocity of the femur-tibia joint are necessary to produce simulated PRCs that show good agreement with the experimental one.

By clustering the simulated PRCs, obtained with the extended 1-leg model, according to the goodness of their fit to the experimental one (Fig. 7), we could determine the nature of the synaptic connections that ensured good agreement between experimental and the simulated PRCs. It thus turned out that, for this, a strong excitatory synaptic connection was required on the "protractor side" and a moderate excitatory one on the "retractor side". Most notably, the inhibitory connections on both sides proved to be irrelevant.

An earlier model of ours comprising the protractor–retractor systems of all three thoracic ganglia (Daun-Gruhn and Toth 2011) was used to model the neuronal mechanisms that might underlie the tetrapod and tripod gaits (coordination patterns) and the transition between them. In that model, the cyclic connection between the "retractor" CPG neurons modulated by sensory signals proved to be sufficient to produce the desired gaits (coordination patterns) and the transition between them. However, when we used it to generate simulated PRCs, we obtained partial agreement at best between the experimental and the simulated PRCs (unpublished results). This finding thus underpins the necessity of the excitatory connection between CPGs on both the "protractor" and the "retractor side".

The above results are in qualitative agreement with the simulation results obtained with the "skeleton" model. There we found a narrow range ($[0.1, 0.18]$ nS) of admissible conductance values of the excitatory synapses in the symmetric case. At the same time, the conductances of the inhibitory synapses could vary over a larger range: $[0.02, 0.2]$ nS. In the asymmetric case, the suitable conductance values of the excitatory synapses roughly correspond to those obtained with the extended 1-leg model ($g_{\mathrm{s,e}}(8, 2) = 0.17$ nS in all four cases, and $g_{\mathrm{s,e}}(7, 1) = 0.1$ nS in three out of four cases). The conductance of the inhibitory synapse on the "protractor side", however, takes values $g_{\mathrm{s,i}}(8, 2) \geq 0.1$ nS, whereas $g_{\mathrm{s,i}}(7, 1)$ can even be equal to zero (no connection). Moreover, stimuli in the "skeleton" model were applied on the "retractor side" of the pro-thoracic CPG. This, in essence, corresponds to the stimulus that excites the "retractor" CPG neuron C1 in the extended 1-leg model via the β signal and, thus, via IN4, while indirectly inhibiting C2 (Fig. 6). However, in the extended 1-leg model, the sensory signals represented by the angular velocity $\mathrm{d}\beta/\mathrm{d}t$ additionally gate the excitatory and inhibitory connections from the pro-thoracic to the meso-thoracic CPG (Fig. 6). The inclusion of this gating function proved crucial because without it, no satisfactory replication of the experimental PRCs could be obtained in the simulations. The (angular) velocity-sensitive gating is, therefore, an indispensable part of the extended model. Nevertheless, it *does not* interfere with the types of dynamic behaviour that were mimicked by earlier versions of the model, since in all of those cases the angular velocity $\mathrm{d}\beta/\mathrm{d}t$ was virtually never zero; hence, the "velocity gates" were always open. Thus, the present, extended, version of the model is, in this respect, fully compatible with earlier ones.

Another important point is the comparability of stimuli in the experiments and simulations. It is obvious that experimental stimuli and those used in the simulation with the "skeleton" model bear little direct analogy. On the other hand, stimuli used in the extended 1-leg model correspond well to (forced) front leg stepping stimuli in the experiments, since in the model, they induce mechanical (lifting) movement of the femur and, thus, both position- and velocity-dependent sensory signals. These signals then act as direct stimuli on the pro-thoracic CPG and determine the actual synaptic connections from the pro-thoracic to the meso-thoracic CPG. Thus, the use of "peripheral stimuli" results in front-leg movement in the model. Hence, to compare the experimental PRCs, obtained with front-leg stepping, to simulated ones is reasonably justified. Moreover, the experimental PRC produced with selective CS stimulation is too noisy to serve as a basis for a comparison with simulated PRCs (cf. Fig. 1b). By contrast, the PRCs obtained from experiments with free and forced stepping animals (Fig. 1c) show very close similarity.

There is yet another, more general point to be dealt with, that is, how to relate the conclusions drawn from the results of the present modelling work to neurophysiological properties of the stick insect. One could, for example, argue that the analogy between the model and the stick insect's nervous system is rather weak since, in the model, single neurons stand

for whole neuron populations in the stick insect's nervous system. Therefore, the properties of the model are not valid in the nervous system. It is certainly true that in our model, single neurons represent neuron populations in the stick insect's nervous system. One can, however, in a thought experiment replace the single neurons by (almost) simultaneously active neuron populations which would act in a similar manner as a single neuron. In this way, the strength of a synaptic connection between two neuronal populations is determined by the strength of individual synaptic connections and the number of the parallel synaptic pathways. Conversely, because of the high degree of spatial summation, this total synaptic connection strength can be reduced to a synaptic connection between single neurons with a synaptic strength that corresponds to the total connection strength of the whole neuron population. Hodgkin–Huxley-type neuron models, and the corresponding synaptic connection models, lend themselves to this approach since their parameters can directly be interpreted in neurophysiological terms. The models we have been using are certainly strong simplifications of the neuronal systems they emulate. They, nevertheless, admit a physiologically meaningful interpretation of the simulation results achieved with them along the lines of the foregoing reasoning.

From these results and reasoning, a more general conclusion can also be drawn. They suggest that the model network we used here, in particular the inter-segmental synaptic connections between the neurons of the thoracic protractor–retractor CPGs in it, might provide a blueprint for a possible implementation of the biological neuronal network that produced the PRCs.

Acknowledgments We thank Drs. J. Schmidt and A. Büschges for helpful discussions in the course of this work. This work was funded by the Deutsche Forschungsgemeinschaft Grants DA1182/1-1 and GR3690/4-1.

References

Akay T, Ludwar BCh, Göritz ML, Schmitz J, Büschges A (2007) Segment specificity of load signal processing depends on walking direction in the stick insect leg muscle control system. J Neurosci 27:3285–3294

Bässler U (1977) Sensory control of leg movement in the stick insect Carausius morosus. Biol Cybern 25:61–72

Bässler U (1983) Neural basis of elementary behavior in stick insects. Springer, Berlin

Borgmann A, Scharstein H, Büschges A (2007) Intersegmental coordination: influence of a single walking leg on the neighboring segments in the stick insect walking system. J Neurophysiol 98:1685–1696

Borgmann A, Hooper SL, Büschges A (2009) Sensory feedback induced by front-leg stepping entrains the activity of central pattern generators in caudal segments of the stick insect walking system. J Neurosci 29:2972–2983

Borgmann A, Tóth TI, Gruhn M, Daun-Gruhn S, Büschges A (2011) Dominance of local sensory signals over inter-segmental effects in a motor system: experiments. Biol Cybern 105:399–411

Büschges A (1995) Role of local nonspiking interneurons in the generation of rhythmic motor activity in the stick insect. J Neurobiol 27:488–512

Büschges A (1998) Inhibitory synaptic drive patterns motoneuronal activity in rhythmic preparations of isolated thoracic ganglia in the stick insect. Brain Res 783:262–271

Büschges A, Gruhn M (2008) Mechanosensory feedback in walking: from joint control to locomotor patterns. Adv Insect Physiol 34:193–230

Cruse H (1990) What mechanisms coordinate leg movement in walking arthropods? TINS 13:15–21

Cruse H (2009) Principles of insect locomotion. In: Arena P, Patane L (eds) Spatial temporal patterns for action-oriented perception in roving robots. Springer, Berlin, pp 1–57

Daun S, Rybak IA, Rubin J (2009) The response of a half-center oscillator to external drive depends on the intrinsic dynamics of its components: a mechanistic analysis. J Comput Neurosci 27:3–36

Daun-Gruhn S, Tóth TI (2011) An inter-segmental network model and its use in elucidating gait-switches in the stick insect. J Comput Neurosci 31:43–60

Daun-Gruhn S, Tóth TI, Borgmann A (2011) Dominance of local sensory signals over inter-segmental effects in a motor system: modeling studies. Biol Cybern 105:413–426

Delcomyn F (1971) The locomotion of the cockroach Periplaneta americana. J Exp Biol 54:453–496

Delcomyn F (1981) Insect locomotion on land. In: Herreid CF, Fourtner CR (eds) Locomotion and energetics in arthropods. Plenum Press, New York, pp 103–125

Grabowska M, Godlewska E, Schmidt J, Daun-Gruhn S (2012) Quadrupedal gaits in hexapod animals—inter-leg coordination in free-walking adult stick insects. J Exp Biol 215:4255–4266

Graham D (1972) A behavioural analysis of the temporal organisation of walking movements in the 1st instar and adult stick insect (*Carausius morosus*). J Comp Physiol A 81:23–52

Graham D (1985) Pattern and control of walking in insects. Adv Insect Physiol 18:31–140

Hill AV (1953) The mechanics of active muscle. Proc R Soc Lond (Biol) 141:104–117

Hodgkin AL, Huxley AF (1952) A quantitative description of membrane current and its application to conduction and excitation in nerve. J Physiol 117:500–544

Hughes GM (1952) The co-ordination of insect movements. I. The walking movements of insects. J Exp Biol 29:167–285

Knops S, Tóth TI, Guschlbauer C, Gruhn M, Daun-Gruhn S (2013) A neuromechanical model for the neuronal basis of curve walking in the stick insect. J Neurophysiol 109:679–691

Laurent G, Burrows M (1989) Distribution of intersegmental inputs to nonspiking local interneurons and motor neurons in the locust. J Neurosci 9:3019–3029

Laurent G, Burrows M (1989) Intersegmental interneurons can control the gain of reflexes in adjacent segments of the locust by their action on nonspiking local interneurons. J Neurosci 9:3030–3039

Ludwar BC, Westmark S, Büschges A, Schmidt J (2005) Modulation of membrane potential in mesothoracic moto- and interneurons during stick insect front leg walking. J Neurophysiol 93:1255–1265

Pearson KG, Franklin R (1984) Characteristics of leg movements and patterns of coordination in locusts walking on rough terrain. Int J Robot res 3:101–112

Ritzmann RE, Büschges A (2007) Adaptive motor behavior in insects. Curr Opin Neurobiol 17:629–636

Schmitz J (1986) The depressor trochanteris motoneurones and their role in the coxa-trochanteral feedback loop in the stick insect Carausius morosus. Biol Cybern 55:25–34

Schmitz J (1986) Properties of the feedback system controlling the coxa-trochanter joint in the stick insect Carausius morosus. Biol Cybern 55:35–42

Schultheiss NW, Prinz AA, Butera RJ (eds) (2012) Phase response curves in neuroscience. Theory, experiment, and analysis. Springer Series in Computational Neuroscience, vol 6. Springer, New York

Tóth TI, Daun-Gruhn S (2011) A putative neuronal network controlling the activity of the leg motoneurons of the stick insect. Neuroreport 22:943–946

Tóth TI, Knops S, Daun-Gruhn S (2012) A neuromechanical model explaining forward and backward stepping in the stick insect. J Neurophysiol 107:3267–3280

Westmark S, Oliveira EE, Schmidt J (2009) Pharmacological analysis of tonic activity in motoneurons during stick insect walking. J Neurophysiol 102:1049–1061

Wilson DM (1966) Insect walking. Ann Rev Entomol 11:103–122

Winfree AT (2000) The geometry of biological time, 2nd edn. Springer, New York

2.3 Phase-locking in the delta-theta frequency band is an EEG marker of movement execution

Svitlana Popovych*, Nils Rosjat*, Tibor Istvan Tóth, Bin Wang, Liqing Liu, Rouhollah Abdollahi, Shivakumar Viswanathan, Christian Grefkes, Gereon Rudolf Fink, Silvia Daun-Gruhn

Under review in the Journal of Neuroscience
*Shared first authorship, alphabetical order

Author Contributions

Conceived the research
Nils Rosjat, Svitlana Popovych
Bin Wang, Rouhollah Abdollahi
Shivakumar Viswanathan, Christian Grefkes
Gereon Rudolf Fink, Silvia Daun-Gruhn

Performed the experiments
Bin Wang, Rouhollah Abdollahi, Shivakumar Viswanathan

Analyzed the data
Nils Rosjat, Svitlana Popovych
Liqing Liu, Silvia Daun-Gruhn

Figure Preparation
Svitlana Popovych, Nils Rosjat
Liqing Liu

First version of manuscript
Svitlana Popovych

Wrote the paper
Tibor Istvan Tóth, Nils Rosjat
Svitlana Popovych, Silvia Daun-Gruhn

Contributed materials/analysis tools
Christian Grefkes, Gereon Rudolf Fink
Silvia Daun-Gruhn

Phase locking in the delta-theta frequency band is an EEG marker of movement execution

S.Popovych[1,2,*], N.Rosjat[1,2,*], T.I.Tóth[1], B.Wang[2], L.Liu[1,2], R.Abdollahi[2], S.Viswanathan[2,3], C.Grefkes[2,3], G.R.Fink[2,3], S.Daun-Gruhn[1,2]

[1] Heisenberg Research Group of Computational Biology, Department of Animal Physiology, Institute of Zoology, University of Cologne

[2] Cognitive Neuroscience, Institute of Neuroscience and Medicine (INM-3), Research Centre Jülich

[3] Department of Neurology, University Hospital Cologne

** shared first authorship*

Abbreviated title:

EEG marker of movement execution

Correspondence to:

Silvia Daun-Gruhn, PhD
Cognitive Neuroscience,
Institute of Neuroscience and Medicine (INM-3),
Research Centre Jülich, 52425, Jülich, Germany
Tel: +49-2461-61 8638
Fax: +49-2461-61 1518
Email: s.gruhn@fz-juelich.de

Number of pages: 31
Number of figures: 9
Number of words for Abstract: 247
Number of words for Introduction: 643
Number of words for Discussion: 1077
Total number of words: 8680

Acknowledgements

This works was funded by the University of Cologne Emerging Groups Initiative (CONNECT group) implemented into the Institutional Strategy of the University of Cologne and the German Excellence Initiative. SDG gratefully acknowledges additional support from the German Research Foundation (GR3690/2-1, GR3690/4-1). GRF was supported by the Marga and Walter Boll foundation.

Conflict of Interest

The authors declare no competing financial interests.

Abstract

Motor actions result from a complex interplay of various brain regions. These are assembled into different functional networks depending on the specifics of the action. Identifying the neural signals that encode an action's component remains a challenge. In this study, we sought to identify neural markers of the execution of a movement that are invariant despite differences in the type of movement initiation and hence the neural processes and functional networks involved. To this end, EEG activity was continuously recorded from 18 right-handed healthy participants while they performed a simple motor task consisting of button presses with the left or right index finger. The movement was performed either in response to a visual cue or at a self-chosen, i.e. non-cued point in time. Despite substantial difference in how the actions were initiated, properties of the EEG signals common to both conditions could be identified using time-frequency and phase locking analyses of the EEG data: In both conditions, a significant phase locking effect was observed that started prior to the movement onset in the δ-θ frequency band (2-7 Hz), and that was strongest at the electrodes above the contralateral motor regions (M1). Results suggest that phase locking in the δ-θ frequency band is a neural marker of movement execution, which is invariant under differences in the functional networks involved in movement initiation. This enhanced synchronization is likely to present a neural state necessary to facilitate the convergence of simultaneously active distinct cortical pathways onto the common motor output.

Significance statement

In this study, we identified phase locking in the δ-θ frequency band as an electrophysiological marker of movement execution, which is invariant despite differences in the functional networks involved in the initiation of a movement. We suggest that this enhanced synchronization prior to the start of the movement

can serve as a mechanism by which distinct simultaneously active cortical pathways converge onto the common motor output and thereby forms the basis necessary for the activation of the processes that trigger the actual motor task.

Introduction

Motor actions are basic functions of living organisms. In humans, they have reached immense complexity and sophistication. A voluntary action is defined by its 'internal' origin. Consequently, voluntary actions are often compared to actions triggered by 'external' stimuli. Multiple lines of evidence have established that internally- and externally-triggered actions are effectuated by distinct cortical pathways whose simultaneous activities converges onto a common final efferent pathway, which predominantly consists of the primary motor cortex (M1) and the corticospinal tract (CST) (Jenkins et al., 2000; Waszak et al., 2005; Hughes et al., 2011; Krieghoff et al., 2011). However, for motor actions to be executed accurately and efficiently, a precise timing of the action potentials fired by the neurons, which project from M1 into the CST where in turn the appropriate motor neurons drive the muscles, is crucial. The nature and properties of neural markers of such a timing mechanism remain as yet unclear in humans.

Previous studies have ascribed a crucial role to synchronization dynamics during movement execution. For instance, Baker et al. (1997, 2001) suggested that synchrony of neural assemblies in the primary motor cortex of monkeys during a precision grip task is of functional importance, since it was strongly modulated during different phases of the task and correlated with synchronous activity in the hand muscles performing the task.

Furthermore, synchronization of oscillatory activity is important for shaping functional connections between different brain areas. Uhlaas and colleagues, for instance, have shown that synchronized neural oscillations in the low (δ, θ, α) and high (β, γ) frequency bands constitute fundamental mechanisms that enable coordinated activity in the normally functioning brain (Uhlhaas et al., 2010). Consequently, the primary goal of our study was the search for neural markers related to synchronous activity in the human motor system.

To achieve this goal, we examined neural markers of the execution of a movement that are invariant despite profound differences in the functional

networks, which trigger them. We hypothesized that such neural markers would be indicative of a common synchronization mechanism. Such a mechanism is likely to facilitate the convergence of the simultaneous activities of the functional pathways from these networks onto the common motor output.

The electroencephalogram (EEG) has a high temporal resolution and is well suited to study and analyze neuronal processes, in particular neural synchrony, on a millisecond scale. EEG activity was, therefore, continuously recorded from 18 right-handed healthy participants while they performed a simple motor task consisting of button presses with the left or right index finger. The movement was performed either (i) in response to a visual cue or (ii) at a self-chosen, i.e. non-cued point in time. Importantly, although such button presses are (i) simple to perform and (ii) involve only a small group of skeletal muscles, they are complex enough to engage the most important motor brain areas (e.g., Gerloff et al., 1998; Witt et al., 2008; Michely et al., 2012). They are hence suitable to enable the systematic investigation of the physiological processes that take place during motor activities.

We carried out time-frequency (wavelet) analysis (e.g., Blinowska and Durka, 1994; Sanei and Chambers, 2013) and used methods to uncover phase locking (Lachaux et al., 1999; Wang et al., 2006) in the EEG signals. We found phase locking in the δ-θ (2-7 Hz) frequency band around movement onset at all electrodes above the cortical motor areas: C1, C3 and C2, C4 above the left and right primary motor cortex (lM1, rM1), respectively, FC3 and FC4 above the left and right pre-motor cortex (lPM, rPM), respectively, as well as FCz and Cz above the supplementary motor area (SMA). Phase locking was strongest at the electrodes lying above the motor regions contralateral to the moving index finger (left and right), in particular M1, but it was independent of how the movement was initiated. Phase locking did, however, not occur in the higher frequency bands.

Material and methods

Participants

Twenty-one healthy participants were recruited from which 18 could be used for data analysis (11 women and 7 men; age range 22-35 years). Data from three participants were excluded due to insufficient quality of the recordings (see EEG pre-processing section). The participants had normal or corrected-to-normal vision and no history of neurological or psychiatric diseases. The experimental protocol was approved by the Ethics Committee of the Medical Faculty, University of Cologne, and the participants provided informed, written consent before the start of the experiment. According to the selection criteria, all participants were right handed, had no mental or physical illness and did not use any psycho-active or psycho-tropic substance. We utilized the Edinburgh Handedness Inventory (Oldfield, 1971) to identify the dominant hand of the participants.

Task design

Subjects were asked to perform button presses with their index finger of the left or right hand. There were two motor conditions: (i) self-initiated movements and (ii) movements upon appearance of a visual cue. In addition, a third condition with identical visual stimulation but without motor responses served as control condition to estimate EEG activity evoked by the visual stimuli in the absence of response-related activity.

In the first condition ('self-initiated movements'), subjects were allowed to choose when and with which hand to perform the button press. Apart from the fixation point that was displayed for the entire duration of the block (Figure 1A), there were no additional visual stimuli to indicate (i) when, and (ii) with which hand each of these responses were to be performed. The following constraints applied: (i) responses had to be given with an inter-trial interval of approximately 4-8 seconds; (ii) subjects had to roughly balance the number

of left and right hand responses, and (iii) subjects had to avoid regular sequences (e.g., alternating between left and right hand).

In the second condition ('visually-cued movements'), a right or left-pointing arrow (2° wide and 1.2° high expressed as visual angles), was presented first for 200 ms on a presentation screen with inter-stimulus intervals (ISI) of varying length ≥ 4 s. The participant had to press the button, as soon as possible after the visual stimulus had appeared, with either the left or the right index finger, depending on the direction of the arrow. That is, he/she had to press with the right index finger if the arrow was pointing to the right, and with the left index finger, if the arrow was pointing to the left.

In the third condition ('vision-only'), the same visual stimulus (i.e., a left or right-pointing arrow) was presented as in the visually-cued tapping condition but now the participant was instructed to pay attention to the arrow, only, without pressing the button. Thus, no motor action was performed in this condition.

Before the start of the experiment, participants were introduced to the experimental procedure. They were given instructions on how to perform the task while the electrode cap was put on. They were also intensively trained in order to achieve good task performance and for fulfilling the above mentioned criteria. In order to help the subjects to remember the actual condition, we used unique geometric objects as indicated in the panels 1-3 of Fig. 1A, for each condition. All visual stimuli were generated using the software 'Presentation' (version 11.0, Neurobehavioral Systems, Albany, CA).

The whole experiment lasted about 70 minutes, and consisted of 16 blocks of each condition. These 16 blocks were divided into 4 runs with each run (approximately 17 minutes long) containing four blocks of each condition. Each condition was presented for 60 seconds after which the participant was informed about his/her performance. After the feedback, there was a white fixation period of 10 s in order to produce a baseline between two subsequent conditions. All blocks started with the self-initiated tapping condition but the other two conditions appeared in random order. The recorded inter-response-

intervals of the self-initiated tapping condition were used as the inter-stimulus intervals in the vision-only and visually-cued conditions, after randomizing the order. Additionally, intervals with a duration less than 4 s were replaced with a random duration ranging from 4 s to 8 s. This adaptive procedure limited the influence of poorly timed responses in the self-initiated condition on the other conditions. Additionally, it ensured that the total number of responses, proportion of left/right responses, and the timing between responses were closely matched across conditions. Between blocks, the participants had 1 min resting time. During the entire experiment, every participant performed 80-90 button presses per condition.

Procedure

After the preparation of the electrode cap, participants were seated in a comfortable chair in a sound-proof room, and their head was kept in static position by a chin-rest. The distance of their eyes from the presentation screen was approximately 70 cm. During the EEG signal acquisition, the room lights were dimmed. Accelerometer sensors (Brain Products GmbH, Munich, Germany) were attached to the dorsal tip of both index fingers, and fixed by tapes. We used these accelerometer sensors to identify the onset of the finger movement and the movement time, i.e., the time between movement onset and button press. Subjects were then asked to perform the task. While doing so, their body (apart from the active hand, if applicable) had to be kept steady and at rest. Task performance was monitored online by the examiner via a video camera to ensure that the participants were alert and did not fall asleep. It was also ensured by the same means that the self-initiated tapping was not regular. Moreover, the participants were asked to minimize the number of eye blinks during the recording. After the experiment, the participants were interviewed about their strategy to perform the task in the self-initiated tapping condition. This was done in order to ensure that they neither counted mentally the number of left- and right-hand tappings nor tried to measure the time (e.g.,

by counting the seconds) between two button presses.

Recording of EEG and acceleration signals

EEG data were acquired using 64 active Ag/AgCl electrodes (Brain Products GmbH, Munich, Germany) placed according to the international 10-20 system in a spherical array. Bilateral horizontal and left vertical electro-oculograms (EOG) were recorded by three of the 64 scalp electrodes (FT9, FT10, TP10 in the 10-20 system) placed bilaterally at the outer canthi and under the left eye, respectively. The reference electrode was placed at the left earlobe. At the beginning and the end of the experiment, the impedance of each electrode was measured to ascertain that it was smaller than 15 kΩ. The EEG signals were amplified, band-pass filtered in the frequency band 0.87-500 Hz, and digitized at a sample rate of 2500 Hz.

Two acceleration sensors, one for each hand, were attached to the index fingers for the detection of finger movements throughout the experiment. The sensors generated voltage signals, which were recorded simultaneously with the EEG signals using separate channels. Each sensor signal had three components that encoded the instantaneous accelerations in the X, Y, and Z direction. The first derivative of the X, Y, and Z components of the acceleration signal were computed and then combined to obtain the scalar (Euclidean) magnitude of the instantaneous acceleration change at each time point (Wyatt, 1998). This time-series was then smoothed, rescaled and a threshold was set to identify the earliest time point in a 125 ms window prior to each button press that showed a continuous increase in acceleration rate. All trials in which the movement onset could not be unambiguously detected were excluded from further analysis.

We used accelerometers as our key measure of motor-output as the acceleration signals are highly sensitive to detect the start of a movement and are not restricted to a muscle group and a specific movement direction like, e.g., surface EMG (Keil et al., 1999). Additionally, the use of accelerometers also

allowed us to exclude trials with excessive or mirror movements.

Preprocessing of the recorded data

For preprocessing and analysis of the EEG data, we used the EEGLAB toolbox (Delorme and Makeig, 2004) and scripts in Matlab R2014a (MathWorks Inc.). First, the data were band-pass filtered in the frequency band 0.5-48 Hz, and then down-sampled from 2500 Hz to 200 Hz in order to achieve a substantial data reduction, and, thereby, a shortening of the processing time. Next, the continuous raw EEG data were visually inspected for paroxysmal and muscular artifacts not related to eye-blinks. Eye-blink related artifacts were removed by using ICA (see below). Noisy portions of the EEG signal were excluded from further analysis. The trials in the self-initiated tapping condition with inter-trial intervals shorter than 4 s were removed, as well as trials in the visually-cued tapping condition in which the time between the stimulus and the onset of the movement (accelerometer signal) was longer than 1 s. This led to a reduction of the data by 10-20 %.

In the next step, the EEG recordings were epoched to single trials, i.e., they were subdivided into intervals of 4 s depending on the experimental condition. In the vision-only condition, the reference point (time zero) was assigned to the start of the visual stimulus. The intervals reached from 1500 ms before the stimulus to 2500 ms after it: [-1500, 2500] ms. In the self-initiated tapping condition, the onset of the finger movement as determined by the accelerometer signal was set to be the reference point (time zero). Here, the 4 s intervals started 2500 ms before the onset of the movement and lasted until 1500 ms after it ([-2500, 1500] ms). In the visually-cued tapping condition, two different subdivisions, henceforth intervals, were used. In one case, the reference point was assigned to the start of the visual stimulus, and we used the same interval [-1500, 2500] ms as in the vision-only condition. In the other, the reference point (time zero) was set to the onset of the finger movement, and the interval reached from 2000 ms before the onset of the finger movement until 1500 ms after it ([-2000, 1500] ms), as illustrated in Fig. 1B. The use of the two

different intervals in the visually-cued tapping condition was necessary in order to preserve the comparability of the results with those obtained in the vision-only condition, and with those in the self-initiated tapping condition. In the self-initiated tapping condition, the onset of the finger movement is the only point in time that can serve as reference. It is usually preceded by the build-up of the so-called readiness potential (Bereitschaftspotential), which takes about 2000 ms (Shibasaki and Hallett, 2006). In the visually-cued tapping condition, by contrast, the motor action is triggered by an external visual stimulus. Therefore, this condition has two potential reference points, i.e., response-locked or stimulus-locked ($t = 0$). The length of 4000 ms for the intervals was chosen such as to avoid overlaps between subsequent trials. This applies to all conditions.

After subdividing the data into single trials, data were further corrected for artifacts. All trials with an amplitude larger than 100 μV in any of the recording channels, or showing a drift that exceeded 75 μV over the whole interval (abnormal drift) were rejected. This is a common procedure, see e.g. Herz et al. (2012). Trials with other artifacts (blinks, eye movements, muscle activity, and infrequent single-channel noise) were identified by means of a semi-automated procedure based on independent components analysis (ICA) (Jung et al., 2000a,b; Hyvärinen et al., 2004; Langlois et al., 2010). ICA was used with the Info-Max ICA algorithm implemented in EEGLAB (Langlois et al., 2010). Signals containing blink/oculomotor artifacts or other artifacts that were clearly of different origin were subtracted from the data by using the procedure ADJUST from EEGLAB (Mognon et al., 2011). Noisy channels were automatically detected by EEGLAB. The noisy signals were corrected by interpolation of adjacent noise-free channels using spherical splines (Perrin et al., 1989). Finally, the trials were baseline-corrected taking the first 1000 ms of each interval as baseline. In order to improve the spatial resolution and to eliminate the influence of distortions due to the reference electrode, we used the so-called small Laplacian (e.g., McFarland et al., 1997) for all EEG channels, except for the boundary ones.

Data analysis

There are many ways of time-frequency decomposition of EEG data. They mainly differ in the choice of the basis functions. We chose the complex Morlet wavelets as basis function, which are often used for time-frequency decomposition of EEG/MEG data (Lachaux et al., 1999). They are sinusoidal, weighted by a Gaussian kernel, hence they can capture local oscillatory components in the time series. Contrary to the standard short-time Fourier transform, wavelets have variable resolution in time and frequency (Sanei and Chambers, 2013). When choosing the wavelet, we, in essence, made a trade-off between temporal and spectral resolution. The analysis of EEG signals yielded spectral power and phase of the signals in different conditions such as self-initiated or visually-cued tapping. These quantities were, in practice, computed by means of procedures implementing the aforementioned wavelet transform as part of the software package SPM12 (Friston et al., 2006).

The time-frequency analysis was performed in all main frequency bands: delta (1-3 Hz), theta (4-7 Hz), alpha (8-12 Hz), beta (13-30 Hz), and low-gamma (30-48 Hz) and for all EEG channels. A detailed analysis, however, is only presented for the following EEG channels: C2 and C4 over the right primary motor cortex: rM1; C1 and C3 over the left primary motor cortex: lM1; FC3 over the left pre-motor cortex: lPM; FC4 over the right pre-motor cortex: rPM; FCz and Cz over the supplementary motor area: SMA. The occipital electrode Oz above the primary visual cortex V1 was used to record and monitor the activity of V1 in the visually-cued tapping and the vision-only condition. We did not carry out source identification for two reasons: first, all electrodes of interest were positioned directly above the motor areas of interest, i.e. above the very sources; secondly, as we used (the small) Laplacian in preprocessing the EEG data, this method might have interfered with source identification (Michel et al., 2004).

The Morlet transformation provided two (physical) quantities for each trial

and each electrode: the (instantaneous) phase $\varphi\,(t, f)$ and the (instantaneous) amplitude (power) $A\,(t, f)$, which depend on the time (t) and the oscillatory frequency (f). We computed the amplitude and the phase dynamics in each condition and tried to derive properties common across trials. An important characteristic of the phase dynamics between the trials is the phase locking index (PLI), also denoted as the so-called inter-trial phase locking or inter-trial coherence. PLI is defined as

$$PLI\,(t,f) = \left|\frac{1}{N}\sum_{k=1}^{N} \exp\,(i\varphi_k(t,f))\right|$$

where N is the number of trials, and φ_k is the phase of trial k at time t and at a given frequency f; i is the imaginary unit: $i^2 = -1$. It is a measure of similarity of the phases of a signal over many repetitions. PLI ranges from 0 to 1. PLI $= 1$ means identical phase of the signal across the trials. Low values of PLI suggest temporal heterogeneity of the phases in the individual trials. Thus, PLI measures the degree of inter-trial variation in phase between the responses to stimuli and thereby quantifies phase locking of the oscillatory activity irrespective of its amplitude (Herrmann et al., 2005; Tass, 2007).

We carried out a simple statistical analysis of the data to verify that our results are statistically significant. For this, we calculated the average value of PLI over the frequency band 2-7 Hz in both tapping conditions and for both hands. We then performed a pointwise t-test on each of the average PLI curves in both (self-initiated and visually-cued tapping) conditions. We compared the PLI obtained for each of these conditions with the corresponding baseline at the significance level of $p \leq 0.05$ with a False Discovery Rate (FDR) correction (Benjamini and Hochberg, 1995). In self-initiated tapping, the baseline was computed using the interval [-2300, -1500] ms, whereas in visually-cued tapping the baseline was computed using the interval [-1800, -1000] ms. In both conditions, the baseline ended at least 1 s before the onset of the movement,

thereby ensuring that the baseline was not contaminated by the movement itself or by stimulus-related activity (cf. epoching of data described in the section 'Preprocessing of the recorded data'). The first 200 ms of the trial intervals were cut in both conditions to make sure that edge effects from the wavelet transform did not distort the baseline.

Results

Amplitude and PLI were computed from single-trial data in the frequency range from 2 to 48 Hz using Morlet wavelet functions as implemented in SPM 12 (Friston et al., 2006).

Amplitude dynamics

First, we investigated the amplitudes (power) of the wavelet transforms (cf. Material and methods) near the onset of the movement.

Fig. 2 shows the changes in amplitude with respect to the baseline in self-initiated tapping (A) and visually-cued tapping (B) with the right (top rows) and left (bottom rows) index finger at the electrodes C3 (lM1) and C4 (rM1) in the frequency range 2-48 Hz. A decrease of power in the α and β frequency bands around movement onset and during the movement can clearly be discerned in both conditions and for both hands. Additionally, an increase of power in these frequency bands upon termination of the movement can be observed in both tapping conditions at the electrode contralateral to the moving hand (i.e., C3 for right hand and C4 for left hand tapping). At the electrode ipsilateral to the moving hand, no or only a weak increase in the α and β amplitude band can be seen. Finally, an increase in amplitude in the δ-θ frequency band around movement onset can be observed at the electrode contralateral to the moving hand in both tapping conditions. This increase was also observed at the electrode ipsilateral to the moving hand in the visually-cued tapping condition.

In summary, our results replicate the well-known event-related desynchronization (ERD) and event-related synchronization (ERS) related to the onset and the termination of the movement in the α, β, and the low frequency bands (e.g., Pfurtscheller and da Silva, 1999; Neuper et al., 2006) and underpin the validity of our dataset.

Phase dynamics

Next, we investigated the phases of the wavelet transforms (cf. Material and methods) and their dynamics near the onset of the movement. Fig. 3 shows the group average of the PLI over 18 participants in the frequency range 2-48 Hz at the electrode C4 in the self-initiated (A), and the visually-cued tapping condition (B) when tapping was done with the left hand. As this figure reveals, PLI changed only in the δ-θ frequency band (2-7 Hz) around the onset of the movement. Hence, we restricted our further investigations to this frequency band. In Fig. 4, the group average of the PLI over 18 participants for all 61 channels are displayed for the self-initiated (A,B) and visually-cued (C,D) tapping condition (A,C: left hand tapping, B,D: right hand tapping). Each small panel is placed according to the position of the corresponding EEG electrode. In each of them, the PLI obtained from the EEG signal that was recorded by the corresponding electrode is shown. In the panels, the horizontal axis is the time and the vertical axis is the frequency from 2 Hz to 7 Hz. An increase of PLI can clearly be discerned around the onset of the movement at the central electrodes, which are located close to the motor regions, in both conditions (Fig. 4A-D), as well as at the electrodes lying above the occipital regions in the visually-cued condition (Fig. 4C-D).

As described in the Material and Methods section, we selected the electrodes C1-C4, FC3-FC4, FCz, and Cz, i.e. the central electrodes, which are located close to the motor regions, in order to perform a more detailed analysis. Visual activity in the visually-cued tapping condition was recorded and monitored at the electrode Oz. Fig. 5 illustrates, how PLI changed at the aforementioned

electrodes. In all panels of Fig. 5, the horizontal axis is the time interval [-1000, 1000] ms around the onset of the movement (determined by the accelerometer signal), which is marked by a black, vertical line at $t = 0$. The vertical axis is the frequency f in the δ-θ band (2-7 Hz). PLI is shown in color-coded form at a given time t and frequency f. Figs. 5A and 5B display the results for the self-initiated tapping condition performed with the left or right hand, respectively. Figs. 5C and 5D show the equivalent data for the visually-cued tapping condition. As illustrated, PLI increases before the onset of the movement in all movement conditions for both left and right finger tapping. Furthermore, in both conditions, the maximum PLI values are highest at the electrodes lying above the SMA (electrode Cz) and above the primary motor cortex (M1) contralateral to the moving hand. These are the electrodes C2, C4 for left and C1, C3 for right finger movements, respectively. In the visually-cued tapping condition, PLI was larger than in the self-initiated tapping condition.

To test whether this finding is a statistically significant result, we carried out a simple statistical analysis of the data. We calculated the average value of PLI over the frequency band 2-7 Hz in both conditions. The results are displayed in Fig. 6. The horizontal axis represents time, while the vertical axis shows the average values of PLI at each instant of time. Fig. 6A shows the PLIs as functions of time in self-initiated tapping in blue and those in visually-cued tapping in green for left hand tapping. Analogous results are displayed in Fig. 6B for right hand tapping. In both sets of panels, the onset of the movement is at $t = 0$. We then performed a pointwise t-test on each of the average PLI curves in both (self-initiated and visually-cued tapping) conditions. We compared PLI obtained in each of these conditions with the corresponding baseline at the significance level of $p \leq 0.05$ with FDR correction for multiple comparisons. Intervals with significant differences to baseline are marked in red for the self-initiated condition and in blue for the visually-cued condition. The results clearly reveal that the intervals in which PLI was significantly different from baseline were longer in the visually-cued

tapping condition than in the self-initiated tapping condition at most of the electrodes. It can be seen that at all nine electrodes, the interval of significant difference started earlier in visually-cued tapping than in self-initiated tapping, and in most of them it also finished later.

In summary, these results show that PLI was significantly different from its baseline value in a time interval around the onset of the movement at all electrodes of interest, in both conditions, and for both hands (except of course at Oz in the self-initiated tapping condition, because of the lack of the visual stimulus). This means that in both conditions, the neural activity in the respective areas of the motor cortex (i.e. PM, SMA and M1) had already been highly synchronized before the movement was executed. Furthermore, the presence of the visual stimulus in the visually-cued condition increased the time of neural synchrony in the motor cortex before and after movement execution.

Hemispheric dependence of PLI

Having confirmed that neural synchrony in the regions of the motor cortex was significantly enhanced around movement onset in both conditions, we next investigated whether the PLI exhibited spatial differences.

To assess inter-hemispheric differences in EEG activity, we computed a lateralization index (LI) (Deiber et al., 2012). With regard to PLI, it measures the cumulative asymmetry between the PLI values in the right and left hemisphere. It is defined as follows:

$$LI = \frac{\left[PLI_{C4,left} - PLI_{C3,left}\right] + \left[PLI_{C3,right} - PLI_{C4,right}\right]}{2}$$

Here $\mathrm{PLI}_{C4,left}$ is the value of PLI at the electrode C4 when the tapping is done with the left hand. The other $\mathrm{PLI}_{Cx,h}$ ($x = 3, 4$, $h = left$, or $right$) quantities are defined analogously. Fig. 7 illustrates the time course of *LI* in both tapping conditions in the interval 500 ms before until 700 ms after the

start of the motor action ($t = 0$). The blue curve corresponds to self-initiated tapping, and the green one to visually- cued tapping. The figure shows that the cumulative asymmetry (*LI*) of the function of the hemispheres is large and about of the same size in the interval [-500, 700] ms in both conditions. This means that phase locking was stronger in the motor regions, in particular M1, contralateral to the moving hand in a time interval around the motor action in both the self-initiated and the visually-cued tapping condition.

Furthermore, when the tapping was performed with the left hand, phase locking was strongest at electrode C4 (rM1) in both conditions (cf. Fig. 6). An analogous result holds true when tapping was done with the right hand. In this case, the strongest effect occurred at C1 (lM1) and Cz (SMA) in both conditions. The strength of phase locking was defined by the length of the time interval in which PLI was significantly different from its baseline as well as by its maximum value (cf. Fig. 6). In both conditions and for both hands, these intervals started already approximately 400-500 ms before the onset of the movement at the electrodes C1 and C4, which lie above the left and right M1.

In summary, our results suggest that phase locking in the δ-θ frequency band is a neural marker of movement execution, since it remains unchanged despite differences in the functional networks involved in the initiation of a movement. We further suggest that this enhanced synchronization before the start of an action paves the way for distinct active cortical pathways to converge onto the common motor output. The synchronization thus establishes the basis necessary for the activation of the processes that generate the actual movement. The activation was therefore always the strongest in M1 contralateral to the moving hand.

Effect of the visual stimulus on PLI

In order to verify that PLI found in the motor cortex in the visually-cued tapping condition was not solely due to visual stimulation, we compared the PLI in the visually-cued tapping condition with that in the vision-only condition in the time interval [-2000, 1500] ms with respect to the onset of

559 the visual stimulation ($t = 0$). This test was necessary to ensure that a pure
560 motor effect common to externally or internally triggered movements was
561 identified.

562 Fig. 7 exhibits the differences in the PLI values in the 2-30 Hz frequency
563 band at the electrodes Oz, C4, and C3 in the vision-only condition with left-
564 pointing arrow (left column) and in the visually-cued tapping condition with
565 left hand tapping (right column). Phase locking appears not only in the δ-θ
566 frequency band, but also in the α and β frequency bands. Here $t = 0$ is the
567 onset of stimulation. It is evident from this figure that the PLI was
568 significantly larger in the motor cortex (cf. C4 and C3) in the visually-cued
569 tapping condition than in the vision-only condition (t-test, $p \leq 0.05$ FDR
570 corrected). The large signals in the motor cortex (C4, C3) are therefore
571 unlikely to result from effects of the visual stimulation, only.

572
573
574 *The relation of PLI to behavior*
575
576

577 Next, we tested whether the observed increase in neural synchronization within
578 the regions of the motor cortex or the occipital regions could be linked to the
579 behavioral performance of the individual subjects. To this end, processing time
580 (PT) was defined as the time that elapsed from the onset of the stimulus until
581 the onset of the movement (defined by the accelerometer) and movement time
582 (MvT) as the time from the onset of the movement to the button press (cf.
583 Fig. 1B). In the visually-cued tapping condition, a significant correlation
584 between the individual PTs of the 18 participants and the maximum PLI
585 values was found in the occipital region (Oz) (Pearson, left p=0.0145 and right
586 p=0.0429, respectively). This underpins the physiological validity of the data,
587 since the visual stimulus was processed in this brain region.

588 Furthermore, we found a significant correlation between the MvTs of the 18
589 participants and the maximum values of PLI obtained from the EEG at the
590 electrode C1 and C2 for left hand tapping (Pearson, p=0.0332) and for right
591 hand tapping (Pearson, p=0.0087), respectively, in the self-initiated tapping

condition. This means that the stronger the phase locking preparing the movement in a given motor region, the faster the movement performed with the contralateral hand.

Discussion

The objective of the current study was to identify EGG markers related to the mechanisms involved in the precise timing of the neural signals underlying isolated finger movements. We hypothesized that such neural markers would be specific forms of synchronization dynamics that are invariant in the functional networks irrespective of the initiation of an action. To this end, we carried out EEG recordings on 18 right-handed young healthy human subjects who had to perform simple motor tasks probing internal and external initiation of finger movements. We used a rather simple task, since it has the advantage of being simple enough to be used in studies of both healthy subjects and patients suffering from neurological disorders affecting the motor system.

We analyzed the EEG recordings with respect to changes in amplitude (power) and phase locking index (PLI) over the trials in each subject for every instant of the sampled time and at every integer frequency in the frequency band 2-48 Hz. We found that in the δ-θ frequency band PLI was significantly different from its baseline value in a time interval around the onset of the movement at all electrodes of interest (C1-C4, FC3-FC4, and FCz, Cz and Oz), in both conditions and for both hands (except, of course, at Oz in the self-initiated tapping condition, because of the lack of the visual stimulus). We furthermore found, by calculating the lateralization index LI, that this phase locking was stronger in the motor regions contralateral to the moving hand in both the self-initiated and the visually-cued tapping condition. This phase locking cannot be attributed to the effects of sensory feedback from the tapping, since the PLI started to become significantly different from baseline in the primary motor area 500 ms before the onset of the movement, i.e.,

about 600 ms before the button press. The significant presence of PLI in the visually-cued tapping condition was not due to the visual stimulus alone, since phase locking was stronger at the electrodes lying above the motor regions in the visually-cued than in the vision-only condition at the onset of the stimulus. One can therefore regard those changes of PLI in the EEG signals as general markers of movement execution, which are present irrespective of how the motor action is initiated and which hand is used.

The analysis of phase locking properties in the EEG data constitutes a novel finding of our work. The widely known bio-markers of movement preparation and execution (e.g., Pfurtscheller and da Silva, 1999; Neuper et al., 2006) are based on changes of amplitudes (ERD and ERS), only, and do not take phase-locking effects into account. Our results replicate the well-known event-related-desynchronization (ERD) and event-related-synchronization (ERS) related to the onset and the termination of the movement in the power of the α and β and the lower frequency bands (e.g., Gerloff et al., 1998; Pfurtscheller and da Silva, 1999; Luu and Tucker, 2001; Neuper et al., 2006) and thereby demonstrate the physiological validity of our data. However, our results strongly support the importance of calculating the phase in addition to the amplitude when investigating event-related changes of brain activity.

It remains to be tested whether this newly identified neural marker of movement execution, i.e., the increase of the PLI around movement onset, is (i) effector dependent, and (ii) dependent on actual physical execution. Pfurtscheller and colleagues, for instance, intensively investigated changes in amplitudes of EEG/MEG signals during motor preparation, execution and imagery of internally and externally triggered index finger, thumb, hand and foot movements (e.g., Pfurtscheller and da Silva, 1999, Neuper and Pfurtscheller, 2001; Pfurtscheller, 2001; Neuper et al. 2006; Pfurtscheller et al. 2006). ERD/ERS were identified as generally occurring effects in all of those movements. However, the changes in amplitude differed depending on the electrodes as well as the frequency bands at which the ERD and ERS effects were apparent.

654 A relationship between decision making and EEG activity in the δ-θ
655 frequency band (2-7 Hz) has recently been established (e.g. Cohen and Donner,
656 2013). However, previous studies investigating EEG activity during finger tapping
657 tasks (Gerloff et al., 1998; Zhao et al., 2014) did not report a phase locking of
658 EEG signals in the δ-θ band. Recently, Igarashi et al. (2013) showed that θ
659 oscillations play a part in the neuronal coordination during motor activity, in
660 particular motor planning and output, albeit in the rat. The authors
661 demonstrated a close (functional) connection between θ oscillation and layer-
662 dependent firing of cortical neurons (at high and low β frequencies). These
663 data, at least indirectly, support our results concerning the role of δ-θ
664 oscillations as markers of human motor actions.
665 As far as the physiological significance of our results, i.e., the enhanced
666 synchronization just before the start of the motor action, is concerned, we
667 hypothesize that the spike rate of the motor neurons projecting from M1 to the
668 spinal cord increases at a certain preferred phase angle of the δ-θ cycle. This
669 concept is illustrated in Fig. 9. Here the cosine of the phase of each trial k is
670 shown for all trials of one subject at a frequency of 3 Hz (with maximal PLI)
671 in the visually-cued tapping condition. The red line indicates the time at which
672 we expect this increase in the spike rate to occur, i.e., the instant of time at which
673 the command to move the finger is send from M1 to the spinal cord, which is
674 $\approx$ 50 ms before the onset of the movement.
675 This interpretation is in line with a study by Lee et al. (2005) who
676 investigated local field potentials and single unit activity from multi-electrodes
677 placed in the extrastriate visual cortex of monkeys while the animals were
678 performing a working memory task. The authors found that θ oscillations had a
679 systematic effect on single neuron activity, with neurons emitting more action
680 potentials near their preferred phase angle of each θ cycle. Lee and colleagues
681 therefore suggested that extrastriate visual cortex is involved in short-term
682 storage of information and that θ oscillations provide a mechanism for
683 structuring the interaction between neurons in different brain regions that

underlie working memory.

Finally, we suggest that phase locking in the δ-θ frequency band, being most pronounced in M1 contralateral to the moving hand, constitutes a mechanism by which distinct active cortical pathways, which initiate voluntary and stimulus-triggered movements, converge to the common motor output. This mechanism may thus form the basis for the activation of the appropriate muscles, via the motor neurons, to perform the movement.

References

Baker S, Olivier E, Lemon R (1997) Coherent oscillations in monkey motor cortex and hand muscle EMG show task-dependent modulation. J Physiology 501:225–241.

Baker S, Spinks R, Jackson A, Lemon R (2001) Synchronization in monkey motor cortex during a precision grip task. i. task-dependent modulation in single-unit synchrony. J Neurophysiol 85:869–885.

Benjamini Y, Hochberg Y (1995) Controlling the false discovery rate: a pratical and powerful approach to multiple testing. Journal of the Royal Statistical Society B57(1):289–300.

Blinowska K, Durka P (1994) The application of wavelet transform and matching pursuit to the time-varying EEG signals. Intell engineering systems through artificial neural networks 4:535–540.

Cohen MX, Donner TH (2013) Midfrontal conflict-related theta-band power reflects neural oscillations that predict behavior. J Neurophysiology 110:2752–2763.

Deiber MP, Sallard E, Ludwig C, Ghezzi C, Barral J, Ibañez V (2012) EEG alpha activity reflects motor preparation rather than the mode of action

718 selection. Front Integrative Neuroscience 6: 59
719
720 Delorme A, Makeig S (2004) EEGLab: an open source toolbox for
721 analysis of single-trial EEG dynamics including independent component
722 analysis. J Neuroscience Methods 134:9–21.
723
724 Friston KJ, Ashburner JT, Kiebel SJ, Nichols TE, Penny WD (2006)
725 Statistical parametric mapping: the analysis of functional brain images. Elsevier,
726 London.
727
728 Gerloff C, Richard J, Hadley J, Schulman AE, Honda M, Hallett M (1998)
729 Functional coupling and regional activation of human cortical motor areas
730 during simple, internally paced and externally paced finger movements. Brain
731 121:1513–1531.
732
733 Gerloff C., Uenishi N, Nagamine T, Kunieda T, Hallett M, et al. (1998)
734 Cortical activation during fast repetitive finger movements in humans: steady-
735 state movement-related magnetic fields and their cortical generators.
736 Electroencephalogr Clin Neurophysiol 109:444-453.
737
738 Herrmann C, Busch N, Grigutsch M (2005) EEG oscillations and wavelet
739 analysis. In: Event-related potentials: A methods handbook (Handy TC, ed),
740 pp229-259, Cambridge: MIT press.
741
742 Herz DM, Christensen MS, Reck C, Florin E, Barbe MT, Stahlhut C,
743 Pauls KAM, Tittgemeyer M, Siebner HR, Timmermann L (2012) Task-
744 specific modulation of effective connectivity during two simple uni-manual
745 motor tasks: a 122-channel EEG study. Neuroimage 59:3187–3193.
746
747 Hughes G, Schütz-Bosbach S, Waszak F (2011) One action system or
748 two? Evidence for common central preparatory mechanisms in voluntary and
749 stimulus-driven actions. J Neurosci 31:16692–16699.
750
751 Hyvärinen A, Karhunen J, Oja E (2004) Independent component analysis,

752 Vol. 46 John Wiley & Sons.
753
754 Igarashi J, Isomura Y, Arai K, Harukuni R, Fukai T (2013) A θ–γ
755 oscillation code for neuronal coordination during motor behavior. J Neurosci
756 33:18515–18530.
757
758 Jenkins IH, Jahanshahi M, Jueptner M, Passingham RE, Brooks DJ. (2000)
759 Self-initiated versus externally triggered movements. Brain 123:1216–1228.
760
761 Jung TP, Makeig S, Humphries C, Lee TW, Mckeown MJ, Iragui V,
762 Sejnowski TJ (2000a) Removing electroencephalographic artifacts by blind
763 source separation. Psychophysiol 37:163–178.
764
765 Jung TP, Makeig S, Westerfield M, Townsend J, Courchesne E,
766 Sejnowski TJ (2000b) Removal of eye activity artifacts from visual event-
767 related potentials in normal and clinical subjects. Clin Neurophysiol 111:1745–
768 1758.
769
770 Keil A, Elbert T, Taub E (1999) Relation of accelerometer and EMG
771 recordings for the measurement of upper extremity movement. J Psychophysiol
772 13:77.
773
774 Krieghoff V, Waszak F, Prinz W, Brass M (2011) Neural and behavioral
775 correlates of intentional actions. Neuropsychol 49:767–776.
776
777 Lachaux JP, Rodriguez E, Martinerie J, Varela FJ et al. (1999)
778 Measuring phase synchrony in brain signals. Hum Brain Mapping 8:194–208.
779
780 Langlois D, Chartier S, Gosselin D (2010) An introduction to
781 independent component analysis: Infomax and fastica algorithms. Tutorials
782 Quant Methods for Psychol 6:31–38.
783
784 Lee H, Simpson GV, Logothetis NK, Rainer G (2005) Phase locking of
785 single neuron activity to theta oscillations during working memory in monkey

786 extrastriate visual cortex. Neuron 45:147 – 156.
787
788 Luu P, Tucker DM (2001) Regulating action: alternating activation of midline
789 frontal and motor cortical networks. Clin Neurophysiol 112:1295-1306.
790
791 McFarland DJ, McCane LM, David SV, Wolpaw JR (1997) Spatial filter
792 selection for EEG-based communication. Electroencephalogr Clinical
793 Neurophysiol 103:386–394.
794
795 Michel CM, Murray MM, Lantz G, Gonzalez S, Spinelli L, de Peralta
796 RG (2004) EEG source imaging. Clin Neurophysiology 115:2195–2222.
797
798 Michely J, Barbe MT, Hoffstaedter F, Timmermann L, Eickhoff SB,
799 Fink GR, Grefkes C (2012) Differential effects of dopaminergic medication on
800 basic motor performance and executive functions in parkinson's disease.
801 Neuropsychol 50:2506–2514.
802
803 Mognon A, Jovicich J, Bruzzone L, Buiatti M (2011) Adjust: An
804 automatic EEG artifact detector based on the joint use of spatial and temporal
805 features. Psychophysiol 48:229–240.
806
807 Neuper C, Wörtz M, Pfurtscheller G (2006) ERD/ERS patterns
808 reflecting senso-rimotor activation and deactivation In: Event-Related
809 Dynamics of Brain Oscillations (Neuper C, Klimesch W, eds), pp211-222, Vol.
810 159 of Progress in Brain Research. Elsevier.
811
812 Neuper C, Pfurtscheller G (2001) Event-related dynamics of cortical rhythms:
813 frequency-specific features and functional correlates. International Journal of
814 Psychophysiology 43:41-58.
815
816 Oldfield RC (1971) The assessment and analysis of handedness: The
817 Edinburgh Inventory. Neuropsychol 9:97-113.
818
819 Perrin F, Pernier J, Bertrand O, Echallier J (1989) Spherical splines for

scalp potential and current density mapping. Electroencephalogr Clinical Neurophysiology 72:184-187.

Pfurtscheller G (2001) Functional brain imaging based on ERD/ERS. Vision Research 41:1257-1260.

Pfurtscheller G, da Silva FL (1999). Event-related EEG/MEG synchronization and desynchronization: basic principles. Clin Neurophysiol 110:1842-1857.

Pfurtscheller G, Brunner C, Schlögl A, da Silva FL (2006) Mu rhythm (de)synchronization and EEG single-trial classification of different motor imagery tasks. NeuroImage 31:153-159.

Sanei S, Chambers JA (2013) EEG signal processing John Wiley & Sons.

Shibasaki H, Hallett M (2006) What is the Bereitschaftspotential? Clin Neurophysiol 117:2341–2356.

Tass PA (2007) Phase resetting in medicine and biology: stochastic modelling and data analysis, Vol. 172 Springer Science & Business Media.

Uhlhaas PJ, Roux F, Rodriguez E, Rotarska-Jagiela A, Singer W (2010) Neural synchrony and the development of cortical networks. Trends Cogn Sci 14:72 – 80.

Wang Y, Hong B, Gao X, Gao S (2006) Phase synchrony measurement in motor cortex for classifying single-trial EEG during motor imagery. In: Engineering in Medicine and Biology Society. EMBS'06. 28th Annual International Conference of the IEEE, p. 75–78. IEEE.

Waszak F, Wascher E, Keller P, Koch I, Aschersleben G, Rosenbaum D, Prinz W (2005) Intention-based and stimulus-based mechanisms in action selection. Exp Brain Res 162:346–356.

Witt ST, Laird AR, Meyerand ME (2008) Functional neuroimaging correlates of finger-tapping task variations: an ALE meta-analysis. Neuroimage 42:343–356.

Wyatt HJ (1998) Detecting saccades with jerk. Vision Research 38:2147-2153.

Zhao K, Gu R, Wang L, Xiao P, Chen YH, Liang J, Hu L, Fu X (2014) Voluntary pressing and releasing actions induce different senses of time: Evidence from event-related brain responses. Sci Reports 4.

Figure legends

Fig. 1

(A) Scheme of organization of the experiments. See text for further details.
(B) Typical trial epoched with respect to movement onset or visual stimulus. The visual stimulus was applied in the interval [-519, -245] ms with respect to the start of the motor action. Pressing the button in both cases took place in the interval [62, 98] ms after the onset of the movement.

Fig. 2

Group average of the amplitude over 18 participants in the frequency range 2-48 Hz at the electrodes C3 and C4 in the self-initiated tapping condition (A) when tapping was done with the right (top row) or left hand (bottom row) and in the visually-cued tapping condition (B) when tapping was done with the right (top row) or left hand (bottom row).
The onset of the movement as determined by the accelerometer is marked by a black vertical line.

Fig. 3

Group average of the phase locking index over 18 participants in the frequency

range 2-48 Hz in the self-initiated (A) and the visually-cued tapping condition (B) at electrode C4.

The onset of the movement as determined by the accelerometer is marked by a black vertical line.

Fig. 4

Phase locking index at all channels in self-initiated tapping with the left hand (A) or right hand (B); and in visually-cued tapping with the left hand (C) or right hand (D). In all panels, the horizontal axis is time in the interval [-1400, 1400] ms, and the vertical axis is frequency in the δ-θ band (2-7 Hz). The onset of the movement, as determined by the accelerometer, is set to $t = 0$. The color bar is the same as in Fig. 2.

Fig. 5

Phase locking index at the electrodes of interest. Their locations are above different regions of the motor cortex. C2,C4: right primary motor area (rM1); C1,C3: left primary motor area (lM1); FC3: left pre-motor area (lPM); FC4: right pre-motor area (rPM); FCz,Cz: supplementary motor area (SMA); Oz: primary visual area V1. Self-initiated tapping with the left hand (A) or the right hand (B). Visually-cued tapping with the left hand (C) or the right hand (D). In all panels, the horizontal axis is the time in the interval [-1000, 1000] ms; the black vertical line represents the onset of the movement, $t = 0$. The vertical axis is the frequency in the band 2-7 Hz. The value of the phase locking index is shown by means of a color-coded scale (below the panels). The edge effects of PLI reach until 8-10 Hz at some of the electrodes in this condition.

Fig. 6

Average PLIs over the 2-7 Hz frequency band in visually-cued tapping (green curves), and in self-initiated tapping (blue curves). The time intervals of statistical significance ($p \leq 0.05$, FDR corrected) are determined by the red

shaded regions in self-initiated tapping, and by the light-blue shaded regions in visually-cued tapping. Left hand tapping (A), right hand tapping (B). The horizontal-axis is the same as in Fig. 4. The vertical axis shows the values of the phase locking index.

Fig. 7

The lateralization index related to the phase locking index in self-initiated (blue curve), and in visually-cued tapping (green curve) at the electrodes C3 and C4. The coordinate axes are the same as in Fig. 4. For further explanation, please, see text.

Fig. 8

Phase locking index around the onset of the visual stimulus ($t = 0$) at the electrodes Oz, C4, and C3 in the vision-only condition with left-pointing arrow (left column), and in the visually-cued tapping condition with left hand tapping (right column). Time is again on the x-axis and frequency (2-30 Hz) on the y-axis.

Fig. 9

The cosine of the phase φ derived from the individual trials k of the EEG data of a single participant at a frequency of 3 Hz at the electrode C4 for self-initiated tapping with the left hand.

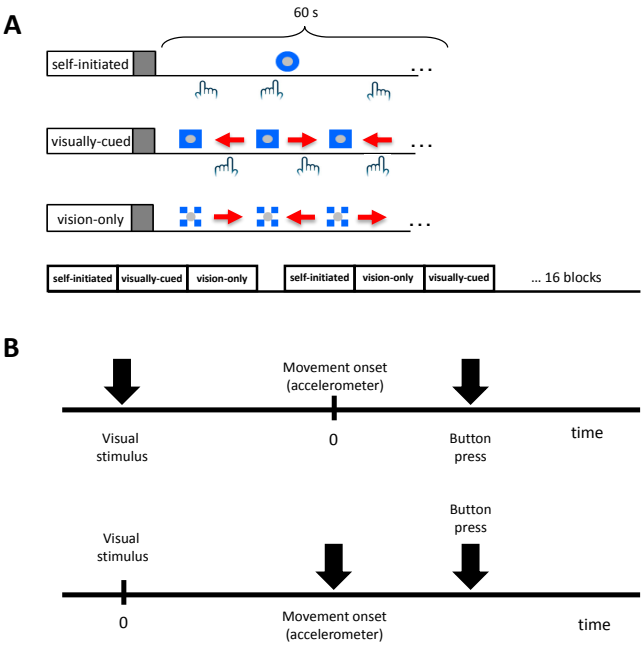
A
60 s
self-initiated
visually-cued
vision-only
self-initiated
visually-cued
vision-only
self-initiated
vision-only
visually-cued
... 16 blocks
B
Movement onset
(accelerometer)
Visual
stimulus
0
Button
press
time
Button
press
Visual
stimulus
0
Movement onset
(accelerometer)
time

Figure 1

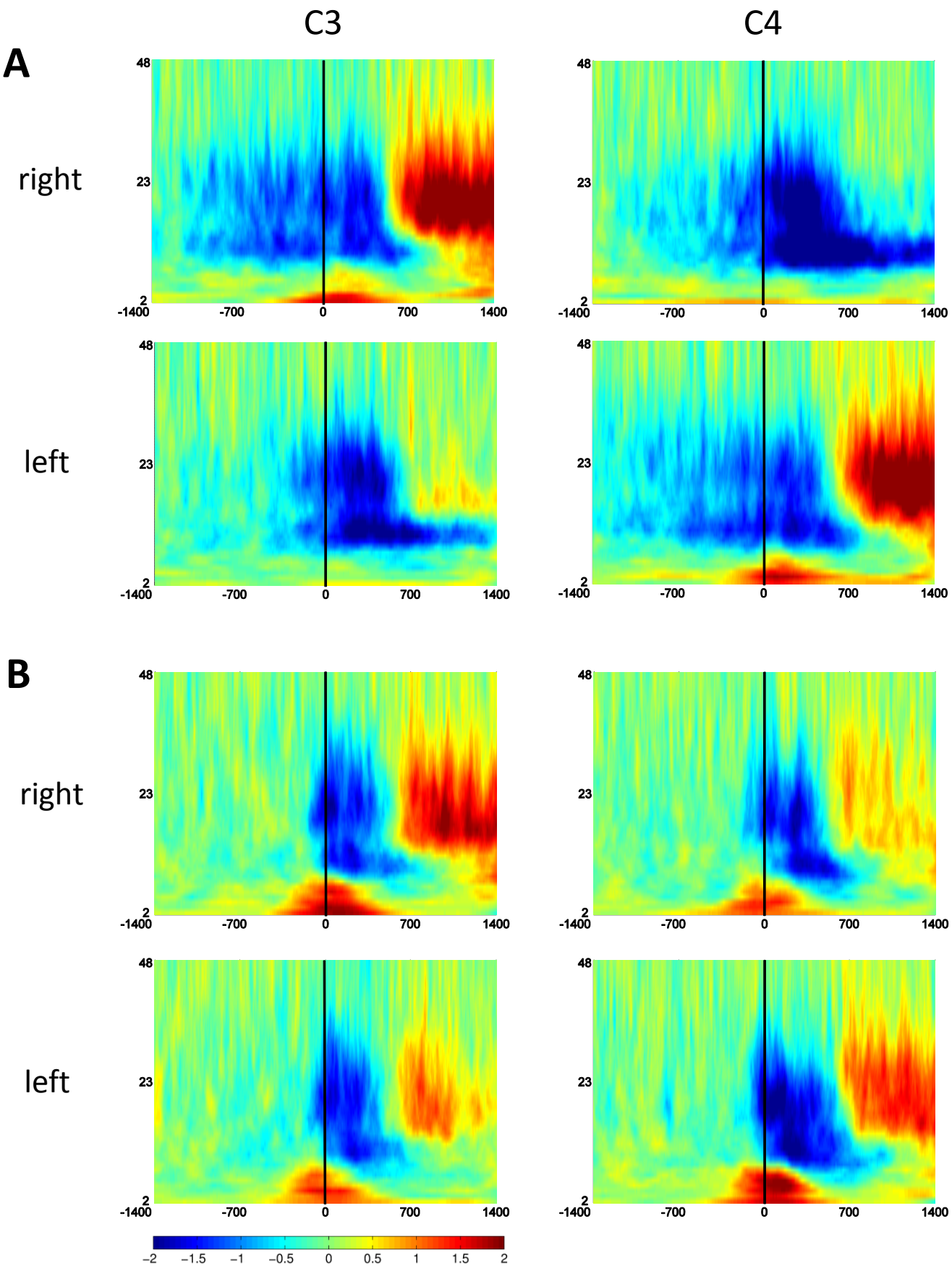
C3
C4
A
right
left
B
right
left
48
23
2
-1400
-700
0
700
1400
−2
−1.5
−1
−0.5
0
0.5
1
1.5
2

Figure 2

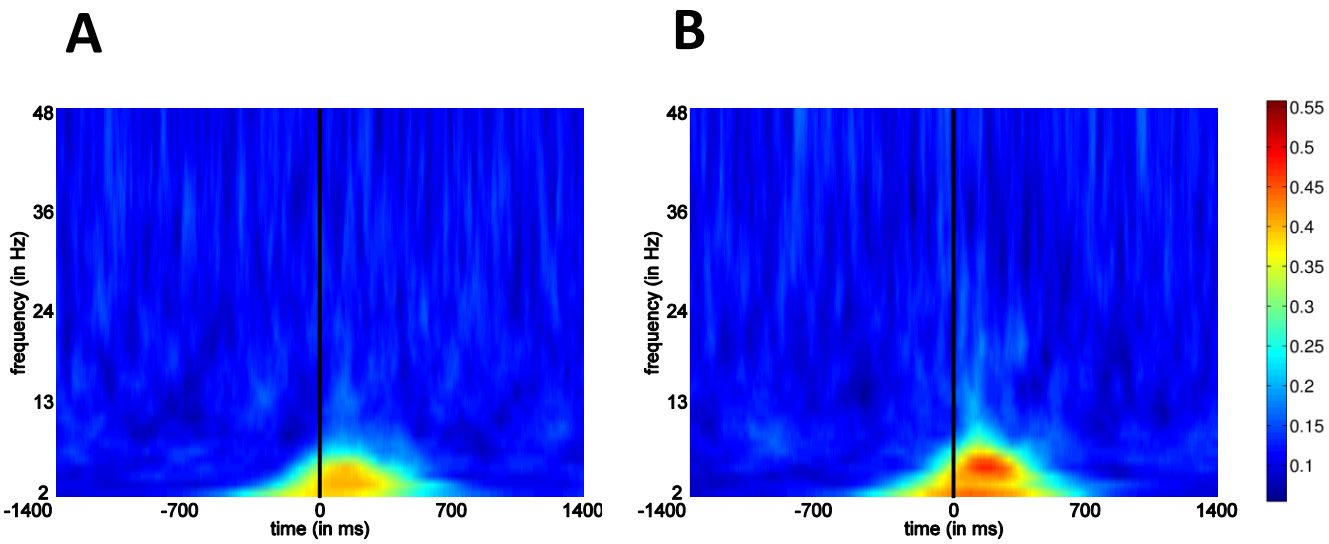
A
B
48
36
24
13
2
frequency (in Hz)
-1400
-700
0
700
1400
time (in ms)
0.55
0.5
0.45
0.4
0.35
0.3
0.25
0.2
0.15
0.1

Figure 3

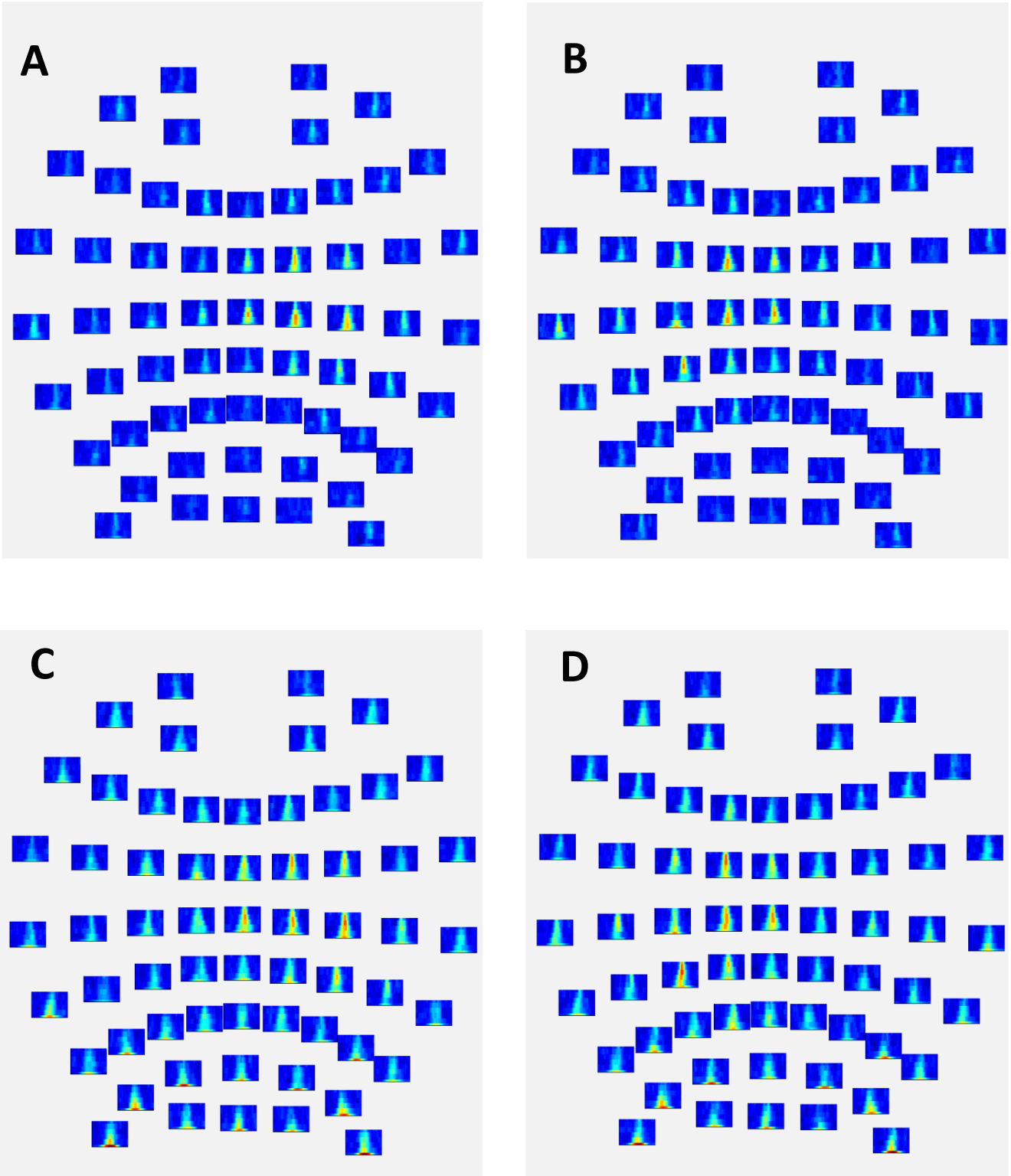

Figure 4

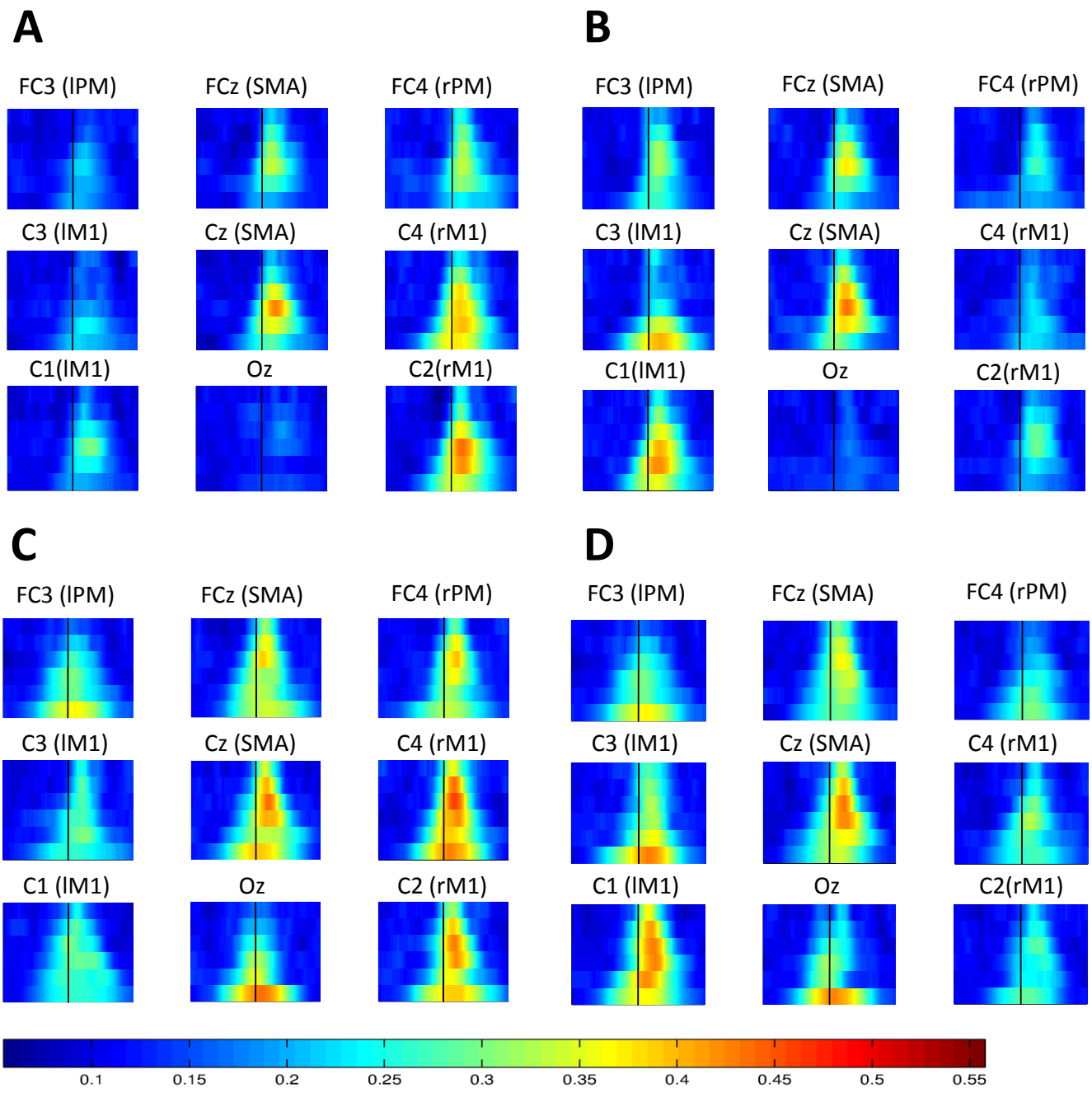
A
FC3 (lPM)
FCz (SMA)
FC4 (rPM)
C3 (lM1)
Cz (SMA)
C4 (rM1)
C1(lM1)
Oz
C2(rM1)
B
FC3 (lPM)
FCz (SMA)
FC4 (rPM)
C3 (lM1)
Cz (SMA)
C4 (rM1)
C1(lM1)
Oz
C2(rM1)
C
FC3 (lPM)
FCz (SMA)
FC4 (rPM)
C3 (lM1)
Cz (SMA)
C4 (rM1)
C1 (lM1)
Oz
C2 (rM1)
D
FC3 (lPM)
FCz (SMA)
FC4 (rPM)
C3 (lM1)
Cz (SMA)
C4 (rM1)
C1 (lM1)
Oz
C2(rM1)
0.1
0.15
0.2
0.25
0.3
0.35
0.4
0.45
0.5
0.55

Figure 5

A

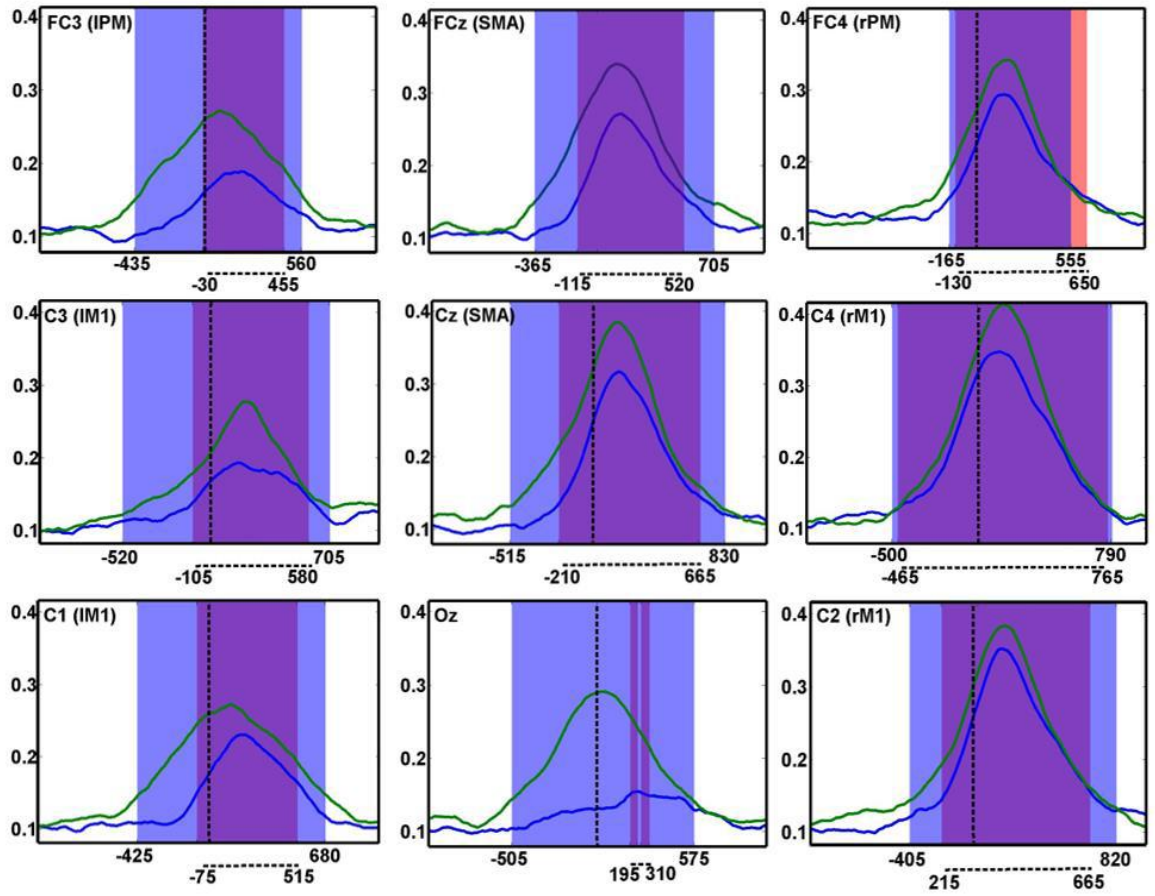
FC3 (IPM)
-435 560
-30 455
FCz (SMA)
-365 705
-115 520
FC4 (rPM)
-165 555
-130 650
C3 (IM1)
-520 705
-105 580
Cz (SMA)
-515 830
-210 665
C4 (rM1)
-500 790
-465 765
C1 (IM1)
-425 680
-75 515
Oz
-505 575
195 310
C2 (rM1)
-405 820
215 665

B

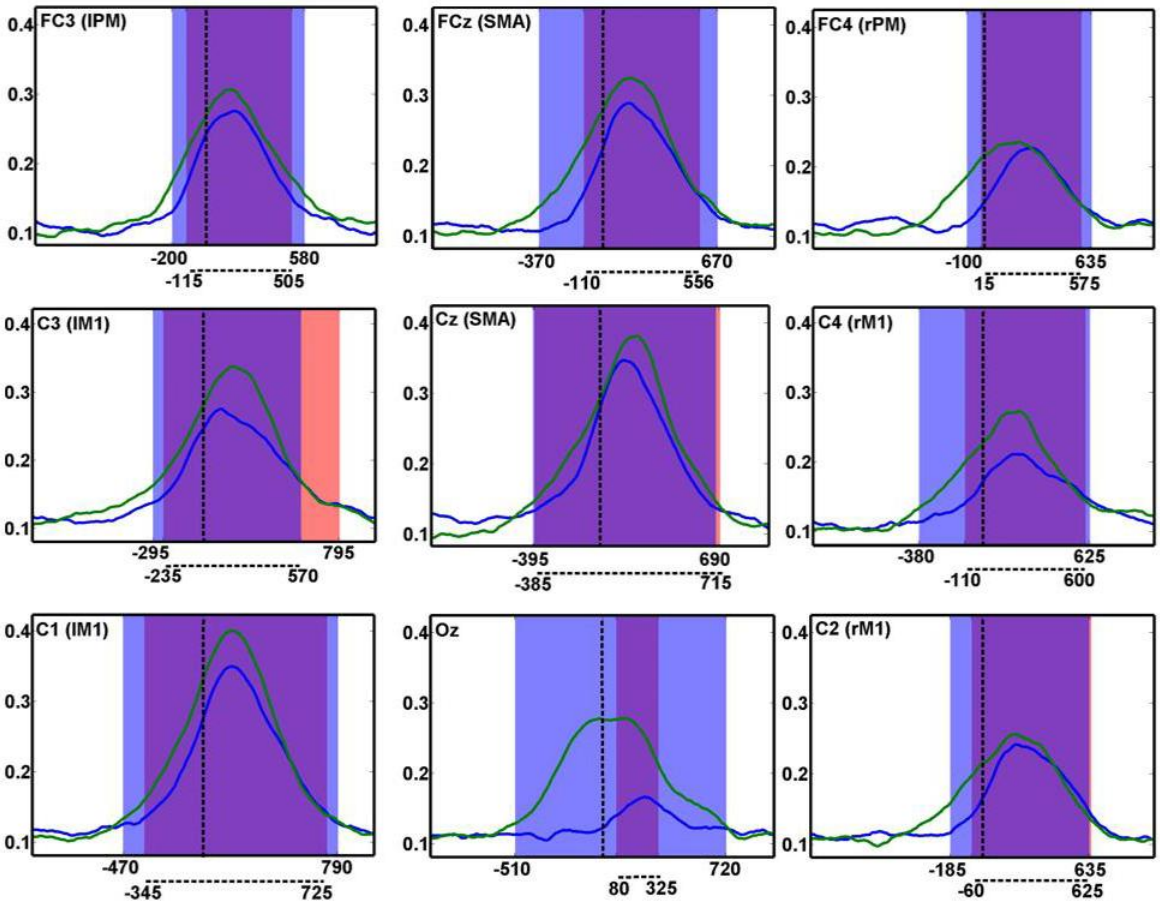
FC3 (IPM)
-200 580
-115 505
FCz (SMA)
-370 670
-110 556
FC4 (rPM)
-100 635
15 575
C3 (IM1)
-295 795
-235 570
Cz (SMA)
-395 690
-385 715
C4 (rM1)
-380 625
-110 600
C1 (IM1)
-470 790
-345 725
Oz
-510 720
80 325
C2 (rM1)
-185 635
-60 625

Figure 6

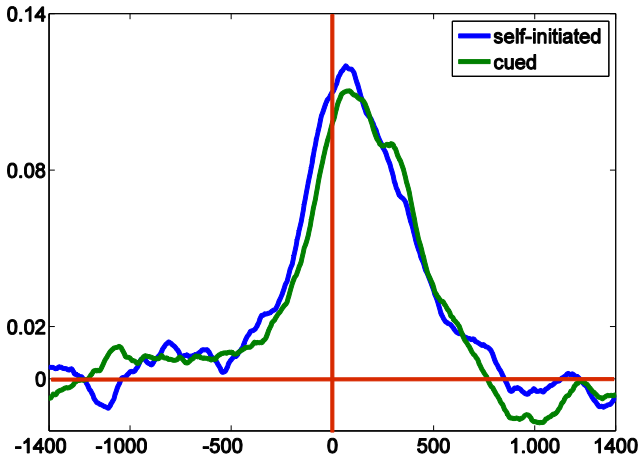
0.14
0.08
0.02
0
-1400
-1000
-500
0
500
1.000
1400
self-initiated
cued

Figure 7

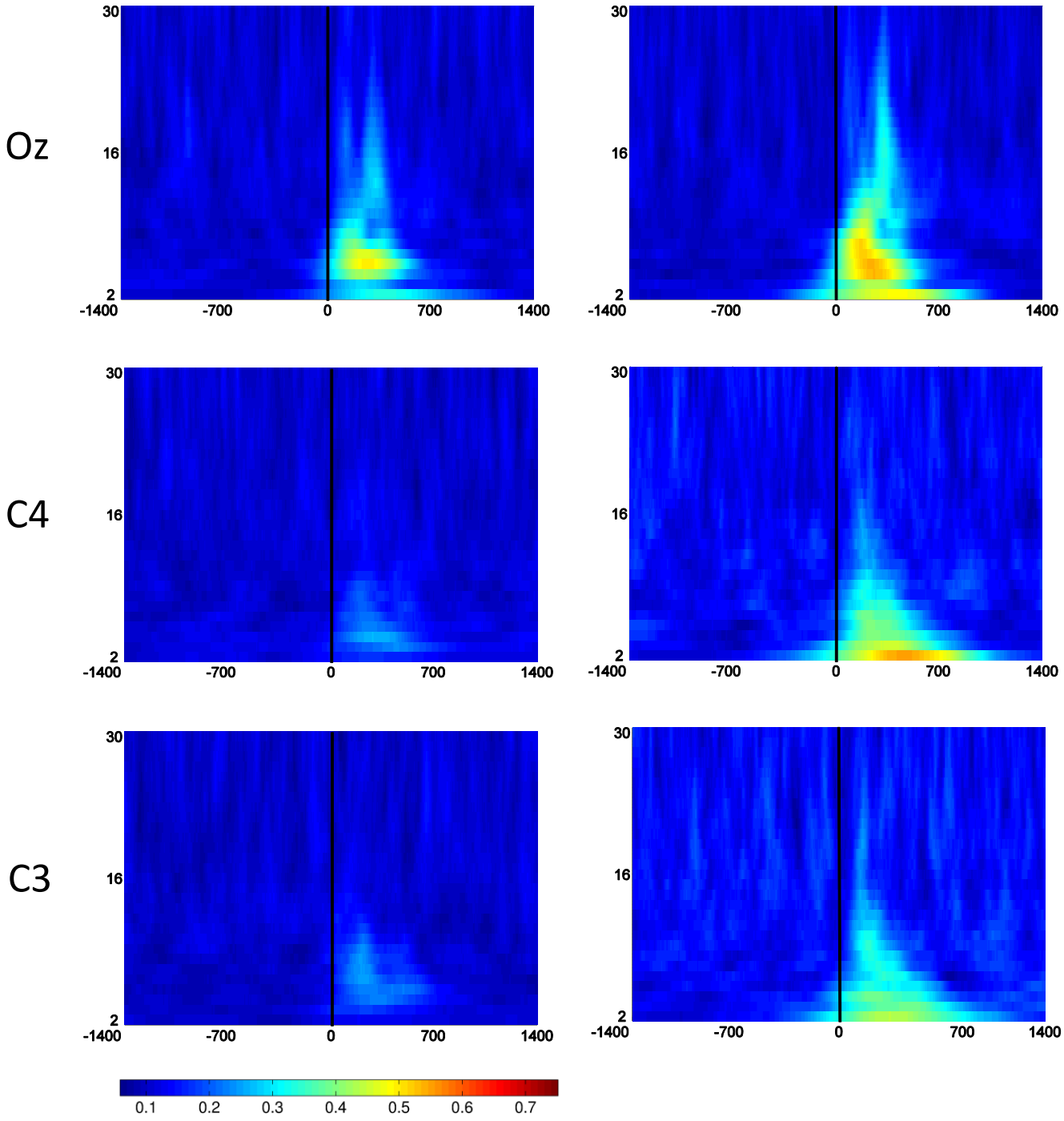

Figure 8

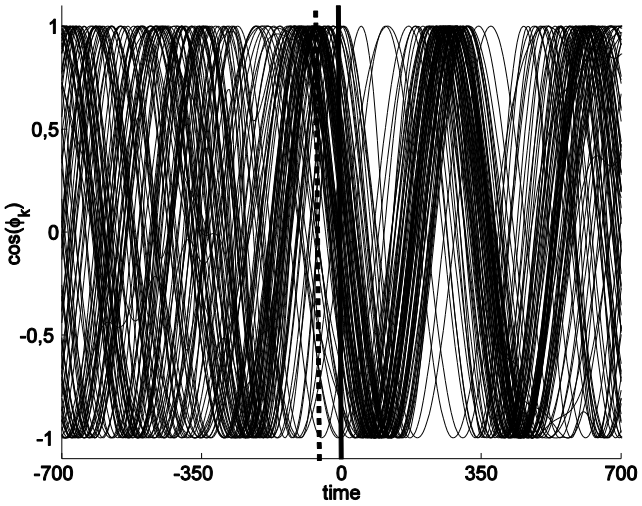

Figure 9

3 Unpublished Studies

3.1 Phase-locking analysis of EEG-data in movement related tasks reveals common underlying network of synchronous activity

Nils Rosjat, Svitlana Popovych, Bin Wang, Rouhollah Abdollahi, Tibor Istvan Tóth, Shivakumar Viswanathan, Christian Grefkes, Gereon Rudolf Fink, Silvia Daun-Gruhn

Author Contributions

Conceived the research
Nils Rosjat, Svitlana Popovych, Bin Wang, Shivakumar Viswanathan Christian Grefkes, Gereon Rudolf Fink, Silvia Daun-Gruhn

Performed the experiments
Bin Wang, Rouhollah Abdollahi, Shivakumar Viswanathan

Analyzed the data
Nils Rosjat

Figure Preparation
Nils Rosjat

First version of manuscript
Nils Rosjat

Wrote the manuscript
Nils Rosjat, Silvia Daun-Gruhn

Contributed materials/analysis tools
Christian Grefkes, Gereon Rudolf Fink, Silvia Daun-Gruhn

Phase-locking analysis of EEG-data in movement related tasks reveals common underlying network of synchronous activity

Nils Rosjat[a,b], Svitlana Popovych[a,b], Bin Wang[b], Rouhollah Abdollahi[b,c], Tibor Tóth[a], Shivakumar Viswanathan[b,c], Christian Grefkes[b,c], Gereon R. Fink[b,c], Silvia Daun-Gruhn[a,b]

[a] *Heisenberg Research Group of Computational Biology, Department of Animal Physiology, Institute of Zoology, University of Cologne*
[b] *Cognitive Neuroscience, Institute of Neuroscience and Medicine (INM-3), Research Centre Jülich*
[c] *Departman of Neurology, University Hospital Cologne*

1. Introduction

The performance of motor actions is a highly complex task where different body parts and brain regions have to be coordinated properly. To ensure this, the interplay of various brain regions of the motor cortex is important. In this study we investigate the communication of different motor related brain regions during simple internally and externally initiated finger movements during their preparation and execution.

In our earlier work, we have shown that intraregional synchronization in δ-θ frequencies is an EEG marker for the motor output during finger tapping tasks [11]. Several studies hypothesized that synchronization between different brain regions and different frequencies plays a crucial role when performing movements [2, 3, 15]. Thus we used time-frequency analysis and investigated the communication of motor related brain regions via interregional phase-locking analysis in the EEG signals. We found strong changes of synchronization in the δ-θ frequency band during movement preparation and movement execution. The calculation of lateralization networks revealed that the phase-locking effect in these frequency bands was stronger in connections between brain regions

from motor regions contralateral of the moving hand to supplementary motor areas than in those on the ipsilateral side. Those interregional synchronizations only appeared when both regions showed a strong intraregional phase locking. Thus intraregional phase locking in δ-θ frequencies seems to be a prerequisite for interregional phase locking. Additionally we could show a strong synchronization in the β-frequency band that appeared after the movement was executed in connections from the primary motor cortex and the pre-motor cortex contralateral to the moving hand to the supplementary motor areas. As previous studies have shown [4, 5] this kind of β phase-synchronization might be linked to movement suppression. Since this synchronization effect is expressed stronger in the self-initiated finger movement, we suggest that it might be related to the suppression of the internal "go" cue after the movement was executed that is not as strong in the visually cued tapping task.

2. Materials and methods

Participants. We investigated 21 healthy individuals (10F/11M, age: 22-35 years). All participants were right-handed according to the Edinburgh Handedness Inventory [9], had normal color vision and no history of psychiatric or neurological disease. All participants gave their written informed consent to the study before the experiment, which was approved by the local ethics committee of the Faculty of Medicine at the University of Cologne. Three subjects had to be excluded due to data quality: one of the subjects had too many noisy trials and two subjects were not able to perform the task properly. Thus 18 subjects were included in our study.

Experimental design. We recorded EEG data of healthy young subjects while they were performing a simple finger movement task (for details of the experiment and methods used to preprocess the data see [11]). The task consisted of three main conditions (Figure 1). The first condition was a self-initiated condition where the subjects were asked to perform voluntary left and right index finger movements each 4-8 s. In the second condition a visual stimulus pointing

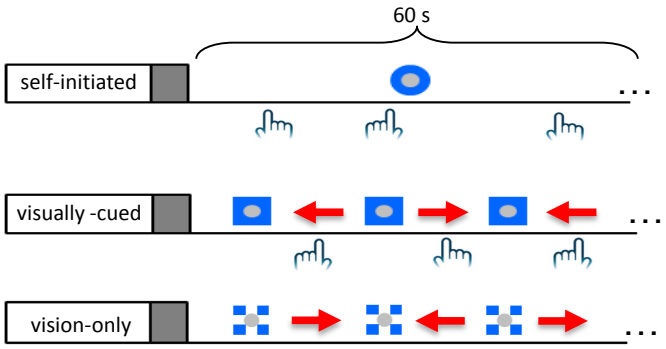

Figure 1: Experimental paradigm used for the finger tapping task. Consisting of 1) uncued, self-initiated voluntary movements, 2) visually triggered movements and 3) vision-only control condition.

to the left or to the right was shown to the subjects using a randomized order of the inter-trial intervals recorded from the self-initiated condition. The subjects were asked to press the button with the corresponding index finger as fast as possible. The last condition was a vision-only condition that was used as a control condition. In this part of the experiment the subjects were shown visual stimuli again, but without any action from the subjects required. The whole duration of the task was about 60-70 min. During that time each participant performed between 80 and 90 trials for each condition.

EEG recording and preprocessing. During the experiment we acquired data continuously from 64 active Ag/AgCl electrodes (Brain Products GmbH, Munich, Germany) that were placed in the order of the international 10-20 system. The reference electrode was placed at the left earlobe since we expected this location to be uninvolved in visual processing, movement planning and execution. Bipolar horizontal and left vertical electro-oculograms (EOG) were recorded using three of the 64 scalp electrodes (FT9, FT10 and TP10 in 10-20 nomenclature). They were placed at the bilateral outer canthi and under the left eye to monitor eye movement and blinks. Before the experiment we made sure that the impedance of the electrodes was below 15 kΩ. EEG signals were amplified,

band-pass filtered from $0.87 - 500$ Hz and digitised at a sampling rate of 2.5 kHz. Two acceleration sensors, one for each index finger, were attached at the finger tip for detection of movement onset. We chose to use these sensors in favor of EMG electrodes since they are more sensitive to small movements and are not restricted to single muscle groups. We also used the information from the acceleration signals to monitor the behaviour of the subjects to exclude errors, e.g. mirror movements.

The details of the preprocessing performed can be found elsewhere [11]. We defined the onset of each finger movement by application of a threshold to the norm of the numerically differentiated acceleration signal [16]. The signals were band-pass filtered from $0.5 - 48$ Hz and downsampled from 2.5 kHz to 200 Hz to reduce the filesize and thereby the amount of computation time. Artifacts were removed by a half-automatic procedure in EEGLAB described in detail in [11]. The data was finally epoched to intervals centered around the movement onset. In both conditions we had different requirements for the epochs. In the self-initiated tapping condition the baseline needed to be located before the start of the Bereitschaftspotential (readiness potential) [13] and in the visually-cued tapping condition we needed to avoid overlap between consecutive trials. Thus in the self-initiated tapping condition the epoch was defined as [-2500,1500] ms with the baseline [-2500,-1500] ms and for the visually-cued tapping condition we set the epoch to [-2000,1500] ms with a baseline interval of [-2000,-1000] ms.

Data analysis. The preprocessed data was re-referenced to small Laplacian reference [8] in order to improve the spatial resolution of the signals. We then transformed the data to the time-frequency domain using Morlet wavelets [7]. These steps were performed using the Statistical Parametric Mapping toolbox (SPM12, Wellcome Trust Centre for Neuroimaging, London, UK) implemented in MatLab R2011b (The MathWorks Inc., Massachusetts, USA). Following we analyzed the phase-information received from the time-frequency decomposition with custom programmed MatLab scripts.

4

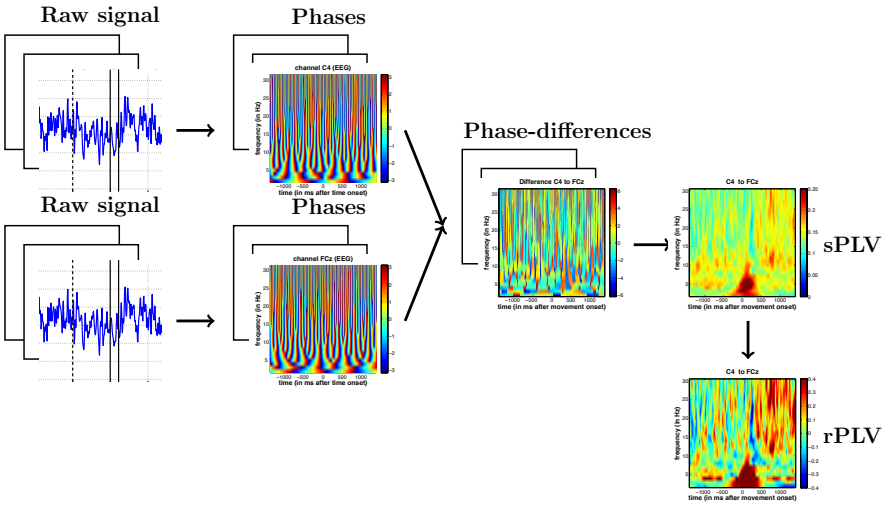

Figure 2: Workflow representing the preprocessing steps for the phase-locking analysis. First column: Raw signals; Second column: extracted phase information; Third column: phase-difference of two channels; Fourth column: single-frequency and relative phase-locking value.

Phase-locking analysis. We analyzed the interregional synchronization of the rhythms produced by different brain regions. We included four major frequency bands: δ (2-3 Hz), θ (4-7 Hz), α (8-12 Hz), β (13-30 Hz). In the following, our analysis will be restricted to EEG channels lying above motor regions. We identified the channels C2 and C4 with the right primary motor cortex rM1, C1 and C3 with the left primary motor cortex lM1, respectively. The frontocentral electrodes FC3 and FC4 representing the left and right pre-motor cortex (lPM, rPM) and the central electrodes Cz, FCz were chosen to analyze activity from the supplementary motor area (SMA, pre-SMA). We added the electrode Oz as a control for activity in the visual area (V1).

The complex Morlet wavelet transformation gives the possibility to analyze two quantities of the signal separately for each frequency, namely the amplitude A(f,t) and the phase $\varphi(f,t)$. Our previous study [11] showed that intraregional phase locking in low frequency bands can serve as a bio-marker of movement ex-

ecution. This led us to focus our attention on the analysis of interregional phase locking to get an insight in possible synchronization mechanisms between different motor regions. As a characteristic for interregional communication or synchronization we used the single-frequency phase-locking value (sPLV) (adapted from phase-locking value defined in [7]). Instead of the widely used technique of filtering the signal to frequency bands of interest and calculating a single phase-locking value for the whole frequency band, we calculated the single-frequency phase-locking value for each single frequency separately in 1 Hz steps (see Figure 2). In this way we got information on the exact contribution of each frequency to the observed phase locking. The sPLV for a channel pair m and n is defined as:

$$sPLV_{m,n}(f,t) = \frac{1}{N}\left|\sum_{k=1}^{N}\exp\left(i(\varphi_{m_k}(f,t) - \varphi_{n_k}(f,t))\right)\right| \tag{1}$$

Here φ_{m_k} represents the phase of channel m in trial number k. The sPLV ranges from 0 to 1. While a sPLV of 0 represents a random distribution of phase-differences over all trials without any coherence at all, a sPLV of 1 means perfect intertrial phase locking of the phase-differences of both channels over all trials.

Since we were more interested in the effects of movement preparation and movement execution and less in constant synchronizations, we normalized the sPLV of each pair of channels to its baseline and calculated the relative change over the whole epoch. We called these normalized sPLVs relative phase-locking values (rPLV):

$$rPLV_{m,n}(f,t) = \frac{sPLV_{m,n}(f,t) - \overline{sPLV_{m,n}(f,t)}}{\overline{sPLV_{m,n}(f,t)}} \tag{2}$$

Here $\overline{sPLV}$ denotes the mean sPLV in the baseline interval, i.e. [-2500,-1500] ms in the self-initiated tapping condition and [-2000,1500] ms in the visually-cued tapping condition.

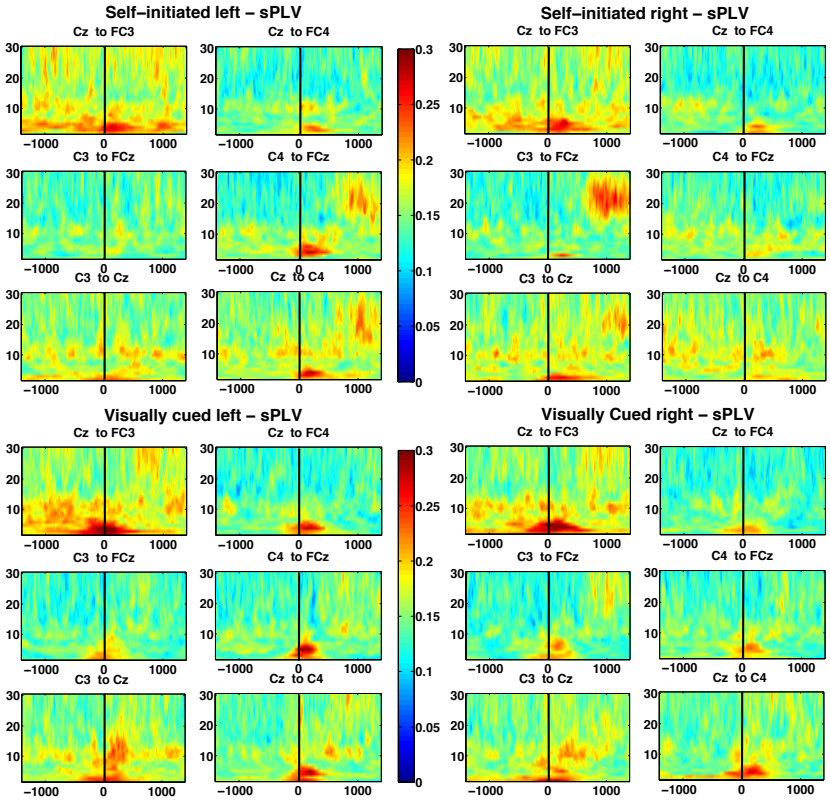

Figure 3: Single frequency phase locking for frequencies 2-30 Hz in all tapping conditions (self-initiated top, visually-cued bottom, left tapping shown left, right tapping shown right) for six example channel pairs.

3. Results

We used the phase-locking approach to get information about the interregional communication of motor areas, represented by six channels located above those areas, during movement preparation and execution. As we have seen in earlier work the only intraregional phase-locking effect could be observed in the δ-θ frequency band [11]. Thus we mainly focused our analysis on the frequencies ranging from 2-7 Hz. We used the morlet wavelet transformation to get the phase-information of each trial on the single subject level and calculated both the sPLV and the rPLV from 2-30 Hz.

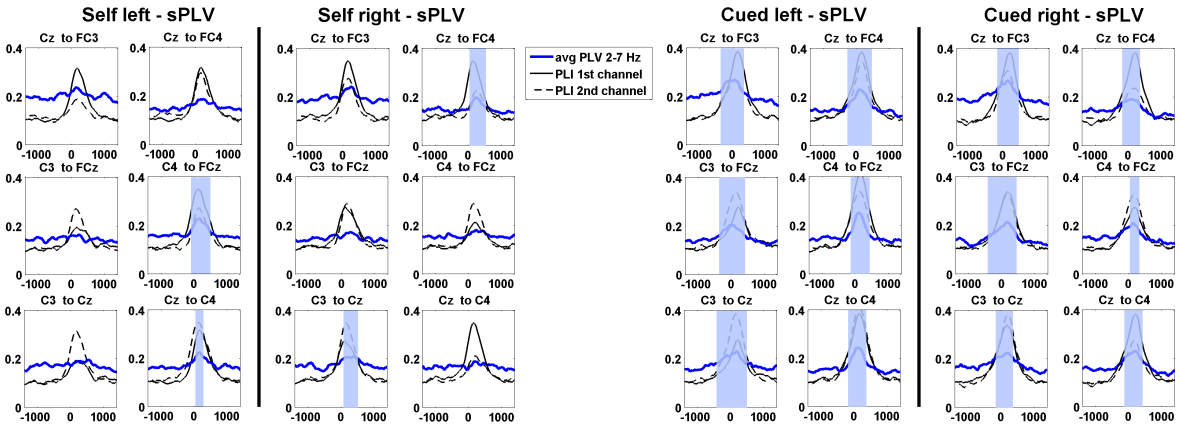

Figure 4: Significant differences in sPLV for 2-7 Hz compared with an artificial baseline (sPLV marked as solid blue line, PLIs marked as black solid line (first channel) and black dashed line (second channel), interval of significant changes marked with light blue box).

Figure 3 shows the group result of the sPLV analysis for self-initiated and visually-cued left and right finger tapping conditions. In general all conditions showed an interregional phase-locking effect in the δ-θ frequency band around movement onset. While this effect was present in almost every tested connection for the visually-cued tapping condition, it was present in the connections contralateral to the moving hand in the self-initiated tapping. Additionally, we found a strong phase locking in β-frequencies after the movement had finished between electrodes lying above the pre- and primary motor cortex and electrodes lying above the supplementary motor area. This β frequency phase locking was not observed in the phase locking within individual regions and appears only in interregional phase locking. Unlike the other effects we observed, e.g. low frequency sPLV and PLI, these effects were significantly stronger in the self-initiated tapping condition compared to the visually-cued tapping condition ($p < .0005$).

For further analysis of the phase locking in the δ-θ frequency band we aver-

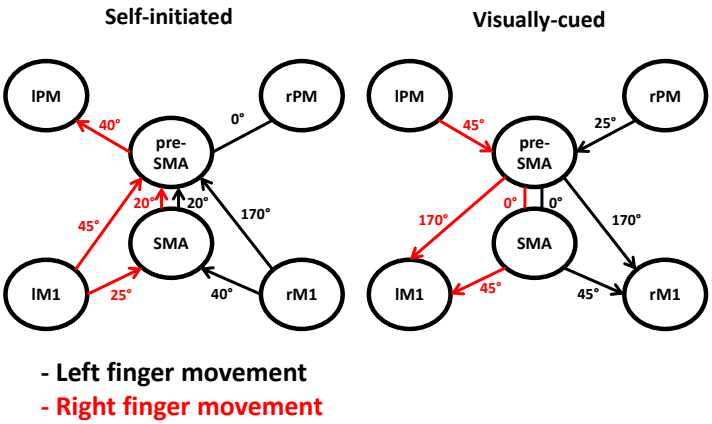

Figure 5: Preferred mean phase-differences in intervals of increased phase locking around movement onset for self-initiated and visually-cued movements (left tapping black solid lines, right tapping red solid lines).

aged the sPLVs over the frequency range from 2-7 Hz (shown in Figure 4). Here we plot the sPLV as a solid blue line and the corresponding intraregional phase-locking indices (PLIs) as dotted and dashed lines (from [11]). The intervals where the sPLV changed significantly from an artificial baseline, that was constructed from the mean value and the standard-deviation in the baseline interval (first second of the epoch), at a significant level of $p < 0.05$ (FDR corrected) are presented as blue boxes. While only few significant changes around movement onset, that primarily consist of electrodes that are located above the hemisphere contralateral to the moving hand, were found in the self-initiated tapping condition, almost every electrode pair showed a significant increase around movement onset in the visually-cued tapping condition. In Figure 6 we can see all pairs of regions that show a significant change around movement onset. While the pairs of channels that show a significant increase were strongly lateralized in the self-initiated left finger tapping, there was no evident lateralization in the self-initiated right finger tapping condition. This lack of lateralization in the right finger movements could be due to the fact that all of our subjects were right handed and thus needed less effort for movements with their dominant

hand. When comparing interregional phase locking to the intraregional one in the corresponding electrodes, it becomes clear that the sPLV only shows significant changes if both electrodes develop a high synchronization in the same time-interval.

An analysis of the phase-differences in the intervals of increased phase locking showed a similar pattern when comparing left to right hand movements of the same condition, but different structures between the conditions (see Fig. 5). In the self-initiated condition phases in M1 were preceding phases in SMA that were followed by PM, while the phases of PM were followed by SMA and M1 in the visually-cued condition. The phase-differences vary between 20-45° with two exceptions in the visually-cued condition where M1 followed pre-SMA by approximately 170° (see Fig. 5).

The β phase synchronization showed a significant increase for connections from pre-SMA to M1 contralateral to the moving hand for self-initiated left and right finger movements as well as visually-cued right finger movements. The visually-cued left movement condition did not show an increase that was significant on a statistical level. However, the same trend can be seen in this condition. The mean phase difference analysis in the intervals of increased β band synchronization showed that M1 lags behind pre-SMA (self-initiated: $\approx 160°$; visually-cued: $\approx 135°$)

In the following we aimed at determining whether the interregional phase locking in the δ-θ frequency band is a lateralized effect that is expressed stronger on one hemisphere than on the other. To exclude high phase-locking values, that resulted from a high baseline synchronization between the two channels that was not related to movement preparation or execution, we calculated the rPLV. In this way we were able to analyze the changes in phase locking relative to the baseline synchronization. Figure 7 shows that the overall effect did not change drastically, but all channel pairs are now normalized in a way that they

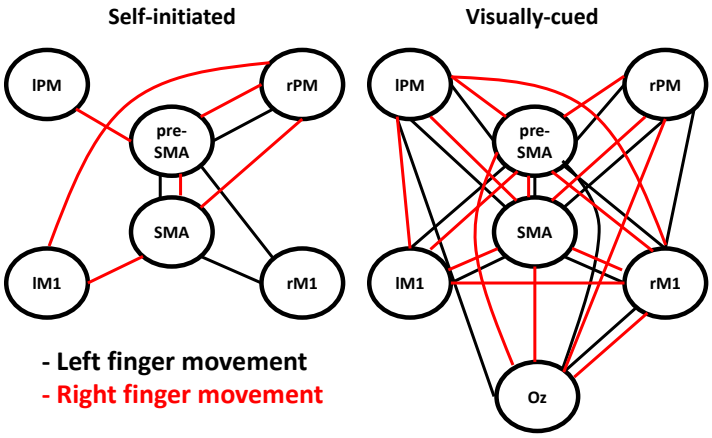

Figure 6: Networks for all channel pairs that show significant changes compared to an artificial baseline around movement onset for self-initiated and visually-cued movements (left tapping black solid lines, right tapping red solid lines).

can be compared to each other. We then averaged the rPLV over frequencies from 2-7 Hz to get the mean response in the δ-θ frequency band and tested the maximal values of channel pairs contralateral to the moving hand to channel pairs on the ipsilateral side of the moving hand. The lateralization index Lat is defined as follows:

$$\mathrm{Lat}(cp_c, cp_i) = \frac{\max(cp_c) - \max(cp_i)}{\max(cp_c) + \max(cp_i)} \tag{3}$$

Here cp_c denotes a channel pair from SMA to pre or primary motor areas contralateral to the moving hand and cp_i denotes the channel pair ipsilateral to the moving hand. This results in positive values when the synchronization on the contralateral hemisphere is stronger than the one on the ipsilateral hemisphere and negative values vice versa. The results of the lateralization analysis are presented in Figure 8. Most of the connections are stronger synchronized to pre- and primary motor regions contralateral of the moving hand (14 out of 18 possible connections) no matter if the left hand (marked with black lines) or the right hand (marked with red lines) is performing the task or whether it is initiated internally or externally.

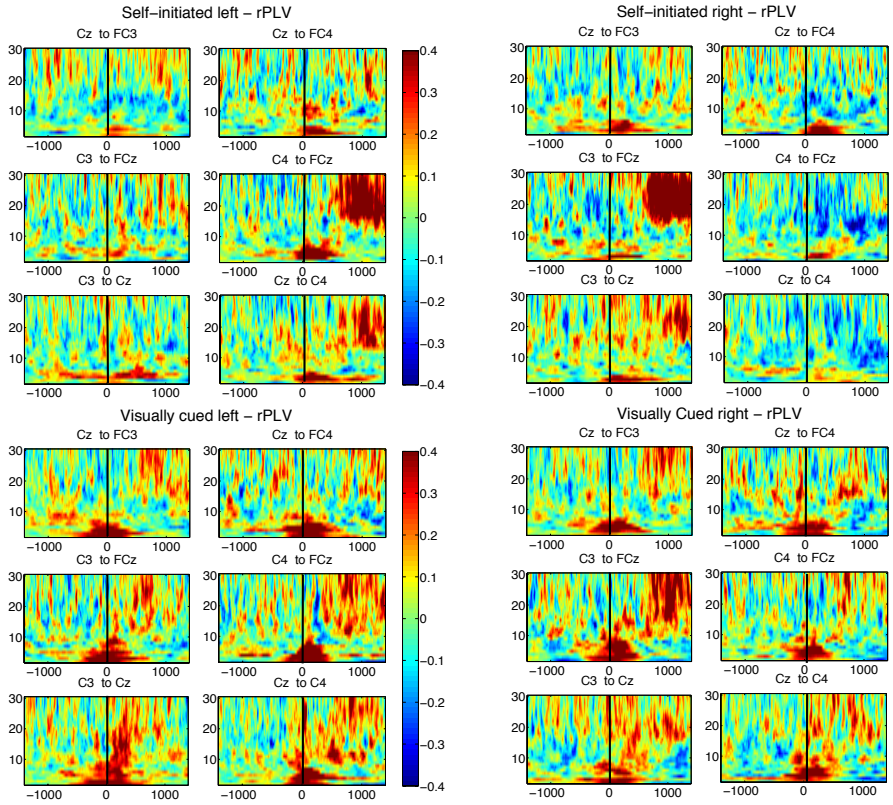

Figure 7: rPLV from 2-30 Hz for all tapping conditions for six example channel pairs.

4. Conclusions

We have performed interregional phase-locking analysis on EEG data during simple self-initiated and visually-cued finger tapping tasks. We have seen that there is a strong interregional phase locking in the δ-θ frequency band around movement onset additional to earlier reported intraregional phase locking [11]. We also observed phase locking in higher β-frequencies after the movement had finished from pre- and primary motor cortex to supplementary motor areas that were not related to intraregional phase locking in this frequency range and that were significantly stronger in the self-initiated tapping condition compared to the visually-cued one.

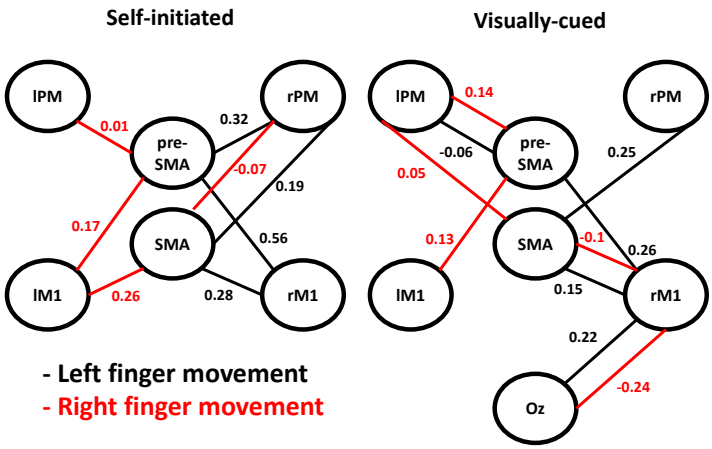

Figure 8: Lateralization network for the self-initiated and visually-cued tapping condition. Corresponding finger movements are marked with black (left) and red lines (right).

The phase differences in the intervals of increased phase locking revealed a different order of the involved brain areas in self-initiated and visually-cued tapping conditions. This order is in accordance with the one obtained from the timepoints of maximal phase locking within the regions (cf. [11]). These findings imply a directionality in the connections between the regions. In the self-initiated tapping condition the signal originates in M1 and proceed to SMA and PM, while it is the inverse direction in the visually-cued condition. Analyses of additional channels above the parietal and frontal cortices will be necessary to check whether the signals in the self-initiated condition are truly initiated in M1 or whether they originate in parietal or frontal regions.

We suggest that the communication of motor-regions and the supplementary motor area represented by an increase in phase locking in $\delta - \theta$ frequencies is necessary to establish and maintain the movement of the finger. Even though we found a different order of the involved brain areas in different movement conditions, they showed similar synchronization patterns in M1 and SMA during movement execution as they converge to the same motor output. The event-

related β synchronization in the amplitude dynamics is often interpreted as idling of the motor cortex after movement execution [10], however there is a hint that phase locking in the β-frequencies can be linked to the suppression of movement after execution [4, 5]. Our results showed that the phase of the SMA is preceding the phase of M1. Thus, further motor output from M1 might be suppressed by phase locking to the phase of the β rhythm in SMA. It will be necessary to investigate if the β phase locking is reduced in subjects that have problems with terminating the movements, e.g. elderly subjects or subjects suffering from Parkinson's disease.

In future investigations these findings will be compared for different groups of subjects, e.g. elderly subjects and stroke patients. The interregional phase-locking effects might be reduced in general in both of the groups. Additionally it is reasonable to assume that stroke patients show a strong reduction of phase locking and also in the lateralization-indices when using their affected hand. This might then be used as a basis for mathematical modelling of the underlying network using populations of phase-oscillators (cf. [12]). This mathematical model would then be able to give information on the differences in interregional coupling strengths between different groups. The hypotheses derived from the mathematical model could then be verified by additional experiments using transcranial magnetic stimulation (TMS). This technique can be used to alter the activity in certain brain regions [c.f. 1, 6, 14]. In this way, it can be tested whether an alteration in the same region of the mathematical model shows similar effects.

References

[1] **Baeken C, De Raedt R**. Neurobiological mechanisms of repetitive transcranial magnetic stimulation on the underlying neuro circuitry in unipolar depression. *Dialogues clinical neuroscience* 13: 139, 2011.

[2] **Baker S, Olivier E, Lemon R**. Coherent oscillations in monkey motor cortex and hand muscle emg show task-dependent modulation. *The J physiology* 501: 225–241, 1997.

[3] **Baker S, Spinks R, Jackson A, Lemon R**. Synchronization in monkey motor cortex during a precision grip task. i. task-dependent modulation in single-unit synchrony. *J Neurophysiol* 85: 869–885, 2001.

[4] **de Hemptinne C, Ryapolova-Webb ES, Air EL, Garcia PA, Miller KJ, Ojemann JG, Ostrem JL, Galifianakis NB, Starr PA**. Exaggerated phase–amplitude coupling in the primary motor cortex in parkinson disease. *Proc Natl Acad Sci United States Am* 110: 4780–4785, 2013.

[5] **de Hemptinne C, Swann NC, Ostrem JL, Ryapolova-Webb ES, San Luciano M, Galifianakis NB, Starr PA**. Therapeutic deep brain stimulation reduces cortical phase-amplitude coupling in parkinson's disease. *Nat Neurosci* 18: 779–786, 2015.

[6] **Fitzgerald PB, Daskalakis ZJ, Hoy K, Farzan F, Upton DJ, Cooper NR, Maller JJ**. Cortical inhibition in motor and non-motor regions: a combined tms-eeg study. *Clin EEG neuroscience* 39: 112–117, 2008.

[7] **Lachaux JP, Rodriguez E, Martinerie J, Varela FJ et al.** Measuring phase synchrony in brain signals. *Hum brain mapping* 8: 194–208, 1999.

[8] **McFarland DJ, McCane LM, David SV, Wolpaw JR**. Spatial filter selection for eeg-based communication. *Electroencephalogr clinical Neurophysiol* 103: 386–394, 1997.

[9] **Oldfield RC**. The assessment and analysis of handedness: the edinburgh inventory. *Neuropsychol* 9: 97–113, 1971.

[10] **Pfurtscheller G, Jr. AS, Neuper C**. Post-movement beta synchronization. a correlate of an idling motor area? *Electroencephalogr Clin Neurophysiol* 98: 281 – 293, 1996.

[11] **Popovych S, Rosjat N, Wang B, Liu L, Tóth TI, Viswanathan S, Abdollahi RO, Grefkes C, Fink GR, Daun-Gruhn S**. Phase-locking in the delta-theta frequency band is an eeg marker of movement execution. *J Neurosci (submitted)* , 2015.

[12] **Rosjat N, Popovych S, Daun-Gruhn S**. A mathematical model of dysfunction of the thalamo-cortical loop in schizophrenia. *Theor Biol Med Model* 11: 45, 2014.

[13] **Shibasaki H, Hallett M**. What is the bereitschaftspotential? *Clin Neurophysiol* 117: 2341–2356, 2006.

[14] **Terao Y, Ugawa Y**. Basic mechanisms of tms. *J clinical neurophysiology* 19: 322–343, 2002.

[15] **Uhlhaas PJ, Roux F, Rodriguez E, Rotarska-Jagiela A, Singer W**. Neural synchrony and the development of cortical networks. *Trends Cogn Sci* 14: 72 – 80, 2010.

[16] **Wyatt HJ**. Detecting saccades with jerk. *Vis research* 38: 2147–2153, 1998.

3.2 Intersegmental coupling between fictive motor rhythms of pattern generating networks in the stick insect

Nils Rosjat, Charlampos Mantziaris, Anke Borgmann, Ansgar Büschges, Silvia Daun-Gruhn

Author Contributions

Conceived the research
Nils Rosjat, Charlampos Mantziaris
Anke Borgmann, Ansgar Büschges
Silvia Daun-Gruhn

Performed the experiments
Charlampos Mantziaris, Anke Borgmann

Performed the simulations
Nils Rosjat, Anke Borgmann

Analyzed the data
Nils Rosjat, Silvia Daun-Gruhn

Figure Preparation
Nils Rosjat, Anke Borgmann

First version of manuscript
Nils Rosjat

Wrote the paper
Nils Rosjat, Silvia Daun-Gruhn

Contributed materials/analysis tools
Ansgar Büschges, Silvia Daun-Gruhn

Intersegmental coupling between fictive motor rhythms of pattern generating networks in the stick insect

Nils Rosjat[a,c], Charlampos Mantziaris[b], Anke Borgmann[b], Ansgar Büschges[b], Silvia Daun-Gruhn[a,c]

[a] *Heisenberg Research Group of Computational Biology, Department of Animal Physiology, Institute of Zoology, University of Cologne*
[b] *Departman of Animal Physiology, Institute of Zoology, University of Cologne*
[c] *Cognitive Neuroscience, Institute of Neuroscience and Medicine (INM-3), Research Centre Jlich*

Abstract

Walking results from a complex interplay of central pattern generating networks (CPGs), local sensory feedback signalizing position, velocity and forces generated in the legs, and coordinating signals from neighboring limbs. In the stick insect, the neural basis of inter-segmental coordination and the precise effects of sensory information on the central networks in establishing coordinated motor output are largely unknown. The antagonistic muscles of each leg joint are driven by one CPG that can be activated by the muscarinic acetylcholine agonist pilocarpine. Sensory information plays a crucial role in coordinating the different CPGs of one leg and appears to play a major role in inter-segmental coordination of the different legs, too. However, precious little is known about the interactions between the different CPG networks. Here, we aimed to investigate potential coupling between CPGs at the CTr-joint in the different segments, in more detail. Rhythmic motor activity was induced by bath application of the muscarinic receptor agonist pilocarpine. We used phase-difference analysis and dynamic causal modeling (DCM) to investigate the coupling structure and strength of pairs of coupled ganglia. We set up different coupling schemes for DCM and compared them using Bayesian model selection methods. There was a clear preference to models with lateral connections in each segment and ipsilateral connections on both sides to all other tested models. Our results show a high probability for the existence of ipsilateral inter- and lateral intra-segmental

coupling between the CPGs controlling the coxa-trochanteral joint musculature in the stick insect thoracic nerve cord. Furthermore we show that the lateral intrasegmental coupling strength in the mesothoracic ganglion is the strongest and most stable coupling in all three ganglia.

Keywords: Central pattern generator, weak coupling, insect locomotion, intersegmental coordination, dynamic causal modeling, phase-coupling

---

1. Introduction

Various experiments on vertebrate and invertebrate animal models confirm the existence of central pattern generating networks (CPGs). Those networks are responsible for the generation of periodic muscle activity [9, 18] that has to be coordinated to create walking patterns. In the stick insect *Carausius morosus*, each leg is individually controlled by its own CPG located in the pro- (front legs), meso- (middle legs) and metathoracic ganglion (hind legs) [10, 28]. Each leg consists of three leg joints that produce coordinated movements during walking and climbing: The thorax-coxa (ThC) joint is responsible for forward and backward movements, the coxa-trochanter (CTr) joint is able to move the femur of the stick insect in upward and downward direction and finally the femur-tibia (FTi) joint that is responsible for outward and inward movements of the leg. Each of the leg joints is controlled by antagonistic muscle pairs, namely the protractor-retractor (ThC), the levator-depressor (CTr) and the flexor extensor (FTi) muscle pair [11]. When it comes to coordination of the CPGs innervating the motoneuron (MN) pools of legs within the same segment (intra-segmental) or CPGs innervating the MN pools of legs of different segments (inter-segmental), sensory input plays a major role in establishing the coordinated and functional motor output [2, 4, 5, 13, 15]. However, little is known about the interaction between the different CPG networks. In order to understand how a stable locomotor pattern is achieved we need to understand the contribution and the interaction of the central and peripheral components.

So far there is a long and successful history in mathematically describing and modeling central pattern generating networks with phase oscillators. A lot of interesting and fruitful insights come from the models of weakly coupled oscillators [8, 16, 24]. Nevertheless, there is a drawback on this modeling approach. Up to now there is hardly a way to come up with coupling strengths that truly come from the data and not from the model itself. There are some promising approaches for the handling of EEG recordings for example [14, 22]. In this paper we tackle the problem with two different approaches. A simpler and more descriptive approach and a more complex modeling approach in order to assign relative strength of coupling to the connections of the coupling of fictive motor rhythms of levator-depressor CPGs of different hemisegments.

Usually the interaction of oscillators is quantified with coupling strengths. These coupling strengths usually come from a model that was fitted to the data somehow. As there is no direct bridge between recorded data and modeling, we decided to investigate the effect of central coupling from both sides: The side of data analysis, using a more descriptive approach, and the side of modeling, to get an indication about the strength of observed effects in order to characterize the coupling between the CPGs of the different segments in the thoracic nerve cord.

This article is organized as follows: In section *Materials and methods*, we will first review the experimental set up and describe the phase-difference and dynamic causal modeling methods we are going to use for the data analysis. The section *Results* is separated into two parts. In the first part we will present the results of the analysis for the meso- and metathoracic ganglia and in the second part the results for the pro- and mesothoracic ganglia.

2. Materials and methods

Animals. The experiments were carried out on adult female Indian stick insects, *Carausius morosus* [3]. The animals are obtained from our colony maintained at 22-24°C, at approximately 60% humidity and under a 12 h light / 12 h dark cycle.

Preparation. We recorded the CPG activity of C2 leg nerves innervating the *depressor trochanteris* muscles extracellularly from contralateral nerves on pro-, meso- and metathoracic ganglia using 'hook' electrodes [25] (for detailed descriptions of the preparation, experimental setup and electrophysiology see [17]). Therefore all legs of the stick insects were removed, all lateral and connective nerves, except the ones of interest, were cut off (isolated and deafferented preparation). Also sensory axons were destroyed to avoid sensory feedback and peripheral input being recorded. Rhythmic activity in leg motoneuron pools was then induced by bath application of the muscarinic receptor agonist *pilocarpine* [6].

We used phase analysis to detect the intrasegmental (within one segment) and intersegmental (between two segments) ganglia coupling of motor outputs. The intersegmental analysis will be done for the meso- and metathoracic ganglia first and second for the pro- and mesothoracic ganglia.

Data analysis. The collected data was preprocessed offline using Spike2 7.09 (CED, Cambridge, UK). We used the signal processing functions DC-remove, Rectify and Smooth to get rectified and smoothed waveforms that are corrected for DC shifts. This data was then downsampled to 200 Hz, extracted as a time-series and further processed with MatLab R2011b (The MathWorks Inc., Massachusetts, USA). Phase-difference analysis was done using custom programmed MatLab scripts, while we used the Statistical Parametric Mapping toolbox (SPM12, Wellcome Trust Centre for Neuroimaging, London, UK) implemented in MatLab for dynamic causal modelling.

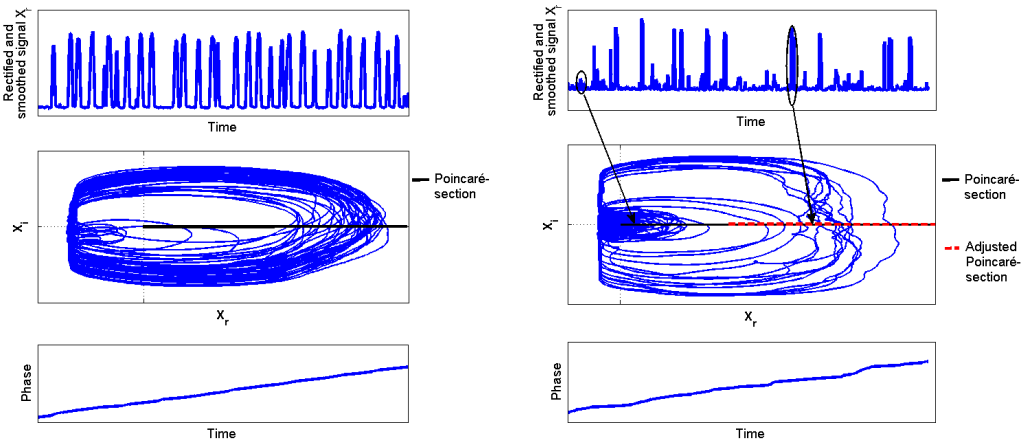

Figure 1: Top: Rectified and smoothed signal X_r (Left: Meso-Meta, Right: Pro-Meso); Middle: Discrete-time analytic Discrete-Timesignal with Poincar-section marked in black (normal) and red (adjusted for small units) (Left: Meso-Meta, Right: Pro-Meso); Bottom: Resulting instantaneous phase φ (Left: Meso-Meta, Right: Pro-Meso).

Phase-connectivity approach. We analyzed the coordination of the rhythms produced by the CPGs controlling the leg movements in the stick insect in the absence of sensory input on the phase level, to investigate possible coupling of those units. This analysis was performed according to established methods described elsewhere [24, 26]. Using this approach we got information about the development of multiple rhythms in relation to each other.

For this, we analyzed the phase development of each nerve recording. To do this the preprocessed extracellular recordings were transformed to the complex plane via the so-called discrete-time analytic signal

$$X = X_r + iX_i, \tag{1}$$

such that X_i is the Hilbert transform of the real data vector X_r [19]. Then a Poincarè-section was used to define the onsets of the bursts and thereby the phase onset of the rhythm. The phase ϕ of each recording was then defined to

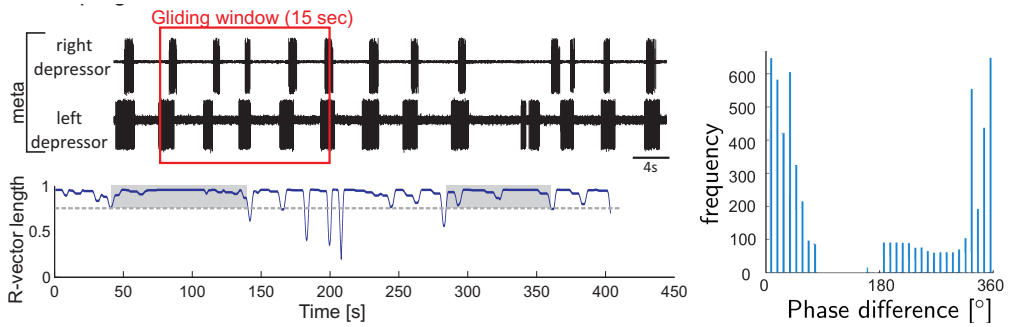

Figure 2: Left top: Sample recording of left and right depressor activity in the metathoracic ganglion, with an example gliding window marked in red; Left bottom: Development of the R-vector length of left-right metathoracic phase-differences over a whole recording, coupled regions marked with grey boxes; Right: Phase-histogram shown for the coupled interval $\approx$ [50,140]

increase linearly from 0 to 1 (2π) during one cycle. In a last step this phase was unwrapped, i.e. we let it grow continuously from the first to the last cycle (Figure 1, left). The signal in the prothoracic ganglion showed activities with small amplitudes additionally to the high amplitude bursts, thus we added a second analysis where we adjusted the Poincar-section such that only the big amplitudes were marked as burst onsets (Figure 1 right).

To investigate the coupling of two CPGs, we calculated the phase-difference. The signals are assumed to be coupled if their phase-difference remains constant over a time-period, i.e.

$$||\varphi_1(t) - \varphi_2(t)|| = c + \varepsilon, \qquad \varepsilon \text{ small} \tag{2}$$

In our analysis we ensured this by demanding the following two criteria, for the R-vector (cf. [1]) which is measuring the similarity of the phase-differences of the coupled phases.

1. The R-vector length in a 15 s long gliding time-window should stay above a length of 0.8 for at least 50 s (corresponds to 10 cycles) (Figure 2, left).

2. Over the whole time-interval defined above the R-vector should stay above 0.3 and have a clear peak in the histogram (Figure 2, right). This criterium prevents a drifting of the phases over the *coupled* interval.

Both thresholds for the R-vectors were adjusted manually in a way that the program was able to correctly assign clearly coupled or clearly uncoupled intervals to the right group. We defined *coupling strength* as the likelihood of coupling over the whole recording, i.e. the sum of all interval lengths in which coupling occurred relative to the total length of the corresponding recording, while recordings without coupling were taken into account with 0 s of coupling.

Dynamic causal modeling approach. In the second approach we used Dynamic causal modeling (DCM) [14] to investigate the coupling structure and the coupling strength of intra- and inter-segmental couplings between the thoracic ganglia of the levator-depressor system of the stick insect. This approach is widely used in the analysis of coupling strengths of EEG and fMRI data [7, 12, 27] and in the analysis of local field potentials [22].

This approach uses neural mass models [20, 21] to describe the neuronal activity of the recorded sources. Therefore the parameters will be fed into a set of differential equations that are coupled after a predefined coupling structure to simulate the recorded source activity.

$$\dot{z} = (A + uB)z, \tag{3}$$

where z is the output of the sources, the coupling structure is defined in A and possible connectivity changes between different experimental conditions is modeled with B. The coupling strengths saved in A and B will then be fitted to be optimal for the recorded activity. After testing for the best coupling structure via bayesian model selection (BMS) [23], this gives us the possibility to investigate intra- and intersegmental coupling strengths in the preferred model architecture.

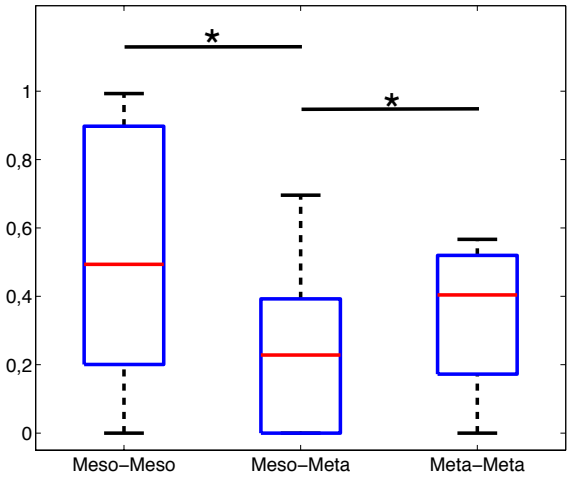

Figure 3: Coupling strength in the meso-meta thoracic ganglia over all experiments using the phase-connectivity approach (N=10).

3. Results

In this study we applied methods commonly used for EEG analysis to analyze pharmacologically induced rhythmicity in MN pools of an invertebrate system. Coupling of the CPG motor output of the CTr-joint of multiple segments, either meso-meta or pro-meso connectivity, was investigated first on the phase level of the bursting behavior and second via mathematical model fits reproducing the recorded depressor MN activity.

Meso-Meta thoracic ganglia. The first part of the experiment consisted of recordings from the C2 nerves of the meso- and metathoracic ganglia. In 9 animals we collected data from both sides in the meso- and metathoracic ganglion.

The results of the phase-coupling approach are presented in Figure 3. The likelihood of coupled segments was highest for the intra-segmental couplings, i.e. the coupling between both sides of the mesothoracic ganglion (meso-meso) and the coupling between both sides of the metathoracic ganglion (meta-meta). The likelihood of inter-segmental coupling (meso-meta) was significantly lower

($p = 0.0396$) than the intra-segmental coupling, while intra-segmental couplings in the meso- and metathoracic ganglia itself showed no significant difference ($p = 0.2224$).

Then we used the bilateral recorded data for the DCM analysis. First we tested different possibilities for the predefined coupling structure. The tested models consisted of unconnected (2), fully connected (3), cross connected with (4) and without lateral connections (5), intrasegmental unconnected (6), intersegmental unconnected (7) ganglia and a circular connected model (1) (Figure 4 (A)). All models were tested with excitatory and inhibitory connections. Here we show only the results of excitatory coupling, since both groups (excitatory and inhibitory) showed the same winning model structure. Over all the winning model with excitatory connections had the highest probability. The BMS showed that the coupling structure best fitting the recorded data was model 1 (Figure 4 (B)).

We used this coupling structure as the basis for further analysis of the coupling strengths. We decided to analyze the recordings in two steps. First we used biased intervals that were defined as coupled from the phase-coupling approach and second we analyzed unbiased arbitrary chosen time-intervals. With this approach it was possible to get information about differences in coupling strengths during phase-synchronized time-intervals in comparison to unsynchronized ones.

The analysis of the biased intervals lead to coupling strengths that are depicted in Figure 5. In agreement with the phase-coupling approach we can see the highest coupling strengths in the meso-meso and meta-meta connectivity, while the meso-meta connectivity was significantly lower (meso-meso: $p = 0.013$, meta-meta: $p = 0.041$). Then we looked at five unbiased intervals of 15 s duration each that were merged together (Figure 6, right). When comparing the coupling strengths of the same animal in the biased intervals, we see that the coupling strengths in the mesothoracic ganglion and the intersegmental coupling

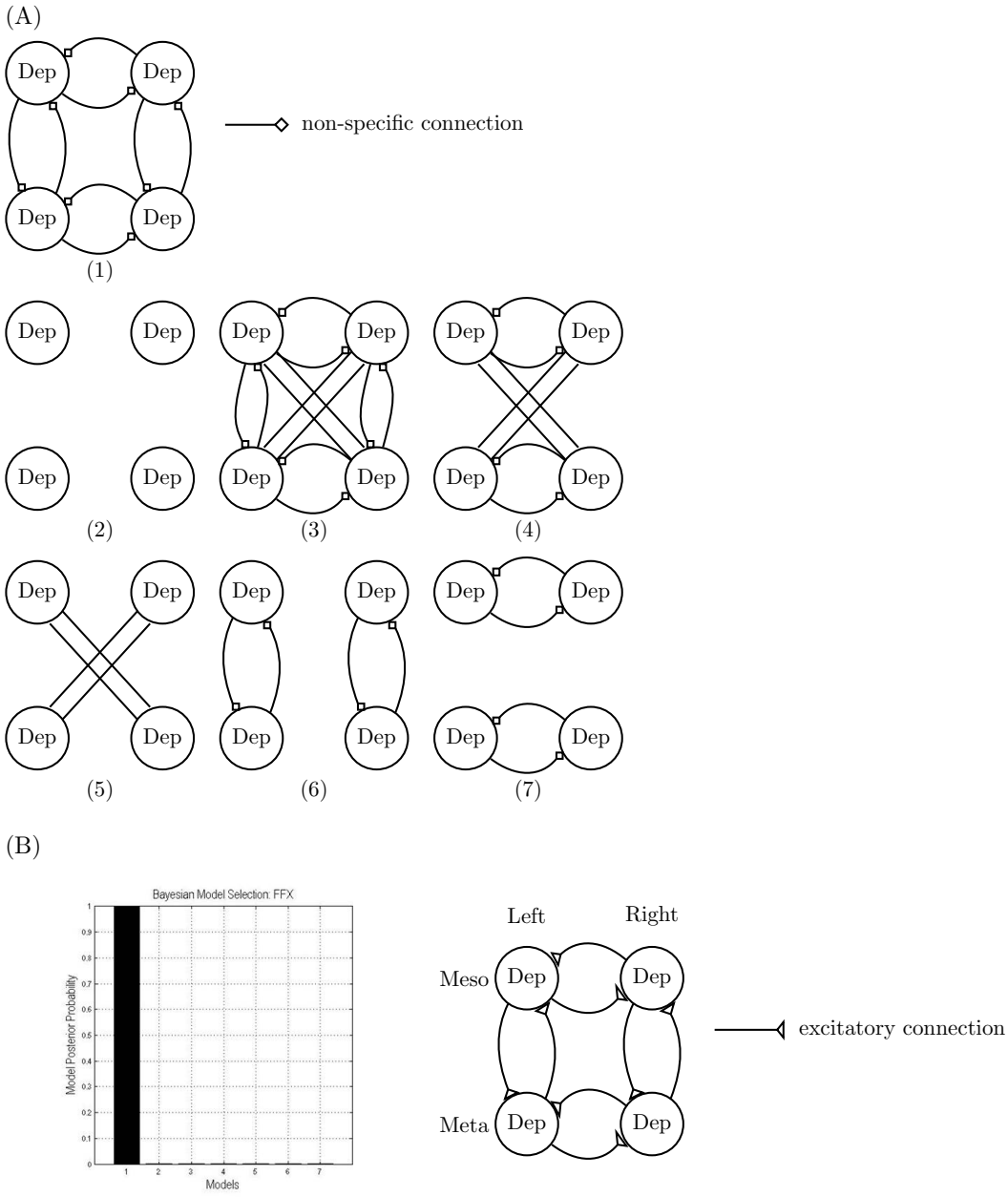

Figure 4: (A) Model architectures tested with DCM (B) Model selection; left: Result of Bayesian Model selection for the meso-meta thoracic ganglia; right: Structure of the winning model (1), triangles marking excitatory connections between CPGs.

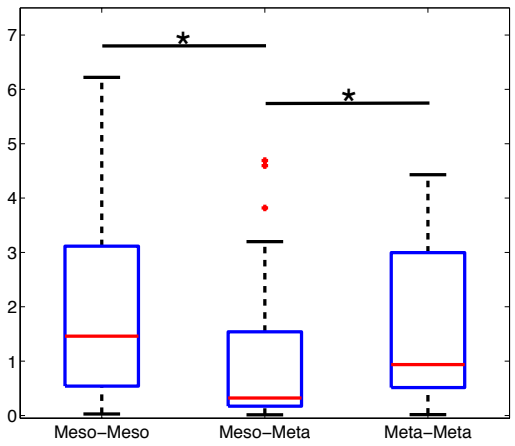

Figure 5: Coupling strength in the meso-meta thoracic ganglia over all experiments using the DCM approach (N=5, n=11) for biased intervals already identified as coupled by the phase-coupling approach.

strengths stay roughly at the same levels, while the coupling strengths in the metathoracic ganglion is decreased by a factor of five. This result suggests that the mesothoracic intra-segmental coupling remains high throughout the whole experiment whereas the coupling in the metathoracic ganglion is strong only in the intervals where the phases are also coupled to each other.

Since DCM was developed for EEG data of the human brain, we performed an analysis to test whether it is able to be applied to extracellular recordings, in particular to reproduce coupling strengths that we would expect to exist in the animal. Therefore we added a second experimental condition to the experiment where the connectives between the meso- and metathoracic ganglia were cut. In this case the connectivity between both segments is destroyed. This time we set up DCM to calculate coupling strengths for the case of connected segments (A-matrix) and the changes from these values in the case of cut connectives (B-matrix). We did not give any prior information on which connections should be changed by DCM. The model showed a strong decrease, 90% on the left side and 95% on the right side, of connection strength between the meso- and

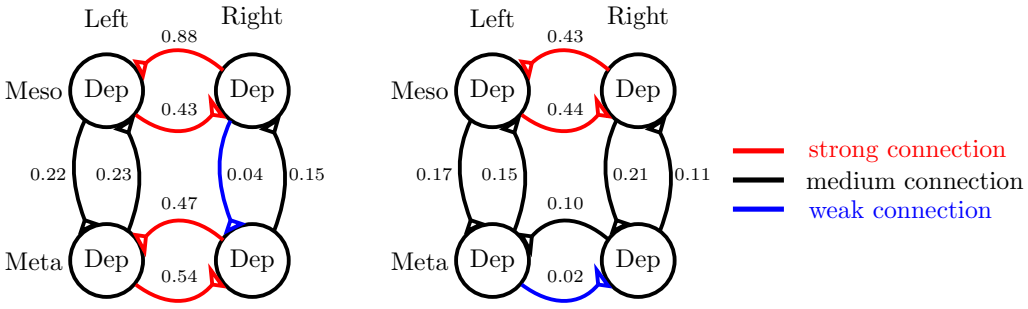

Figure 6: Coupling strength for the same animal. Left: biased interval of 50 s length, Right: unbiased interval from 5 intervals of 15 s length each. Red lines mark strong connections, black lines medium connections and blue lines weak connections respectively.

metathoracic ganglion (Figure 7). The connection between both segments was not removed completely by DCM. This is due to the fact that DCM is set to use at least a minimal strength for the connection whenever it is defined to be present. In addition to the intersegmental decrease, there was a strong increase in the intrasegmental coupling in the mesothoracic ganglion (2-20x as strong) and a decrease in connectivity in the metathoracic ganglion (1/2x as strong). This fits to [17] where they could demonstrate that the mesothoracic ganglion showed phase-coupling even in the isolated state, while the metathoracic ganglion needed to be connected to the mesothoracic ganglion to show phase-coupling.

Pro-Meso thoracic ganglia. In the second part we analyzed the coupling between the pro- and the mesothoracic ganglia. We recorded the activity of the C2 nerve on both sides of both ganglia in 5 animals, on both sides of the mesothoracic ganglion and on one side of the prothoracic ganglion in 3 animals and on both sides of the prothoracic and on one side of the mesothoracic ganglion in 5 animals.

Since there was a lot of small unit activity, we added a second analysis with an adjusted Poincaré section to just mark the onset of the bursts of the big units, i.e. add a threshold for the amplitude of the signal (cf. Figure 1, right).

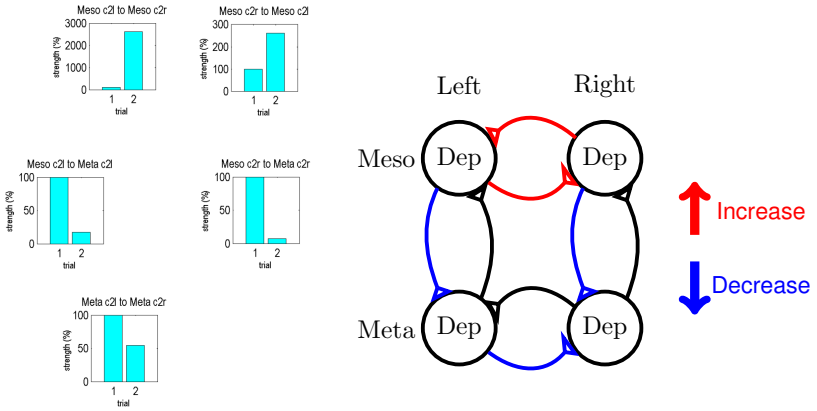

Figure 7: Differences in connectivity from connected segments (trial 1) to unconnected segments (trial 2). Left: Changes of connectivity strength, with trial 1 normed to 100% coupling strength; Right: Changes of connectivity compared to trial 1, red lines mark an increase in connectivity, blue lines a decrease in connectivity and black lines no reliable connectivity change (above 70%).

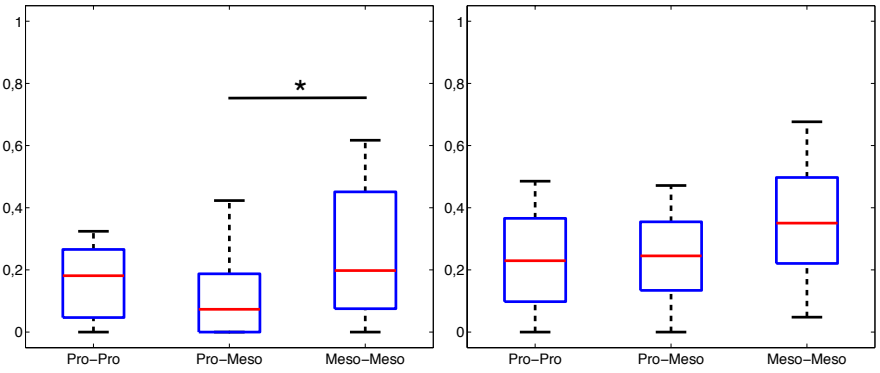

Figure 8: Coupling strength in the pro-meso thoracic ganglia over all experiments using the phase-coupling approach (N=8). Left: without adjustment to the Poincar-section, Right: With Poincar-section adjusted to big units.

The analysis of the uncorrected phase-differences revealed weak intersegmental coupling and weak intrasegmental coupling in the prothoracic ganglion, while the coupling strength was increased in the mesothoracic ganglion compared with the intersegmental coupling strength ($p = 0.0394$, Figure 8, left). In the adjusted analysis the mean mesothoracic coupling strength was still higher than the prothoracic and the intersegmental coupling strength. However, this difference was not significant on a statistical level (pp-mm $p = 0.29$, pm-mm $p = 0.541$, pm-pp $p = 0.437$).

We then investigated the data with the DCM approach. First we started again with the selection of the best fitting coupling structure for the data with the same models tested as in the meso-meta thoracic ganglia (Figure 4 (A)). The BMS showed the same result (Figure 4), which is why we used the same coupling structure for the analysis of the pro-meso thoracic ganglia. In the biased coupling intervals (N=5,n=10) we can see that the intrasegmental meso-meso coupling ($p = 0.003$) and the intersegmental pro-meso coupling ($p = 0.013$) are significantly stronger than the intrasegmental pro-pro coupling (Figure 9, left). The same trend can be seen for unbiased intervals (Figure 9, right). Here we used 4 intervals from 2 animals that were arbitrarily chosen with a length of 50 s. The pro-meso ($p = 0.025$) and meso-meso coupling ($p = 0.001$) strengths are again significantly stronger than the pro-pro coupling strength.

4. Conclusions

Our results show a strong evidence that weak inter- and intrasegmental central coupling is present in the stick insect. In figure 10 we sum up the connectivity results from both approaches. We have seen that there is a coupling present in each ganglion, but with a different coupling strength. In the DCM approach the intrasegmental coupling strength of the prothoracic ganglion was the weakest coupling present (Figure 10). In the phase-coupling approach this connection was amongst the weakest that were analyzed, however it was not significantly

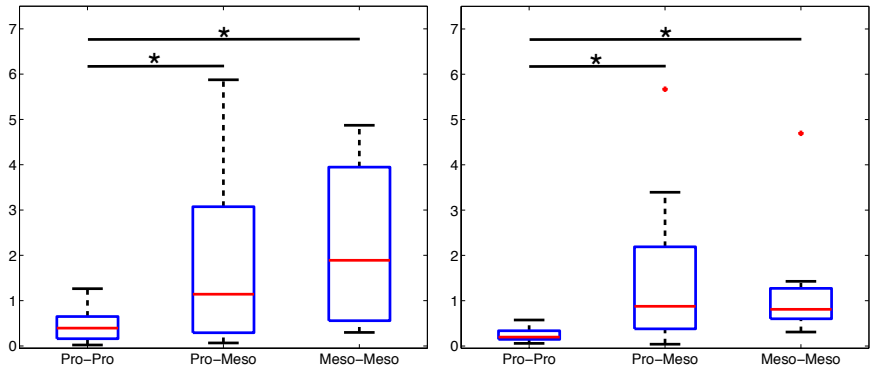

Figure 9: Coupling strength in the pro-meso thoracic ganglia over all experiments using the DCM approach. Left: Coupling strength for biased intervals (N=5 , n=10); Right: Coupling strength for unbiased intervals (N=2, n=4).

weaker than all other connections. This reflects the role of the front legs that are also heavily involved in searching movements. Thus it is necessary for the stick insect to be able to move both legs independently, what would be guaranteed by a weaker coupling between both sides of the front leg CPGs.

Our analysis revealed that the intrasegmental coupling of the mesothoracic ganglion is the strongest of all connections, no matter if we are looking at the phase-difference approach or the biased or unbiased DCM approach (Figure 10). The cut-connective experiment also showed that the presence of the meso-meta connection was needed for a strong intrasegmental coupling in the metathoracic ganglion. This result is also supported by [17] where they could show that the phase-coupling of the recordings in the metathoracic ganglion became more stable when the meso- and metathoracic ganglia were interconnected. These findings combined suggest that the information from the mesothoracic CPGs are stabilizing the other segment and act as some kind of a clock generating the rhythm.

In our analysis we showed for the first time that well established methods for an-

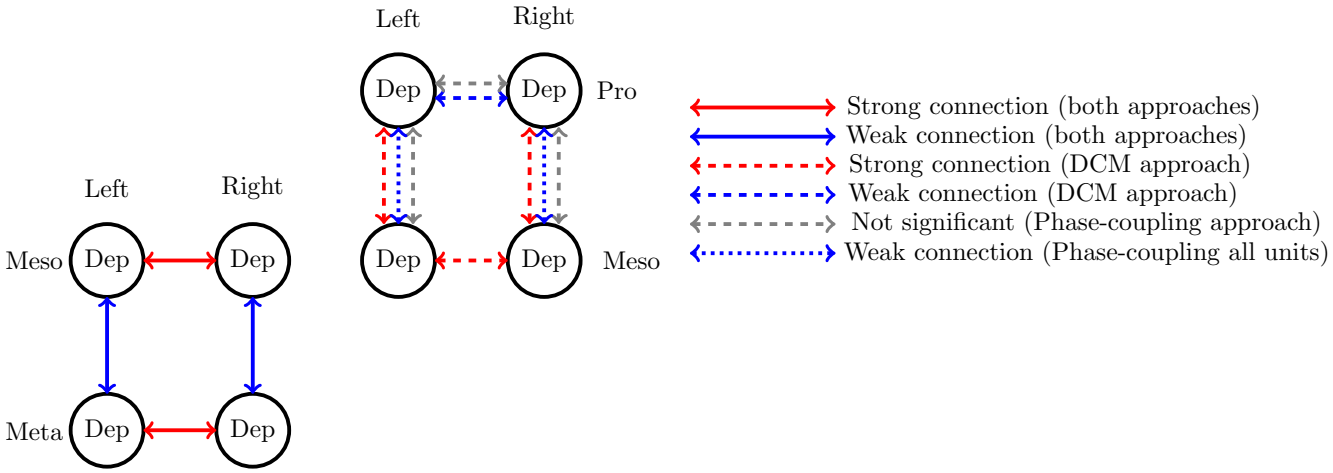

Figure 10: Summary of the differences in coupling strengths obtained by both approaches. Strong connections shown in red, weak connections shown in blue, no significant change is marked in grey.

alyzing EEG data can be adapted for the analysis of pilocarpine induced fictive locomotion pattern of the stick insect *Carausius morosus*. We have seen that the DCM approach that uses neural mass models, that were developed for EEG, was able to detect changes in the system for different experimental conditions. DCM detected the absence of coupling between the meso- and metathoracic ganglia after the connectives were cut.

The next thing to investigate would be to do experiments with electrodes recording from all three segments at the same time to get information on the coupling structure of the pro- and metathoracic ganglion and also to investigate the change of coupling strength that might occur when both connectives anterior and posterior of the mesothoracic ganglion are intact. We are also planning to use the coupling strengths produced by DCM to build models of phase oscillators or more sophisticated models to compare their output to the experimental data.

References

[1] **Berens P**. Circstat: a matlab toolbox for circular statistics. *J Stat Softw* 31: 1–21, 2009.

[2] **Borgmann A, Scharstein H, Büschges A**. Intersegmental coordination: influence of a single walking leg on the neighboring segments in the stick insect walking system. *J Neurophysiol* 98: 1685–1696, 2007.

[3] **Brunner von Wattenwyl K, Redtenbacher J** *Die Insektenfamilie der Phasmiden* W. Engelmann, Leipzig, 1908.

[4] **Büschges A**. Sensory control and organization of neural networks mediating coordination of multisegmental organs for locomotion. *J Neurophysiol* 93: 1127–1135, 2005.

[5] **Büschges A, Akay T, Gabriel JP, Schmidt J**. Organizing network action for locomotion: insights from studying insect walking. *Brain Res Rev* 57: 162–171, 2008.

[6] **Büschges A, Schmitz J, Bässler U**. Rhythmic patterns in the thoracic nerve cord of the stick insect induced by pilocarpine. *The J Exp Biol* 198: 435–56, 1995.

[7] **Chen C, Henson R, Stephan K, Kilner J, Friston K**. Forward and backward connections in the brain: a dcm study of functional asymmetries. *NeuroImage* 45: 453462, 2009.

[8] **Daido H**. Order function theory of macroscopic phase-locking in globally and weakly coupled limit-cycle oscillators. *Int J Bifurc Chaos* 07: 807–829, 1997.

[9] **Delcomyn F**. Neural basis of rhythmic behavior in animals. *Sci* 210: 492–498, 1980.

[10] **Foth E, Bässler U**. Leg movements of stick insects walking with five legs on a treadwheel and with one leg on a motor-driven belt. I. General results and 1:1-coordination. *Biol Cybern* 51: 313–318, 1985.

[11] **Graham D, Epstein S**. Behaviour and motor output for an insect walking on a slippery surface: Ii. backward walking. *J experimental biology* 118: 287–296, 1985.

[12] **Grefkes C, Eickhoff SB, Nowak DA, Dafotakis M, Fink GR**. Dynamic intra- and interhemispheric interactions during unilateral and bilateral hand movements assessed with fmri and {DCM}. *NeuroImage* 41: 1382 – 1394, 2008.

[13] **Hess D, Büschges A**. Sensorimotor pathways involved in interjoint reflex action of an insect leg. *J Neurobiol* 33: 891–913, 1997.

[14] **Kiebel S, Garrido M, Moran R, Friston K**. Dynamic causal modelling for eeg and meg. *Cogn Neurodynamics* 2: 121–136, 2008.

[15] **Ludwar BC, Göritz ML, Schmidt J**. Intersegmental coordination of walking movements in stick insects. *J neurophysiology* 93: 1255–1265, 2005.

[16] **Mallada E, Tang A**. Synchronization of weakly coupled oscillators: coupling, delay and topology. *J Phys A: Math Theor* 46: 505101, 2013.

[17] **Mantziaris B, Borgmann A, Büschges A**. Weak coupling between fictive motor rhythms of levator depressor pattern generating networks in the stick insect. *preparation* , 2015.

[18] **Marder E, Bucher D**. Central pattern generators and the control of rhythmic movements. *Curr Biol* 11, 2001.

[19] **Marple S J**. Computing the discrete-time ldquo;analytic rdquo; signal via fft. *Signal Process IEEE Transactions on* 47: 2600–2603, 1999.

[20] **Moran R, Kiebel S, Rombach N, O'Connor W, Murphy K, Reilly R, Friston K**. Bayesian estimation of synaptic physiology from the spectral responses of neural masses. *NeuroImage* 42: 272–284, 2008.

[21] **Moran R, Kiebel S, Stephan K, Reilly R, Daunizeau J, Friston K**. A neural mass model of spectral responses in electrophysiology. *NeuroImage* 37: 706–720, 2007.

[22] **Moran RJ, Jung F, Kumagai T, Endepols H, Graf R, Dolan RJ, Friston KJ, Stephan KE, Tittgemeyer M**. Dynamic causal models and physiological inference: A validation study using isoflurane anaesthesia in rodents. *PLoS ONE* 6: e22790, 2011.

[23] **Rigoux L, Stephan K, Friston K, Daunizeau J**. Bayesian model selection for group studies – revisited. *NeuroImage* 84: 971–985, 2014.

[24] **Rosenblum M, Pikovsky A, Kurths J, Schäfer C, Tass PA**. Phase synchronization: from theory to data analysis. *Handb biological physics* 4: 93–94, 2001.

[25] **Schmitz J, Büschges A, Delcomyn F**. An improved electrode design for en passant recording from small nerves. *Comp Biochem Physiol Part A: Physiol* 91: 769 – 772, 1988.

[26] **Tass P, Rosenblum MG, Weule J, Kurths J, Pikovsky A, Volkmann J, Schnitzler A, Freund HJ**. Detection of $n : m$ phase locking from noisy data: Application to magnetoencephalography. *Phys Rev Lett* 81: 3291–3294, 1998.

[27] **Walz JM, Goldman RI, Carapezza M, Muraskin J, Brown TR, Sajda P**. Simultaneous eeg-fmri reveals temporal evolution of coupling between supramodal cortical attention networks and the brainstem. *The J Neurosci* 33: 19212–19222, 2013.

[28] **Wendler G**. The co-ordination of walking movements in arthropods. *Symp Soc for Exp Biol* 20: 229–249, 1965.

4 Discussion

In this work I present different approaches for the analysis of couplings and especially the strengths of coupling in neuronal networks that are based on experimental data. First, I will discuss how networks consisting of phase-oscillators can be used to reproduce synchronization effects from EEG data and how the analysis of these models reveals information about the alteration of coupling strengths of different brain regions in the comparison of healthy control subjects and schizophrenia patients (see Rosjat et al., 2014). Next, we used a mathematical model based on Hodgkin-Huxley type neurons to define the coupling strengths between the pro- and mesothoracic ganglion of the protractor-retractor system of the stick insect (see Tóth et al., 2015). In the third study we used intraregional phase locking to define a neurophysiological marker of movement execution from EEG recordings of the human brain during simple motor tasks that were induced either internally or externally by a visual cue (Popovych et al, under review). Following, I present the results from two studies that further analyzed the aforementioned systems in the human brain and the stick insect locomotor system. In the first part phase-locking analysis to identify the synchronization effects caused by interregional coupling between different motor regions of the human brain were applied (see section 3.1, (Rosjat et al., in prep)). In the last part possible applications of analysis methods, developed for EEG recordings, in the analysis of extracellular nerve recordings of the stick insect were demonstrated. There, I used two different approaches, one based on phase-analysis and another one based on dynamic causal modeling, to investigate the intrinsic intra- and intersegmental coupling strengths in the thoracic nerve cord of the stick insect (see section 3.2, (Rosjat et al., in prep)) during fictive locomotion.

In the first study (see Rosjat et al., 2014) the connectivity changes in the thalamo-cortical loop in schizophrenia were analyzed. For this purpose, we built a mathematical model that was based on phase-oscillators in the θ- and $\alpha-$frequency range as an abstract description of the thalamo-cortical loop. Those frequencies were selected, since they were shown to change significantly in patients suffering from schizophrenia in comparison to a control group (c.f. Brockhaus-Dumke et al., 2008). Each cortical region and the thalamic region were modeled by a large number of coupled oscillators. The mathematical model was then used to first reproduce the phase-locking phenomena observed in recordings of a double-click paradigm and then to make hypotheses on the

connectivity changes due to the illness. We have seen that coupling strengths from cortical to thalamic regions was reduced drastically, while the back coupling to the cortical regions was just a little weaker in the patient group. Thus, our model suggested that schizophrenia results from pathological interactions between brain regions. In a next step groups of subjects treated with different drugs, e.g. eicosapentaenoic acid (Peet et al., 2001), pregnenolone (Marx et al., 2009; Ritsner et al., 2010) or antipsychotics (Carlsson, 1978), should be included in the analysis to test whether the reduction of pathological symptoms is also represented in a regained phase locking in the auditory cortex.

In the second study (see Tóth et al. (2014)) we aimed at a better understanding of the structure and function of the inter-segmental coordination between the pro- and mesothoracic neural networks of the stick insect. Therefore, we used mathematical models, at first a simplified "skeleton model" followed by an extended version of the existing 1-leg model (Tóth et al., 2012), to produce simulated PRCs. We made use of corresponding experimental results that were published earlier as well as up to then unpublished results (Borgmann et al., 2009). Our approach was to compare simulated to experimentally obtained PRCs under the assumption that similar PRCs are generated by equally similar underlying networks. Even though the stimuli were applied differently in the simplified "skeleton" model and the extended 1-leg model, they both yield similar results concerning the nature and strengths necessary to produce reasonable PRCs. Both approaches showed that a strong excitatory connection between protractor CPGs and a moderate excitatory connection between retractor CPGs of the pro- and mesothoracic ganglia were crucial for the generation of PRCs which fitted the experimental ones well, while inhibitory connections proved to be irrelevant. Even though models that were solely connected through retractor CPG neurons were able to reproduce the observed walking behaviour, connections only on the retractor side were not sufficient to produce acceptable PRCs.

In the third study (see Popovych et al., under review) we sought to identify EEG markers related to the precise timing of mechanisms underlying isolated finger tapping movements. We hypothesized that such neural markers would be connected with phase-synchronization that is invariant irrespective of the hand performing and the cue triggering the task. For this purpose, we performed EEG recordings on 18 right-handed healthy human control subjects that were asked to perform internally and externally triggered finger tapping movements. The design of the task was held as simple as possible to achieve the aim of the study. This way it will be possible to use the same paradigm also in elderly subjects or patients suffering from neurological disorders affecting the motor system in future investigations. We analyzed the EEG data with respect to the changes in power of certain frequency bands as well as synchronization

measured by the phase-locking index (PLI). We found phase locking during movement preparation and movement execution in the δ-θ frequency band that was significantly increased compared to its baseline value in all electrodes of interest above motor regions in internally and externally triggered movements. Externally triggered movements showed an increased phase locking in visual electrodes in addition. The computation of lateralization indices revealed that phase locking is stronger in the hemisphere contralateral to the moving hand. In contrast to the widely known bio-markers of movement preparation and execution (Bereitschaftspotential, ERD, ERS) that focus on changes in amplitudes only (Shibasaki and Hallett, 2006; Pfurtscheller and da Silva, 1999; Neuper et al., 2006), the PLI is a direct measure of synchronization at the level of neural oscillations.

It remains to be tested whether the increase in phase locking is depending on actual movement execution and whether this effect is specific for index finger movements. For ERD and ERS it has been shown that both can be observed in different kinds of limb movements as well as during motor imaginary tasks (Pfurtscheller and da Silva, 1999; Neuper and Pfurtscheller, 2001; Pfurtscheller, 2001; Neuper et al., 2006; Pfurtscheller et al., 2006), however, the strengths observed and the brain regions showing the effect vary in the different kinds of movements.

We hypothesize that the δ-θ rhythm is reset to a certain preferred phase angle at which the spike rate of the motor neurons projecting from M1 to the spinal cord is increased. As we have seen, this increase in phase locking can be observed at the point in time where the command to move the finger is send from M1 to the spinal cord (approximately 50 ms before the onset of the actual movement). In accordance to this hypothesis Lee et al. (2005) found an increase of firing rate at certain preferred phase angles during the θ cycle in local field potential (LFP) data in monkeys during working memory tasks. They hypothesized that θ oscillations provide a mechanism for structuring the interaction of different brain regions. Thus, we suggest that δ-θ phase locking serves as a common mechanism at which distinct cortical pathways, which initiate internally and externally triggered movements, converge to the same motor output, i.e. the finger movements.

The fourth study (Rosjat et al., in preparation) in chapter 3.1 presents results that build on the third study presented above and showed that the phase-locking effects are not limited to local brain areas, but can also be observed on the interregional level. Interregional phase-locking analyses were performed on the data set consisting of the internally and externally triggered index finger movements of the 18 young healthy right-handed subjects (c.f. Popovych et al., 2015). Phase-locking values similar to the measures suggested by (Lachaux et al., 1999) were calculated to investigate

the phase-locking between the electrodes of interest (C3-C4, Cz-FCz, FC3-FC4, Oz). We found an increase in phase locking between the motor regions in δ-θ frequencies around movement onset in all conditions. In internally triggered movements this effect was mainly visible in pairs of channels with at least one channel on the hemisphere contralateral to the hand performing the task. This lateralization effect turned out to be less pronounced when the subjects were performing the task with their right hand. This could be due to the fact that all our subjects were right-handed and needed less activity when performing the task with their dominant hand. This was also reflected in other measures that have been shown earlier (peak PLI value (Popovych et al., 2015), maximal amplitude in the Bereitschaftspotential (Shibasaki and Hallett, 2006)). However, it still needs to be verified whether a group of left-handed subjects would show a similar reduction in synchronization while using their left hands. Externally triggered movements, on the other hand side, showed a very strong increase in phase locking that resulted in significant changes in nearly all pairs of electrodes investigated. Since the sole analysis of significant changes did not yield much information in this condition, we added an analysis of lateralization. Therefore, the sPLVs were normalized by rescaling to the relative change compared to baseline values. It turned out that even though the changes in externally triggered movements were significant in nearly every pair, the stronger phase locking could be found in the electrodes above the hemisphere contralateral to the moving hand in 70% for externally triggered movements and in 87.5% for internally triggered movements. The analysis of the preferred phase differences revealed different structures for self-initiated and visually-cued tapping conditions. While the interregional phase locking originates in M1 and propagates to SMA and PM in the self-initiated tapping condition, the direction is reversed in the visually-cued tapping condition, namely it originates in PM and propagates to SMA and M1. Analyses of additional channels above parietal and frontal cortices will be necessary to test whether they might be the origin of phase locking in the self-initiated condition.

In contrast to the PLI analysis (see chapter 2.3), this approach showed an additional phase locking in the β-frequency band (13-30 Hz) after the movement has finished. Unlike the low frequency phase locking, this effect was significantly higher in the internally triggered tapping condition as compared to the externally initiated movements. In de Hemptinne et al. (2013, 2015) they found first evidence for the contribution of β synchronization in movement suppression. We suggest that the late high frequency synchronization in our data set might be related to the suppression of a second finger movement after the button press. This effect might be enhanced during the internally triggered movements, because subjects did not react to a certain stimulus and had to prevent multiple voluntary finger movements. The analysis of the preferred phase relation between M1 and SMA during β phase synchronization revealed that M1 is preceding SMA by 130 to 160°. This suggests that SMA is acting on M1 and thereby

might prevent additional finger movements. Analyses of subjects with motor suppression deficits will be needed to test whether they show decreased phase locking in the β frequencies after the movement had finished.

Over the past years several studies have employed the single-trial phase-locking value (PLV) in the detection of imaginary movements in brain-computer interfaces (Brunner et al., 2006; Krusienski et al., 2012; Song et al., 2005; Wang et al., 2006a). They showed an increased predictability of motor imaginary tasks for the PLV compared to methods that are based on amplitude dynamics especially in the first 1-2 s of motor imagination (Song et al., 2005). Their results suggest that PLV is another robust feature for the differentiation between different motor tasks, e.g. left and right finger or foot movements (Brunner et al., 2006). The differences in interregional phase locking and preferred phase relationships, as presented above, might serve as an additional aspect for a differentiation between motor tasks. However, it remains to be checked whether the observed intra- and interregional phase-locking effects are special for motor execution or whether they would be present in motor imagination, too.

In the last study (Rosjat et al., in preparation), in chapter 3.2, I looked at the intrinsic intra- and intersegmental connectivity in the pro-, meso- and metathoracic ganglia of the stick insect levator-depressor system from two different perspectives. Both approaches are purely data driven. While the phase-coupling approach is directly based on synchronization measures of the phases of the recorded signal, the DCM approach utilizes mathematical models fitted to the recorded data to define the appropriate coupling strengths best fitting the data. Even though DCM was first developed for human brain recordings, I was able to substantiate this method with an experiment under a controlled connectivity setting, i.e. after complete removal of certain connections in the network. The analyses showed that the coupling structure, most likely to be present intrinsically, has a cyclic form within pairs of neighbouring segments. Thus, the results suggest that there are no cross-connections from one side of a thoracic ganglion to the other side of a neighbouring thoracic ganglion. Both approaches showed a very high agreement in the coupling strengths in most of the connections underpinning the results. They revealed that the intrasegmental coupling strengths in the meso- and metathoracic ganglia were significantly stronger than the intersegmental coupling strength between both ganglia. While this effect stayed present over different recorded intervals for the mesothoracic intrasegmental connectivity, it got weaker in the metathorax when analyzing randomly selected intervals, i.e. they were not necessarily defined as coupled by the phase-approach. Additionally, after decoupling the mesothoracic ganglion from the metathoracic ganglion, the mesothoracic coupling strength was increased up to twenty times as strong as in the coupled situation. Thus, the intra-segmental coupling strength needed to be increased to maintain the synchronization when the feedback

from the metathoracic ganglion is removed.

Despite some problems in generating regular rhythms in the prothoracic ganglion both approaches showed at least the same trend in the strengths of connections between the pro- and mesothoracic ganglion. While the mesothoracic intrasegmental connectivity was again the highest, the prothoracic intrasegmental connectivity strength was significantly weaker in the DCM approach with the same trend in the phase-approach. However, the difference was not significant on a statistical level in the phase-approach. The special role of the front legs, that are controlled by the CPGs located in the prothoracic ganglion, during walking has been discussed in (Grabowska et al., 2012). They showed that front legs can be moved independently of the walking cycles of the adjacent legs, while the remaining four legs performed coordinated movements that were similar to walking patterns observed in quadrupeds. They suggested that only a weak inter-segmental coupling between the front and the middle legs would be necessary in the decoupled movements, while it would need to be strengthened in a coupled regular hexapedal walking situation. Our results support this hypothesis as they showed large variability of strong and weak intra-segmental coupling between pro- and mesothoracic ganglia. The weaker coupling in the prothoracic ganglion would enable the animal to decouple the front legs from the middle and hind legs to use them for independent movements, e.g. searching movements (Dürr, 2001), while the other two pairs of legs remain unaffected. In our analysis of the pro-, meso- and metathoracic ganglia the intra-segmental mesothoracic connectivity was the strongest and most stable one. This suggests that it might serve as some kind of an internal controller producing a stable locomotor pattern.

The studies presented above investigated the interactions in neuronal networks either in the stick insect locomotor system or in human cortical networks. All results discussed above showed evidences for the high importance of oscillatory phases in the neuronal communication.

The next step in the investigation of the human motor cortex will include experiments on different groups of subjects. These groups might contain young healthy left-handed subjects to get information about the differences arising from the dominant hand. We assume that phase locking as well as amplitudes in the Bereitschaftspotential will be weaker when using the left dominant hand, while it might get more prominent when they perform the experiments with their right hand. Another group consisting of elderly subjects could serve as a control group for non-pathological ageing. The subjects in this group will show slower reactions, make more errors when reacting to visual stimuli and have bigger problems in producing internally triggered movements that fulfill the requirements of the experiment. Therefore, we suppose that the phase-locking effects

will get weaker in general. In a third group we could analyze the effects of pathological ageing in subjects suffering from mental disorders that affect the motor system, e.g. stroke patients. Since these subjects are in the same age range as the group of elderly subjects, they will show similar changes in the phase locking effects, but there will be other additional changes due to the lesioned hemisphere. Those changes in phase locking might include reduction in the lesioned hemisphere as well as an increase in the unaffected hemisphere that has to compensate for the loss of function. We also suspect to observe an increase in PLV lateralization to the channel pairs of the ipsilateral hemisphere when subjects perform finger movements with their affected hand.

Suggestion for a mathematical model of the human motor system

It will now be possible to build mathematical models to analyze the underlying network structure and coupling strengths between the involved motor areas. The connectivity structure best fitting the measured data could be analyzed using dynamic causal modeling (cf. section 3.2, (Kiebel et al., 2008)). Previous fMRI studies for bilateral movements (Grefkes et al., 2008) and EEG studies for unilateral movements (Herz et al., 2012) suggest an all-to-all coupling in the regions of interest in the motor system. Therefore, a first model might consist of a single fully connected hemisphere modeling the effects of unilateral movements that could then be enhanced to a full bilateral system for the analysis of left and right handed tasks. Each of the desired motor regions will be represented by a population of phase oscillators that interact via their mean fields as presented in section 2.1 for the thalamo-cortical loop. Since the strongest phase-locking effects occur in the δ, θ and β frequency bands, as we have seen in section 2.3 and 3.1, those populations are composed of oscillators with natural frequencies lying within these frequency ranges. The internal and external stimuli might then act on different parts of the motor system. As suggested by the phase difference analysis, the external stimulus will act on PM and SMA, while the internal stimulus will act on M1 directly. The increase in synchronization in the primary motor cortex populations, determined by their mean fields, will result in an increase of information send to the motor network to trigger the motor output. The local motoneuron network itself is controlled by CPGs (c.f. Calancie et al., 1994; Zehr et al., 2004). In the model the signals send from the primary motor cortex to the MN network would play the role of the central drive (cf. CPG network of the 1-leg model (Tóth et al., 2012)) that evokes certain patterns produced by the CPG and thereby in the motor output. The different CPG networks controlling the left and right hand movements do not need to be coupled strongly, since

each hand can be moved independent of what the other hand is doing. This situation can be compared to the weakly coupled CPG networks of the prothoracic ganglion in the stick insect that might be due to the role of the front legs in searching movements (cf. section 3.2). CPG networks controlling human left and right leg movements, on the other side, need to be closely linked to each other to prevent simultaneous elevation of both legs. However, it still needs to be checked whether similar phase-locking effects are present during leg movements, too.

These models will help getting insights in the interplay of the involved brain regions and how these interactions change during non-pathological and pathological ageing. The results might then be verified either by comparison to coupling strengths obtained by DCM for phase coupling (Penny et al., 2009) or by further experiments using transcranial magnetic stimulation (TMS). With this technique it is possible to increase or decrease the activity and the connectivity of certain brain areas, e.g. primary motor cortex (Baeken and De Raedt, 2011; Fitzgerald et al., 2008; Terao and Ugawa, 2002). Thereby hypotheses of the model in terms of activity and connectivity changes of certain brain regions in different groups of subjects can be verified by application of similar changes induced by TMS to a control group.

Comparison of the phase oscillator model to different mathematical models

The phase oscillator model suggested above consists of coupled oscillator populations with distributed natural frequencies in certain frequency ranges, as they were used in (Rosjat et al., 2014). A large number of mathematical models of neuronal networks, on the other hand, focus on small networks of local cortical structures.

The model presented in (Jansen and Rit, 1995) deals with the coupling of single cortical columns. They investigated the effect of populations of pyramidal cells that interact with populations of inhibitory and excitatory interneurons. The authors were able to reproduce a large variety of EEG-like activity using this modelling approach. Dynamic Causal Modeling (Friston et al., 2003; Kiebel et al., 2008) is fitting the output of the Jansen-Rit model to recorded EEG data via forward modeling of the produced output to scalp activity. The compositions of the three layers, pyramidal cells, inhibitory and excitatory interneurons, used in the Jansen-Rit model, were developed to reproduce activity of the visual cortex. Thus, the model parameters are set such that they represent a well developed granular layer IV. However, this layer is not prominent in the motor cortex (Amunts et al., 1996; Skoglund et al., 1997; Yamawaki et al., 2015). Thereby, the model used in this approach is not applicable to the motor cortex directly without

further adjustments.

The NEST toolbox (Gewaltig and Diesmann, 2007) simulates the signals recorded with microarrays, i.e. the activity of local networks. The models supported by this toolbox are, among others, integrate-and-fire neuron models and Hodgkin-Huxley type neurons. With this toolbox it is possible to determine local spike-frequency synchronization patterns.

Other models describing the brain dynamics underlying schizophrenia (an der Heiden, 2006; Loh et al., 2007; Rolls et al., 2008) are based on the simulation of networks of pyramidal cells. In (an der Heiden, 2006) they investigated microstructural systems of pyramidal cells. The authors in (Loh et al., 2007; Rolls et al., 2008) used a top-down approach in modelling the symptoms of schizophrenia via leaky integrate-and-fire models to simulate the interaction of populations of pyramidal cells, inhibitory interneurons and AMPA, NMDA and $GABA_A$ synapses. In both approaches, the microstructural one and the top-down approach, certain firing patterns were associated with control behaviour and different symptoms of schizophrenia.

In contrast to these mathematical models of human cortical networks, the suggested phase oscillator model does not include explicit biophysical properties. In this way the model is not restricted to a certain application and it is possible to adapt the described model to match other situations that make it necessary to use different cortical areas or different frequency ranges, e.g. when modelling different mental illnesses like Parkinson's disease or bipolar disorder. It has been shown that these disorders show abnormal effects in α frequencies (bipolar disorder (Kim et al., 2013)) and β frequencies (Parkinson's disease (an der Heiden, 2006)). By focussing on these frequency bands, the phase oscillator model would be able to treat the effects observed in these diseases as well.

5 Conclusion

All the different works in my thesis deal with mechanisms related to coordination of neuronal activity. The studies yield evidence that the communication on level of oscillatory phases is crucial for establishing and maintaining coordinated activity in neuronal networks. My thesis combines studies of local CPG networks in the stick insect locomotor system and large scale cortical control networks in the human motor and auditory cortex. Both parts make use of direct analysis of experimental data as well as mathematical models as tools for the analysis of the underlying networks producing the observed activities.

The studies in chapters 2.2 and 3.2 add to previous experimental studies by (Borgmann et al., 2007, 2009). In the first study we emphasized the importance of intersegmental connections in the protractor-retractor system in the pro- and mesothoracic ganglia of the stick insect. The existence of the excitatory intersegmental connections was crucial to reproduce experimentally obtained PRCs. The results were stable over a large range of connectivity strengths. However, the results presented in chapter 3.2 show evidence for the existence of intrinsic inter- and intrasegmental coupling in the levator-depressor system.

In the studies presented in chapters 2.1, 2.3 and 3.1, we have seen that the communication between several brain areas is necessary to produce normal brain activity. A decrease of coupling strengths between brain regions led to loss of synchronization that could be associated with a loss of cognitive functions in neurological disease. In the extended 1-leg model of the stick insect we have observed that a reduction of inter-segmental coupling strengths will lead to PRCs that are not comparable to the ones observed in experimental data. This could also be interpreted as a pathological behaviour in the stick insect due to insufficient coupling of the segments.

Furthermore, I want to emphasize, that the phase-locking effects reported in 2.3 and 3.1 might serve as another robust marker of movement execution. The sPLV, when calculated over motor imaginary intervals in single trials, would possibly also be applicable as an additional measure in the field of brain-computer interfaces and might improve the predictability of different movement conditions.

The strength of the approaches presented in this thesis is the easy adaptability to different research questions. This is shown by the models of CPG networks (Daun-Gruhn and Tóth, 2011) that can be used for various experimental conditions, e.g. single leg preparations. As it has been shown by (Grabowska, 2014) this basic module can easily be adjusted in such a way that it can also be used to represent multi-legged locomotion in other animals, e.g. crustaceans. The easy adaptability is also shown by the phase oscillator ensemble model (Rosjat et al., 2014), that can be used for studies of different brain areas or different dysfunctions by replacing or adding the necessary oscillator regimes to the neural network.

Literaturverzeichnis

Akay T, Bässler U, Gerharz P, Büschges A (2001) The role of sensory signals from the insect coxa-trochanteral joint in controlling motor activity of the femur-tibia joint. *J neurophysiology* 85:594–604.

Akay T, Haehn S, Schmitz J, Bueschges A (2004) Signals from load sensors underlie interjoint coordination during stepping movements of the stick insect leg. *J neurophysiology* 92:42–51.

Akay T, Ludwar BC, Goeritz ML, Schmitz J, Bueschges A (2007) Segment specificity of load signal processing depends on walking direction in the stick insect leg muscle control system. *J Neurosci* 27:3285–3294.

Amunts K, Schleicher A, Zilles K (1996) Persistence of layer iv in the primary motor cortex (area 4) of children with cerebral palsy. *J fur Hirnforschung* 38:247–260.

an der Heiden U (2006) Schizophrenia as a dynamical disease. *Pharmacopsychiatry* 39.

Baeken C, De Raedt R (2011) Neurobiological mechanisms of repetitive transcranial magnetic stimulation on the underlying neuro circuitry in unipolar depression. *Dialogues clinical neuroscience* 13:139.

Baker S, Olivier E, Lemon R (1997) Coherent oscillations in monkey motor cortex and hand muscle emg show task-dependent modulation. *The J physiology* 501:225–241.

Baker S, Spinks R, Jackson A, Lemon R (2001) Synchronization in monkey motor cortex during a precision grip task. i. task-dependent modulation in single-unit synchrony. *J Neurophysiol* 85:869–885.

Bässler U (1967) On the regulation of the position of the femur-tibial joint of the walking-stick insect carausius morosus at rest and in motion. *Kybernetik* 4:18–26.

Bässler U (1977a) Sense organs in the femur of the stick insect and their relevance to the control of position of the femur-tibia-joint. *J comparative physiology* 121:99–113.

Bässler U (1977b) Sensory control of leg movement in the stick insect carausius morosus. *Biol Cybern* 25:61–72.

Bässler U (1983) *Neural basis of elementary behavior in stick insects* Springer Science & Business Media.

Benjamini Y, Hochberg Y (1995) Controlling the false discovery rate: A practical and powerful approach to multiple testing. *J Royal Stat Soc Ser B (Methodological)* 57:289–300.

Berens P (2009) Circstat: a matlab toolbox for circular statistics. *J Stat Softw* 31:1–21.

Blinowska K, Durka P (1994) The application of wavelet transform and matching pursuit to the time-varying eeg signals. *Intell engineering systems through artificial neural networks* 4:535–540.

Borgmann A, Hooper SL, Büschges A (2009) Sensory feedback induced by front-leg stepping entrains the activity of central pattern generators in caudal segments of the stick insect walking system. *The J neuroscience* 29:2972–2983.

Borgmann A, Scharstein H, Büschges A (2007) Intersegmental coordination: influence of a single walking leg on the neighboring segments in the stick insect walking system. *J neurophysiology* 98:1685–1696.

Borgmann A, Toth TI, Gruhn M, Daun-Gruhn S, Büschges A (2011) Dominance of local sensory signals over inter-segmental effects in a motor system: experiments. *Biol cybernetics* 105:399–411.

Brockhaus-Dumke A, Müller R, Faigle U, Klosterkötter J (2008) Sensory gating revisited: Relation between brain oscillations and auditory evoked potentials in schizophrenia. *Schizophr Res* 99:238–249.

Brodersen K, Deserno L, Schlagenhauf F, Penny W, Buhmann J, Stephan K (2014) Dissecting psychiatric spectrum disorders by generative embedding. *NeuroImage: Clin* 4:98–111.

Brodmann K (1909) Vergleichende lokalisationslehre der groshirnrinde. *Leipzig: Barth* .

Brunner C, Scherer R, Graimann B, Supp G, Pfurtscheller G (2006) Online control of a brain-computer interface using phase synchronization. *Biomed Eng IEEE Transactions on* 53:2501–2506.

Brunner von Wattenwyl K, Redtenbacher J (1908) *Die Insektenfamilie der Phasmiden* W. Engelmann, Leipzig.

Büschges A (2005) Sensory control and organization of neural networks mediating coordination of multisegmental organs for locomotion. *J Neurophysiol* 93:1127–1135.

Büschges A, Akay T, Gabriel JP, Schmidt J (2008) Organizing network action for locomotion: insights from studying insect walking. *Brain Res Rev* 57:162–171.

Büschges A, Schmitz J, Bässler U (1995) Rhythmic patterns in the thoracic nerve cord of the stick insect induced by pilocarpine. *The J Exp Biol* 198:435–56.

Büschges A (1995) Role of local nonspiking interneurons in the generation of rhythmic motor activity in the stick insect. *J neurobiology* 27:488–512.

Büschges A (1998) Inhibitory synaptic drive patterns motoneuronal activity in rhythmic preparations of isolated thoracic ganglia in the stick insect. *Brain research* 783:262–271.

Büschges A, Gruhn M (2008) Mechanosensory feedback in walking: from joint control to locomotor patterns. *Adv Insect Physiol* 34:193–230.

Calancie B, Needham-Shropshire B, Jacobs P, Willer K, Zych G, Green BA (1994) Involuntary stepping after chronic spinal cord injury. *Brain* 117:1143–1159.

Carlsson A (1978) Antipsychotic drugs, neurotransmitters, and schizophrenia. *Am J Psychiatry* 135:164–173.

Carlsson A (2006) The neurochemical circuitry of schizophrenia. *Pharmacopsychiatry* 39:10–14.

Chen C, Henson R, Stephan K, Kilner J, Friston K (2009) Forward and backward connections in the brain: a dcm study of functional asymmetries. *NeuroImage* 45:453—462.

Cohen MX, Donner TH (2013) Midfrontal conflict-related theta-band power reflects neural oscillations that predict behavior. *J neurophysiology* 110:2752–2763.

Cruse H (1990) What mechanisms coordinate leg movement in walking arthropods? *Trends neurosciences* 13:15–21.

Cruse H, Dürr V, Schilling M, Schmitz J (2009) Principles of insect locomotion In *Spatial temporal patterns for action-oriented perception in roving robots*, pp. 43–96. Springer.

Daido H (1997) Order function theory of macroscopic phase-locking in globally and weakly coupled limit-cycle oscillators. *Int J Bifurc Chaos* 07:807–829.

Dale AM, Liu AK, Fischl BR, Buckner RL, Belliveau JW, Lewine JD, Halgren E (2000) Dynamic statistical parametric mapping: combining fmri and meg for high-resolution imaging of cortical activity. *Neuron* 26:55–67.

Daun S, Rubin JE, Rybak IA (2009) Control of oscillation periods and phase durations in half-center central pattern generators: a comparative mechanistic analysis. *J computational neuroscience* 27:3–36.

Daun-Gruhn S, Tóth TI, Borgmann A (2011) Dominance of local sensory signals over inter-segmental effects in a motor system: modeling studies. *Biol cybernetics* 105:413–426.

Daun-Gruhn S, Tóth TI (2011) An inter-segmental network model and its use in elucidating gait-switches in the stick insect. *J computational neuroscience* 31:43–60.

de Hemptinne C, Ryapolova-Webb ES, Air EL, Garcia PA, Miller KJ, Ojemann JG, Ostrem JL, Galifianakis NB, Starr PA (2013) Exaggerated phase–amplitude coupling in the primary motor cortex in parkinson disease. *Proc Natl Acad Sci United States Am* 110:4780–4785.

de Hemptinne C, Swann NC, Ostrem JL, Ryapolova-Webb ES, San Luciano M, Galifianakis NB, Starr PA (2015) Therapeutic deep brain stimulation reduces cortical phase-amplitude coupling in parkinson's disease. *Nat Neurosci* 18:779–786.

Deiber MP, Sallard E, Ludwig C, Ghezzi C, Barral J, Ibañez V (2012) Eeg alpha activity reflects motor preparation rather than the mode of action selection. *Front integrative neuroscience* 6.

Delcomyn F (1980) Neural basis of rhythmic behavior in animals. *Sci* 210:492–498.

Delcomyn F (1971) The effect of limb amputation on locomotion in the cockroach periplaneta americana. *J Exp Biol* 54:453–469.

Delcomyn F (1981) Insect locomotion on land In *Locomotion and energetics in arthropods*, pp. 103–125. Springer.

Delorme A, Makeig S (2004) Eeglab: an open source toolbox for analysis of single-trial eeg dynamics including independent component analysis. *J neuroscience methods* 134:9–21.

Deserno L, Sterzer P, Wüstenberg T, Heinz A, Schlagenhauf F (2012) Reduced prefrontal-parietal effective connectivity and working memory deficits in schizophrenia. *The J Neurosci* 32:12–20.

Dirac P (1953) The lorentz transformation and absolute time. *Phys* 19:888–896.

Dürr V (2001) Stereotypic leg searching movements in the stick insect: kinematic analysis, behavioural context and simulation. *J Exp Biol* 204:1589–1604.

Ferrarelli F, Tononi G (2011) The thalamic reticular nucleus and schizophrenia. *Schizophr Bull* 37:306–315.

Feynman R, Vernon Jr. F (1963) The theory of a general quantum system interacting with a linear dissipative system. *Annals Phys* 24:118–173.

Fitzgerald PB, Daskalakis ZJ, Hoy K, Farzan F, Upton DJ, Cooper NR, Maller JJ (2008) Cortical inhibition in motor and non-motor regions: a combined tms-eeg study. *Clin EEG neuroscience* 39:112–117.

Foth E, Bässler U (1985) Leg movements of stick insects walking with five legs on a treadwheel and with one leg on a motor-driven belt. I. General results and 1:1-coordination. *Biol Cybern* 51:313–318.

Friston K, Harrison L, Penny W (2003) Dynamic causal modelling. *NeuroImage* 19:1273–1302.

Friston KJ (1996) Theoretical neurobiology and schizophrenia. *Br Med Bull* 52:644–655.

Friston KJ (1998) The disconnection hypothesis. *Schizophr Res* 30:115–125.

Friston KJ, Frith CD, Fletcher P, Liddle PF, Frackowiak RS (1996) Functional topography: multidimensional scaling and functional connectivity in the brain. *Cereb Cortex* 6:156–164.

Friston KJ, Ashburner JT, Kiebel SJ, Nichols TE, Penny WD (2006) *Statistical parametric mapping: the analysis of functional brain images* Elsevier, London.

Fuchs E, Holmes P, Kiemel T, Ayali A (2010) Intersegmental coordination of cockroach locomotion: adaptive control of centrally coupled pattern generator circuits. *Front neural circuits* 4.

Gerloff C, Richard J, Hadley J, Schulman AE, Honda M, Hallett M (1998) Functional coupling and regional activation of human cortical motor areas during simple, internally paced and externally paced finger movements. *Brain* 121:1513–1531.

Gewaltig MO, Diesmann M (2007) Nest (neural simulation tool). *Scholarpedia* 2:1430.

Grabowska M (2014) Theoretical and experimental investigations of intra-and intersegmental control networks and their application to locomotion of insects and crustaceans Ph.D. diss., Universität zu Köln.

Grabowska M, Godlewska E, Schmidt J, Daun-Gruhn S (2012) Quadrupedal gaits in hexapod animals–inter-leg coordination in free-walking adult stick insects. *The J experimental biology* 215:4255–4266.

Graham D (1972) A behavioural analysis of the temporal organisation of walking movements in the 1st instar and adult stick insect (carausius morosus). *J Comp Physiol* 81:23–52.

Graham D (1985) *Pattern and control of walking in insects* Academic Press.

Graham D, Epstein S (1985) Behaviour and motor output for an insect walking on a slippery surface: Ii. backward walking. *J experimental biology* 118:287–296.

Grass AM, Gibbs FA (1938) A fourier transform of the electroencephalogram. *J Neurophysiol* 1:521–526.

Green MF (1996) What are the functional consequences of neurocognitive deficits in schizophrenia? *Am J Psychiatry* 153:321–330.

Grefkes C, Eickhoff SB, Nowak DA, Dafotakis M, Fink GR (2008) Dynamic intra- and interhemispheric interactions during unilateral and bilateral hand movements assessed with fmri and {DCM}. *NeuroImage* 41:1382 – 1394.

Greig LC, Woodworth MB, Galazo MJ, Padmanabhan H, Macklis JD (2013) Molecular logic of neocortical projection neuron specification, development and diversity. *Nat Rev Neurosci* 14:755–769.

Grillner S (2003) The motor infrastructure: from ion channels to neuronal networks. *Nat Rev Neurosci* 4:573–586.

Heeger DJ, Ress D (2002) What does fmri tell us about neuronal activity? *Nat Rev Neurosci* 3:142–151.

Herrmann C, Busch N, Grigutsch M (2005) Eeg oscillations and wavelet analysis In Handy TC, editor, *Event-related potentials: A methods handbook*, pp. 229–259. MIT press, Cambridge.

Herz DM, Christensen MS, Reck C, Florin E, Barbe MT, Stahlhut C, Pauls KAM, Tittgemeyer M, Siebner HR, Timmermann L (2012) Task-specific modulation of effective connectivity during two simple unimanual motor tasks: a 122-channel eeg study. *Neuroimage* 59:3187–3193.

Hess D, Büschges A (1997) Sensorimotor pathways involved in interjoint reflex action of an insect leg. *J Neurobiol* 33:891–913.

Hill A (1953) The mechanics of active muscle. *Proc Royal Soc Lond B: Biol Sci* 141:104–117.

Hodgkin AL, Huxley AF (1952) A quantitative description of membrane current and its application to conduction and excitation in nerve. *The J physiology* 117:500–544.

Holmes P, Full RJ, Koditschek D, Guckenheimer J (2006) The dynamics of legged locomotion: Models, analyses, and challenges. *Siam Rev* 48:207–304.

Hughes G, Schütz-Bosbach S, Waszak F (2011) One action system or two? evidence for common central preparatory mechanisms in voluntary and stimulus-driven actions. *The J Neurosci* 31:16692–16699.

Hughes G (1952) The co-ordination of insect movements i the walking movements of insects. *J Exp Biol* 29:267–285.

Hyvärinen A, Karhunen J, Oja E (2004) *Independent component analysis*, Vol. 46 John Wiley & Sons.

Igarashi J, Isomura Y, Arai K, Harukuni R, Fukai T (2013) A θ–γ oscillation code for neuronal coordination during motor behavior. *The J Neurosci* 33:18515–18530.

Jansen BH, Rit VG (1995) Electroencephalogram and visual evoked potential generation in a mathematical model of coupled cortical columns. *Biol cybernetics* 73:357–366.

Jenkins IH, Jahanshahi M, Jueptner M, Passingham RE, Brooks DJ (2000) Self-initiated versus externally triggered movements. *Brain* 123:1216–1228.

Jung TP, Makeig S, Humphries C, Lee TW, Mckeown MJ, Iragui V, Sejnowski TJ (2000a) Removing electroencephalographic artifacts by blind source separation. *Psychophysiol* 37:163–178.

Jung TP, Makeig S, Westerfield M, Townsend J, Courchesne E, Sejnowski TJ (2000b) Removal of eye activity artifacts from visual event-related potentials in normal and clinical subjects. *Clin Neurophysiol* 111:1745–1758.

Keil A, Elbert T, Taub E (1999) Relation of accelerometer and emg recordings for the measurement of upper extremity movement. *J Psychophysiol* 13:77.

Kiebel S, Garrido M, Moran R, Friston K (2008) Dynamic causal modelling for eeg and meg. *Cogn Neurodynamics* 2:121–136.

Kim DJ, Bolbecker AR, Howell J, Rass O, Sporns O, Hetrick WP, Breier A, O'Donnell BF (2013) Disturbed resting state eeg synchronization in bipolar disorder: A graph-theoretic analysis. *NeuroImage Clin* 2:414–423.

Knops S, Tóth TI, Guschlbauer C, Gruhn M, Daun-Gruhn S (2013) A neuromechanical model for the neuronal basis of curve walking in the stick insect. *J neurophysiology* 109:679–691.

Komarov M, Pikovsky A (2003) Dynamics of multifrequency oscillator communities. *Phys Rev Lett* 110:134101.

Komarov M, Pikovsky A (2011) Effects of nonresonant interaction in ensembles of phase oscillators. *Phys Rev E* 84:016210.

Krause M, Hoffmann WE, Hajós M (2003) Auditory sensory gating in hippocampus and reticular thalamic neurons in anesthetized rats. *Biol Psychiatry* 53:244 – 253.

Krieghoff V, Waszak F, Prinz W, Brass M (2011) Neural and behavioral correlates of intentional actions. *Neuropsychol* 49:767–776.

Krusienski DJ, McFarland DJ, Wolpaw JR (2012) Value of amplitude, phase, and coherence features for a sensorimotor rhythm-based brain–computer interface. *Brain research bulletin* 87:130–134.

Lachaux JP, Rodriguez E, Martinerie J, Varela FJ et al. (1999) Measuring phase synchrony in brain signals. *Hum brain mapping* 8:194–208.

Langlois D, Chartier S, Gosselin D (2010) An introduction to independent component analysis: Infomax and fastica algorithms. *Tutorials Quant Methods for Psychol* 6:31–38.

Laurent G, Burrows M (1989a) Distribution of intersegmental inputs to nonspiking local interneurons and motor neurons in the locust. *The J Neurosci* 9:3019–3029.

Laurent G, Burrows M (1989b) Intersegmental interneurons can control the gain of reflexes in adjacent segments of the locust by their action on nonspiking local interneurons. *The J Neurosci* 9:3030–3039.

Lawrie SM, Buechel C, Whalley HC, Frith CD, Friston KJ, Johnstone EC (2002) Reduced frontotemporal functional connectivity in schizophrenia associated with auditory hallucinations. *Biol Psychiatry* 51:1008–1011.

Lee H, Simpson GV, Logothetis NK, Rainer G (2005) Phase locking of single neuron activity to theta oscillations during working memory in monkey extrastriate visual cortex. *Neuron* 45:147 – 156.

Liddle PF (1987) The symptoms of chronic schizophrenia. a re-examination of the positive-negative dichotomy. *Br J Psychiatry* 151:145–151.

Llinás R, Ribary U, Jeanmonod D, Kronberg E, Mitra P (1999) Thalamocortical dyrhythmia: A neurological and neuropsychiatric syndrome characterized by magnetoencephalography. *PNAS* 96:15222–15227.

Loh M, Rolls ET, Deco G (2007) A dynamical systems hypothesis of schizophrenia. *PLoS Comput Biol* 3:e228.

Ludwar BC, Göritz ML, Schmidt J (2005) Intersegmental coordination of walking movements in stick insects. *J neurophysiology* 93:1255–1265.

Ludwar BC, Westmark S, Büschges A, Schmidt J (2005) Modulation of membrane potential in mesothoracic moto-and interneurons during stick insect front-leg walking. *J neurophysiology* 94:2772–2784.

Mackey MC, an der Heiden U (1982) Dynamical diseases and bifurcations: Understanding functional disorder in physiological systems. *Funkt Biol Med* 1.

Magri C, Schridde U, Murayama Y, Panzeri S, Logothetis NK (2012) The amplitude and timing of the bold signal reflects the relationship between local field potential power at different frequencies. *The J Neurosci* 32:1395–1407.

Mallada E, Tang A (2013) Synchronization of weakly coupled oscillators: coupling, delay and topology. *J Phys A: Math Theor* 46:505101.

Marder E, Bucher D (2001) Central pattern generators and the control of rhythmic movements. *Curr Biol* 11.

Marple S J (1999) Computing the discrete-time ldquo;analytic rdquo; signal via fft. *Signal Process IEEE Transactions on* 47:2600–2603.

Marx CE, Keefe RSE, Buchanan RW, Hamer RM, Kilts JD, Bradford DW, Strauss JL, Naylor JC, Payne VM, Lieberman JA, Savitz AJ, Leimone LA, Dunn L, Porcu P, Morrow AL, Shampine LJ (2009) Proof-of-concept trial with the neurosteroid pregnenolone targeting cognitive and negative symptoms in schizophrenia. *Neuropsychopharmacol* 34:1885–1903.

McAlonan K, Brown VJ, Bowman EM (2000) Thalamic reticular nucleus activation reflects attentional gating during classical conditioning. *The J Neurosci* 20:8897–8901.

McFarland DJ, McCane LM, David SV, Wolpaw JR (1997) Spatial filter selection for eeg-based communication. *Electroencephalogr clinical Neurophysiol* 103:386–394.

Meyer-Lindenberg AS, Olsen RK, Kohn PD (2005) Regionally specific disturbance of dorsolateral prefrontal hippocampal functional connectivity in schizophrenia. *Arch Gen Psychiatry* 62:379–386.

Michel CM, Murray MM, Lantz G, Gonzalez S, Spinelli L, de Peralta RG (2004) Eeg source imaging. *Clin neurophysiology* 115:2195–2222.

Michely J, Barbe MT, Hoffstaedter F, Timmermann L, Eickhoff SB, Fink GR, Grefkes C (2012) Differential effects of dopaminergic medication on basic motor performance and executive functions in parkinson's disease. *Neuropsychol* 50:2506–2514.

Mognon A, Jovicich J, Bruzzone L, Buiatti M (2011) Adjust: An automatic eeg artifact detector based on the joint use of spatial and temporal features. *Psychophysiol* 48:229–240.

Moran R, Kiebel S, Rombach N, O'Connor W, Murphy K, Reilly R, Friston K (2008) Bayesian estimation of synaptic physiology from the spectral responses of neural masses. *NeuroImage* 42:272–284.

Moran R, Kiebel S, Stephan K, Reilly R, Daunizeau J, Friston K (2007) A neural mass model of spectral responses in electrophysiology. *NeuroImage* 37:706–720.

Moran RJ, Jung F, Kumagai T, Endepols H, Graf R, Dolan RJ, Friston KJ, Stephan KE, Tittgemeyer M (2011) Dynamic causal models and physiological inference: A validation study using isoflurane anaesthesia in rodents. *PLoS ONE* 6:e22790.

Mueser KT, McGurk SR (2004) Schizophrenia. *The Lancet* 363:2063–2072.

Murakami S, Okada Y (2006) Contributions of principal neocortical neurons to magnetoencephalography and electroencephalography signals. *The J physiology* 575:925–936.

Neuper C, Pfurtscheller G (2001) Event-related dynamics of cortical rhythms: frequency-specific features and functional correlates. *Int journal psychophysiology* 43:41–58.

Neuper C, Wörtz M, Pfurtscheller G (2006) Erd/ers patterns reflecting sensorimotor activation and deactivation In Neuper C, Klimesch W, editors, *Event-Related Dynamics of Brain Oscillations*, Vol. 159 of *Progress in Brain Research*, pp. 211 – 222. Elsevier.

Okada YC, Wu J, Kyuhou S (1997) Genesis of meg signals in a mammalian cns structure. *Electroencephalogr clinical neurophysiology* 103:474–485.

Oldfield RC (1971) The assessment and analysis of handedness: the edinburgh inventory. *Neuropsychol* 9:97–113.

Ott E, Antonsen T (2008) Low dimensional behavior of large systems of globally coupled oscillators. *Chaos* 18.

Ott E, Antonsen T (2009) Long time evolution of phase oscillator systems. *Chaos* 19.

Pearson K, Franklin R (1984) Characteristics of leg movements and patterns of coordination in locusts walking on rough terrain. *The Int J Robotics Res* 3:101–112.

Peet M, Brind J, Ramchand CN, Shah S, Vankar GK (2001) Two double-blind placebo-controlled pilot studies of eicosapentaenoic acid in the treatment of schizophrenia. *Schizophr Res* 49:243–251.

Penny W, Litvak V, Fuentemilla L, Duzel E, Friston K (2009) Dynamic causal models for phase coupling. *J neuroscience methods* 183:19–30.

Perrin F, Pernier J, Bertrand O, Echallier J (1989) Spherical splines for scalp potential and current density mapping. *Electroencephalogr clinical neurophysiology* 72:184–187.

Pfurtscheller G (2001) Functional brain imaging based on erd/ers. *Vis research* 41:1257–1260.

Pfurtscheller G, Brunner C, Schlögl A, Da Silva FL (2006) Mu rhythm (de) synchronization and eeg single-trial classification of different motor imagery tasks. *Neuroimage* 31:153–159.

Pfurtscheller G, da Silva FL (1999) Event-related eeg/meg synchronization and desynchronization: basic principles. *Clin Neurophysiol* 110:1842 – 1857.

Pfurtscheller G, Jr. AS, Neuper C (1996) Post-movement beta synchronization. a correlate of an idling motor area? *Electroencephalogr Clin Neurophysiol* 98:281 – 293.

Pfurtscheller G, Pichler-Zalaudek K, Ortmayr B, Diez J, Reisecker F (1998) Postmovement beta synchronization in patients with parkinson's disease. *J Clin Neurophysiol* 15.

Pikovsky A, Rosenblum M (2008) Partially integrable dynamics of hierarchical populations of coupled oscillators. *Phys Rev Lett* 101.

Pikovsky A, Rosenblum M (2011) Dynamics of heterogeneous oscillator ensembles in terms of collective variables. *Phys D* 240:872–881.

Popovych S, Küpper T, Müller R, Brockhaus-Dumke A (2009) Modelling disturbance in early sensory processing in schizophrenia. *GAMM-Mitteilungen* 32:93–104.

Popovych S, Rosjat N, Wang B, Liu L, Tóth TI, Viswanathan S, Abdollahi RO, Grefkes C, Fink GR, Daun-Gruhn S (2015) Phase-locking in the delta-theta frequency band is an eeg marker of movement execution. *J Neurophysiol (submitted)* .

Potter D, Summerfelt A, Gold J, Buchanan RW (2006) Review of clinical correlates of p50 sensory gating abnormalities in patients with schizophrenia. *Schizophr Bull* 32:692–700.

Proctor J, Kukillaya R, Holmes P (2010) A phase-reduced neuro-mechanical model for insect locomotion: feed-forward stability and proprioceptive feedback. *Philos Transactions Royal Soc Lond A: Math Phys Eng Sci* 368:5087–5104.

Rigoux L, Stephan K, Friston K, Daunizeau J (2014) Bayesian model selection for group studies – revisited. *NeuroImage* 84:971–985.

Ritsner MS, Gibel A, Shleifer T, Boguslavsky I, Zayed A, Maayan R, Weizman A, Lerner V (2010) Pregnenolone and dehydroepiandrosterone as an adjunctive treatment in schizophrenia and schizoaffective disorder: an 8-week, double-blind, randomized, controlled, 2-center, parallel-group trial. *J Clin Psychiatry* 71:1351–1362.

Ritzmann RE, Büschges A (2007) Adaptive motor behavior in insects. *Curr opinion neurobiology* 17:629–636.

Rolls E, Loh M, Deco G, Winterer G (2008) Computational models of schizophrenia and dopamine modulation in the prefrontal cortex. *Nat Rev Neurosci* 9:696–709.

Rosenblum M, Pikovsky A, Kurths J, Schäfer C, Tass PA (2001) Phase synchronization: from theory to data analysis. *Handb biological physics* 4:93–94.

Rosjat N, Popovych S, Daun-Gruhn S (2014) A mathematical model of dysfunction of the thalamo-cortical loop in schizophrenia. *Theor Biol Med Model* 11:45.

Rubinov M, Sporns O (2010) Complex network measures of brain connectivity: uses and interpretations. *Neuroimage* 52:1059–1069.

Sanei S, Chambers JA (2013) *EEG signal processing* John Wiley & Sons.

Schmitz J (1986a) The depressor trochanteris motoneurones and their role in the coxo-trochanteral feedback loop in the stick insect carausius morosus. *Biol cybernetics* 55:25–34.

Schmitz J (1986b) Properties of the feedback system controlling the coxa-trochanter joint in the stick insect carausius morosus. *Biol cybernetics* 55:35–42.

Schmitz J, Büschges A, Delcomyn F (1988) An improved electrode design for en passant recording from small nerves. *Comp Biochem Physiol Part A: Physiol* 91:769 – 772.

Schultheiss NW, Prinz AA, Butera RJ (2011) *Phase response curves in neuroscience: theory, experiment, and analysis* Springer Science & Business Media.

Schusdziarra V, Zyznar E, Boden G (1977) Laminar organization of thalamic projections to the rat neocortex. *Life Sci* 20:2081.

Sherrington C (1941) Man on his nature. *The J Nerv Mental Dis* 94:762–763.

Shibasaki H, Hallett M (2006) What is the bereitschaftspotential? *Clin Neurophysiol* 117:2341–2356.

Shipp S (2007) Structure and function of the cerebral cortex. *Curr Biol* 17:R443–R449.

Skoglund T, Pascher R, Berthold C (1997) The existence of a layer iv in the rat motor cortex. *Cereb Cortex* 7:178–180.

Song L, Gordon E, Gysels E (2005) Phase synchrony rate for the recognition of motor imagery in brain-computer interface In *Advances in Neural Information Processing Systems*, pp. 1265–1272.

Stephan KE, Friston KJ, Frith CD (2009) Dysconnection in schizophrenia: From abnormal synaptic plasticity to failures of self-monitoring. *Schizophr Bull* 35(3):509–527.

Tass P, Rosenblum MG, Weule J, Kurths J, Pikovsky A, Volkmann J, Schnitzler A, Freund HJ (1998) Detection of $n : m$ phase locking from noisy data: Application to magnetoencephalography. *Phys Rev Lett* 81:3291–3294.

Tass PA (2002) Stimulus-locked transient phase dynamics, synchronization and desynchronization of two oscillators. *EPL (Europhysics Lett* 59:199.

Tass PA (2007) *Phase resetting in medicine and biology: stochastic modelling and data analysis*, Vol. 172 Springer Science & Business Media.

Teplan M (2002) Fundamentals of eeg measurement. *Meas Sci Rev* 2.

Terao Y, Ugawa Y (2002) Basic mechanisms of tms. *J clinical neurophysiology* 19:322–343.

Toth TI, Daun-Gruhn S (2011) A putative neuronal network controlling the activity of the leg motoneurons of the stick insect. *NeuroReport* 22:943–946.

Tóth TI, Knops S, Daun-Gruhn S (2012) A neuromechanical model explaining forward and backward stepping in the stick insect. *J neurophysiology* 107:3267–3280.

Uhlhaas PJ, Roux F, Rodriguez E, Rotarska-Jagiela A, Singer W (2010) Neural synchrony and the development of cortical networks. *Trends Cogn Sci* 14:72 – 80.

Van Veen BD, Van Drongelen W, Yuchtman M, Suzuki A (1997) Localization of brain electrical activity via linearly constrained minimum variance spatial filtering. *Biomed Eng IEEE Transactions on* 44:867–880.

Varela F, Lachaux JP, Rodriguez E, Martinerie J (2001) The brainweb: phase synchronization and large-scale integration. *Nat reviews neuroscience* 2:229–239.

Walz JM, Goldman RI, Carapezza M, Muraskin J, Brown TR, Sajda P (2013) Simultaneous eeg-fmri reveals temporal evolution of coupling between supramodal cortical attention networks and the brainstem. *The J Neurosci* 33:19212–19222.

Wang Y, Hong B, Gao X, Gao S (2006a) Phase synchrony measurement in motor cortex for classifying single-trial eeg during motor imagery In *Engineering in Medicine and Biology Society, 2006. EMBS'06. 28th Annual International Conference of the IEEE*, pp. 75–78. IEEE.

Wang Y, Hong B, Gao X, Gao S (2006b) Phase synchrony measurement in motor cortex for classifying single-trial eeg during motor imagery In *Engineering in Medicine and Biology Society, 2006. EMBS'06. 28th Annual International Conference of the IEEE*, pp. 75–78. IEEE.

Waszak F, Wascher E, Keller P, Koch I, Aschersleben G, Rosenbaum D, Prinz W (2005) Intention-based and stimulus-based mechanisms in action selection. *Exp Brain Res* 162:346–356.

Watanabe S, Strogatz S (1994) Constants of motion for superconducting josephson arrays. *Phys D* 74:197–253.

Wendler G (1965) The co-ordination of walking movements in arthropods. *Symp Soc for Exp Biol* 20:229–249.

Westmark S, Oliveira EE, Schmidt J (2009) Pharmacological analysis of tonic activity in motoneurons during stick insect walking. *J neurophysiology* 102:1049–1061.

Wilson DM (1966) Insect walking. *Annu review entomology* 11:103–122.

Winfree AT (2000) *The geometry of biological time*, Vol. 12 Springer Science & Business Media.

Witt ST, Laird AR, Meyerand ME (2008) Functional neuroimaging correlates of finger-tapping task variations: an ale meta-analysis. *Neuroimage* 42:343–356.

Wyatt HJ (1998) Detecting saccades with jerk. *Vis research* 38:2147–2153.

Yamawaki N, Borges K, Suter BA, Harris KD, Shepherd GM (2015) A genuine layer 4 in motor cortex with prototypical synaptic circuit connectivity. *Elife* 3:e05422.

Zehr EP, Carroll TJ, Chua R, Collins DF, Frigon A, Haridas C, Hundza SR, Thompson AK (2004) Possible contributions of cpg activity to the control of rhythmic human arm movement. *Can J Physiol Pharmacol* 82:556–568 PMID: 15523513.

Zendehrouh S, Bakouie F, Gharibzadeh S, Rostami A (2010) Mathematical modeling of schizophrenia. *J Paramed Sci* 1.

Zhao K, Gu R, Wang L, Xiao P, Chen YH, Liang J, Hu L, Fu X (2014) Voluntary pressing and releasing actions induce different senses of time: Evidence from event-related brain responses. *Sci reports* 4.

Acknowledgements

An dieser Stelle möchte ich mich ganz herzlich bei all denjenigen bedanken, die mich bei der Entstehung meiner Arbeit unterstützt haben.

Allen voran bedanke ich mich bei meiner Betreuerin Frau PD Dr. Silvia Gruhn, für die Bereitstellung der spannenden Themen, für die tatkräftige Unterstützung und die mir gelassene Gestaltungsfreiheit in der Umsetzung. Außerdem danke ich ihr für die zahlreichen Möglichkeiten der Weiterbildung, besonders sei hier der Forschungsaufenthalt bei Herrn Prof. Dr. Phil Holmes an der Princeton University erwähnt.

Herrn Prof. Dr. Ansgar Büschges danke ich selbstverständlich für die Übernahme des Zweitgutachtens, aber auch für die vielen fruchtbaren Diskussionen und die daraus entstandenen Ideen.

Ebenso danke ich Herrn Prof. Dr. Martin Nawrot für die freundliche Übernahme des Drittgutachtens.

Ein weiterer Dank gilt Herrn Prof. Dr. Dr. Tassilo Küpper und Herrn Prof. Dr. Phil Holmes, in deren Arbeitsgruppen ich vieles über mathematische Methoden bei der Modellierung neuronaler Netzwerke gelernt habe.

Der Arbeitsgruppe Gruhn, danke ich für die schöne Zeit im mal mehr und mal weniger ruhigen Arbeitsumfeld. Ein besonderer Dank gilt dabei Dr. Tibor Tóth und Dr. Svitlana Popovych, die mir in den letzten Jahren jederzeit mit Rat und Tat zur Seite gestanden sind.

Ein großer Dank gilt Magdalena Borowski, Elzbieta Hammel, Darinka Hansen, Marko Kapitza, Patrick Müller, Christoph Quadfasel und Dr. Azamat Yeldesbay dafür, dass sie sich daran gewagt haben einige Abschnitte dieser Arbeit Korrektur zu lesen, obwohl die Gefahr droht “vor lauter neurologischer und mathematischer Fachbegriffe” beim Lesen einzuschlafen.

Meinen Eltern und meiner Schwester gilt ein besonders großer Dank, dafür dass sie mich immer bei all meinen Entscheidungen unterstützt haben und mir immer wieder

den Mut zugesprochen haben unbekannte Pfade zu erforschen.

Zum Schluss gilt mein Dank der Person, ohne die ich wahrscheinlich nicht bis hierher gekommen wäre, meiner Freundin Darinka. Sie war immer da, um sich meiner Sorgen und Probleme anzunehmen und hat mir gerade zum Ende meiner Promotion etliche Lasten abgenommen. Jederzeit wusste sie, wie sie mich ablenken konnte, um mich wieder zum Lachen zu bringen.

Teilpublikationen

1 List of Publications

Rosjat, N., Popovych, S., Daun-Gruhn S., (2014). A mathematical model of dysfunction of the thalamo-cortical loop in schizophrenia, Theoretical Biology and Medical Modelling

Tóth, T. I., Grabowska, M., **Rosjat, N.**, Hellekes, K., Borgmann, A., Daun-Gruhn, S., (2015). Investigating inter-segmental connections between thoracic ganglia in the stick insect by means of experimental and simulated phase response curves, Biological Cybernetics

Popovych, S., **Rosjat, N.**, Wang, B., Liu, L., Tóth, T., Viswanathan, S., Grefkes, C., Fink, G. R., Daun-Gruhn S., (under review). Phase locking in the delta-theta band is an EEG marker of movement execution

Rosjat, N., Mantziaris, C., Borgmann, A., Büschges, A., Daun-Gruhn S., (in preparation). Intersegmental coupling between fictive motor rhythms of pattern generating networks in the stick insect

Rosjat, N., Popovych, S., Wang, B., Liu, L., Tóth, T., Viswanathan, S., Grefkes, C., Fink, G. R., Daun-Gruhn S., (in preparation). Phase-locking analysis of EEG-data in movement related tasks reveals slow frequency motor system synchronisation

2 Short Communications

Rosjat N., Popovych S., Wang B., Liu L., Tóth T., Viswanathan S., Grefkes C., Fink G., Gruhn S., 2015.
Phase-locking analysis of EEG-data in movement related tasks reveals common underlying network of synchronous activity, Poster präsentiert auf dem SfN Meeting 2015 Chicago.

Rosjat N., Tóth T., Mantziaris C., Borgmann A., Gruhn S., 2014.
Using dynamic causal modeling in the study of the stick insect locomotor system, Poster präsentiert auf dem SfN Meeting 2014 Washington.

Rosjat N., Wang B., Tóth T., Popovych S., Grefkes C., Fink G.R., Daun-Gruhn S., 2014.
A dynamic Modeling Brain Connectivity of Networks engaged in the Movement Generation: DCM of EEG data, Poster präsentiert auf der Neurovision 10 Jülich.

Rosjat N., Daun-Gruhn S., Popovych S., Modeling of the dysfunction of the thalamo-cortical loop in schizophrenia, 2013. Poster präsentiert auf der Brain Modes 2013 Amsterdam.

Rosjat N., Popovych S., Daun-Gruhn S., Modeling thalamo-cortical activity during dysfunction in schizophrenia, 2013. Poster präsentiert auf der Neurovision 9 Köln.

Rosjat N., Daun-Gruhn S., Popovych S., Mathematical model of the thalamo-cortical loop by dysfunction in schizophrenia, 2013. Poster präsentiert auf der CNS 2013 Paris.

Rosjat N., Müller R., Brockhaus-Dumke A., Popovych S., Daun-Gruhn S., 2012.
Dysfunction of the thalamo-cortical loop in schizophrenia: EEG data and mathematical model, Poster präsentiert auf der Neurovision 8 Aachen.

Erklärung

Ich versichere, dass ich die von mir vorgelegte Dissertation selbständig angefertigt, die benutzten Quellen und Hilfsmittel vollständig angegeben und die Stellen der Arbeit – einschließlich Tabellen, Karten und Abbildungen –, die anderen Werken im Wortlaut oder dem Sinn nach entnommen sind, in jedem Einzelfall als Entlehnung kenntlich gemacht habe; dass diese Dissertation noch keiner anderen Fakultät oder Universität zur Prüfung vorgelegen hat; dass sie – abgesehen von unten angegebenen Teilpublikationen – noch nicht veröffentlicht worden ist, sowie, dass ich eine solche Veröffentlichung vor Abschluss des Promotionsverfahrens nicht vornehmen werde. Die Bestimmungen der Promotionsordnung sind mir bekannt. Die von mir vorgelegte Dissertation ist von PD Dr. Silvia Gruhn betreut worden.

Köln, den 12. November 2015

Nils Rosjat